2016-01-01

Effects Of Fabrication Conditions On Mechanical Properties Of Ti-6al-4v Fabricated By Powder Bed Fusion Additive Manufacturing

Paola Azani
University of Texas at El Paso, pmcordero@miners.utep.edu

EFFECTS OF FABRICATION CONDITIONS ON MECHANICAL PROPERTIES OF TI-6AL-4V FABRICATED BY POWDER BED FUSION ADDITIVE MANUFACTURING

PAOLA AZANI

Master's Program in Metallurgical and Materials Engineering

APPROVED:

Ryan B. Wicker, Ph.D., Chair

Devesh Misra, Ph.D.

David A. Roberson, Ph.D.

Charles Ambler, Ph.D.
Dean of the Graduate School

This Thesis is dedicated to my mother

EFFECTS OF FABRICATION CONDITIONS ON MECHANICAL PROPERTIES OF TI-6AL-4V FABRICATED BY POWDER BED FUSION ADDITIVE MANUFACTURING

by

PAOLA AZANI, B.S.M.M.E

THESIS

Presented to the Faculty of the Graduate School of

The University of Texas at El Paso

in Partial Fulfillment

of the Requirements

for the Degree of

Master of Science

Department of Metallurgical and Materials Biomedical Engineering

THE UNIVERSITY OF TEXAS AT EL PASO

May 2016

ACKNOWLEDGEMENTS

The work that I present here has been possible by the guidance I have had from individuals with extraordinary minds investing in the best ideas to be ready to take on any challenge, and conserve the humbleness to share their knowledge with those who envision their yearning. Foremost, I would like to express my deepest gratitude to Dr. Ryan Wicker, Director of the W.M. Keck Center for 3D Innovation (Keck Center), for providing me with the opportunity to embark in this research. I am honored to have worked under his mentorship for the last year and half during which I developed my background in additive manufacturing. I am and will always be thankful to Dr. Sara Gaytan and Jorge Mireles for the excellent guidance during my research. Dr. Gaytan's meticulous attention to every aspect of a project made her admirable before me. In addition, Jorge's extensive knowledge in additive manufacturing facilitated my learning processes that hasten the successful completion of my research. I would also like to thank all my professors in the metallurgy and materials department, whom have shaped and polished the career I hold today with their teachings, patience, and devotion to the profession. My sincere thanks also go to my fellow researchers: Mohammad S. Hossain, Shakerur Ridwan, and Philip Morton for the insightful comments that contributed to solutions and for the help they provided throughout the process of my research. I cannot imagine spending this time with more caring and knowledgeable people than the ones that form part of the Keck Center. I thank the National Science Foundation (NSF) for the support provided to make the completion of this work possible.

I would also like to thank my family whose unconditional love and support gave me strength and fueled me with valor to continue my path. Finally, I would like to thank my mother, the person I most admire and love. I wish to let you know that, today I am who I am because of you and I will be eternally thankful for the privilege of calling you, mother.

ABSTRACT

At the writing of this thesis, additive manufacturing (AM) also known as 3D printing, has been popularized for its diversity in applications ranging from home and personal use, medical, industrial, consumer products, aerospace, architecture, automotive, military, fashion, food, art and more. Industries taking advantage of the design freedom and complexity offered by AM have exploded the growth of the technologies. Specifically, technologies that process metals using electron and laser beams have been recognized by the aerospace industry as a promising avenue for re-engineered components leading to reduced weight and improved engineering efficiencies for components like engine brackets and nozzles. However, the direct implementation of AM has not been straightforward primarily because AM processes are not fully trusted to produce reliable and reproducible parts. Continued research, including the subject of this thesis, is aimed at better understanding process variations in the AM of metals via powder bed fusion.

Electron Beam Melting (EBM) is an AM is a technology in the category of powder bed fusion that is seeing increased adoption by a variety of industries for part production. EBM was the focus of this study for the fabrication of solid and porous parts using precursor powder composed of Ti-6Al-4V. This research is centered on evaluating mechanical properties, analyzing microstructures, and correlating the fabrication process to inherent characteristics of solid and porous parts fabricated utilizing EBM. For dense parts, data were documented on the effects on mechanical and microstructural properties from neighboring parts and building location. In the case of porous, or lattice structures, data were documented on the effect of parameter modifications, such as processing currents and number of scan passes, on the final part mechanical response and microstructure. Solid and lattice components were mechanically tested and microstructural features were obtained by the use of computer software MATLAB.

Microstructural and factrographic analyses were performed on samples prepared for such analysis and the prepared surfaces were used for hardness testing.

Several variables in part production exist for AM, including, but not limited to, part orientation, part location, processing parameters, and geometry. For the solid components fabricated for this thesis, the core objective was to determine the effect that surrounding parts have on mechanical properties. The study was expanded to also determine how part location within a build area affects the mechanical properties. Mechanical information of a material was obtained by tensile testing that provided values for the following properties: yield strength (YS), ultimate tensile strength (UTS), modulus of elasticity (E), and elongation (%EL). Twenty-seven total parts were fabricated, machined, and tested. Further comparison between build characteristics and microstructure was evaluated by performing metallographic analysis. The surfaces prepared for metallographic analysis were subsequently subjected to hardness testing and fractography analysis was performed as a means to construct a correlation between the gathered information and the potential cause(s) contributing to the ductile failure mode observed.

Results from surface area variations, in general, demonstrated change in YS, UTS, and E. Percent elongation reflected significant improvements from the increased surface areas. Noteworthy was the significant decrease in standard deviation as melt surface area increased. The typical Widmänstatten lath morphology was observed by all EBM-fabricated Ti-6Al-4V parts; however, increases in α lath width were evident from the increased surface area. For the study consisting of spatial distribution within a build, in general, an increase in YS, UTS and E was observed for parts located toward the back of the fabrication system, with respect to the front of the system. Percent elongation decreased from the back to the front of the machine.

The fabrication of generic structures provided the information on features produced using the standard commercial methodology, which would generally be used by industry. One of the benefits provided to Arcam users is the ability to access the process menu for customize build parameters. The previous deigns presented a study on features for solid structures fabricated without processing parameter variations. This furthering task presents for modification of processing parameters on lattice structures. The area that has been studied adds to improvements on features by additive manufacturing in general, enabling sophisticated designs with tailored properties while optimizing material and weight.

A particular focus of this research was the study of lattice structures fabricated by EBM. Mechanical information of a material was obtained through compression testing, which provided values for the following properties: young's modulus of elasticity (E), ultimate compression strength (UCS), the fracture load, and the displacement seen at such. Twenty-seven total lattice specimens were fabricated and tested. A correlation between microstructure and properties was explored using metallography analysis. Samples that displayed considerable property differences within a single build were chosen for analysis and consequently subjected to hardness testing. Fractography analysis was also performed on selected specimens to examine the potential cause(s) contributing to the bimodal failure mode.

Of pertinence to lattice structures is removing the detrimental martensitic phase created during rapid solidification, which causes brittle mode fracture. Lattice structures provide a light weighting alternative to the typically utilized solid implant that will offer physical properties compatibility. Implants are just one example of the products lattice structures can be utilized for, however the possibilities include the industries already mentioned . The structures cannot be included in production unless performance away from catastrophic failure, as the one the

martensitic phase mentioned would promote is ensure. In order to change the microstructure of lattice structures, it was necessary to make parameter modifications on the fabrication process. The processing currents studied for comparison included a standard build and three sets of modified scan speeds and currents. A second investigation involved the mechanical response of increasing layer-by-layer scans. The melts studied included a single scan, a double scan, and a triple scan. In the case of the study consisting of varying processing speeds and currents, in general, the results showed a change in properties from the standard because of parameter modifications. The E and UCS values do not change notably and fracture load observed varied considerably. A decrease in α lath width was observed as processing current decreased. In the case of the study consisting of increasing melts, in general, the change in mechanical properties showed improvements across all parameters of E, UCS, and fracture load. Microstructurally, this research demonstrated the removal of the detrimental martensitic phase in lattice structures by altering the thermal environment within the build chamber (through changing scanning strategies) during the build. The study conducted in this thesis achieved the reengineering of the microstructure observed in lattice components to a complete Widmänstatten lath morphology with the appearance of α equiaxed grains.

Overall, the research outcome of this thesis provided further characterization of the EBM fabrication process and presented some potential improvements to unique lattice structures. The mechanical response obtained by increase of surface area and varying locations showed that certain variations are present and users need to be aware of these part-to-part differences. In the case of components containing lattice structures, the mechanical response obtained by variation of the processing current within a single build and increasing scan passes suggested that detrimental martensite phase that typically occurs in the standard build process can be removed from in-process modifications.

TABLE OF CONTENTS

LIST OF TABLES

LIST OF FIGURES

CHAPTER 1: INTRODUCTION

PROJECT OVERVIEW

At the writing of this thesis, additive manufacturing (AM) also known as 3D printing, has been popularized for its diversity in applications ranging from home and personal use, medical, industrial, consumer products, aerospace, architecture, automotive, military, fashion, food, art and more. A critical milestone for AM has been the expiration of patents over the years, with one of the most notable patents owned by Stratasys for material extrusion technology, which expired 2009. Industries taking advantage of the design freedom and complexity offered by AM have exploded the growth of the technologies. Specifically, technologies that process metals using electron and laser beams have been recognized by the aerospace industry as a promising avenue for re-engineered components leading to reduced weight and improved engineering efficiencies for components like engine brackets and nozzles. However, the direct implementation of AM has not been straightforward primarily because AM processes are not fully trusted to produce reliable and reproducible parts. Continued research, including the subject of this thesis, is aimed at better understanding process variations in the AM of metals via powder bed fusion.

Powder bed fusion electron beam melting (EBM) AM is a technology that is seeing increased adoption by a variety of industries for part production. EBM will be the focus of this research and utilized in these studies for the fabrication of solid and porous parts using precursor powder composed of Ti-6Al-4V. This research is centered on evaluating mechanical properties, analyzing microstructures, and correlating the fabrication process to inherent characteristics of solid and porous parts fabricated utilizing EBM. For dense parts, data were documented on the effects on mechanical and microstructural properties from neighboring parts and building location. In the case of porous, or lattice structures, data were documented on the effect of

parameter modifications, such as processing currents and number of scan passes, on the final part mechanical response and microstructure. Solid and lattice components were mechanically tested and microstructural features were obtained by the use of computer software MATLAB. Microstructural and factrography analyses were performed on samples prepared for such analysis and the prepared surfaces were used for hardness testing.

Several variables in part production exist for AM, including, but not limited to, part orientation, part location, processing parameters, and geometry. For the solid components fabricated for this thesis, the core objective was to determine the effect that surrounding parts have on mechanical properties. The study was expanded to also determine how part location within a build area affects the mechanical properties. Mechanical information of a material was obtained by tensile testing that provided values for the following properties: Yield Strength (YS), Ultimate Tensile Strength (UTS), Modulus of Elasticity (E), and percent Elongation. Twenty-seven total parts were fabricated, machined, and tested. Further comparison between build characteristics and microstructure was evaluated by performing metallographic analysis. The surfaces prepared for metallographic analysis were further subject to hardness testing and fractography analysis was performed as a means to construct a correlation between the gathered information and the potential cause(s) contributing to the ductile failure mode observed.

Results from surface area variations, in general, demonstrated change in YS, UTS, and E. Percent elongation reflected significant improvements from the increased surface areas. Noteworthy was the significant decrease in standard deviation as melt surface area increased. The typical Widmänstatten lath morphology was observed by all EBM-fabricated Ti-6Al-4V parts; however, increases in α lath width were evident from the increased surface area. For the study consisting of spatial distribution within a build, in general, an increase in YS, UTS and E was

observed for parts located toward the back of the fabrication system, with respect to the front of the system. Percent elongation decreased from the back to the front of the machine.

The fabrication of generic structures provides the information on features produced using the standard commercial methodology, which would generally be used by industry. One of the benefits provided to Arcam users are the ability to access the process menu for customize building parameters. The previous deigns presented a study on features for solid structures fabricated without processing parameter variations. This furthering task presents for modification of processing parameters on lattice structures. The area that has been studied adds to improvements on features by additive manufacturing in general, enabling sophisticated designs with tailored properties while optimizing material and weight.

A particular focus of this research was the study of lattice structures fabricated by EBM. Mechanical information of a material was obtained through compression testing, which provided values for the following properties: Young's Modulus of Elasticity (E), Ultimate Compression Strength (UCS), the fracture load, and the displacement seen at such. Twenty-seven total lattice specimens were fabricated and tested. A correlation between microstructure and properties was explored using metallography analysis. Samples that displayed considerable property differences within a single build were chosen for analysis and consequently subjected to hardness testing. Fractography analysis was also performed on selected specimens to examine the potential cause(s) contributing to the bimodal failure mode.

Of interest to lattice structures is removing the detrimental martensitic phase create during rapid solidification, which causes brittle mode fracture. In order to change the microstructure of lattice structures, it was necessary to make parameter modifications on the fabrication process. The processing currents studied for comparison included a standard build and three sets of modified

scan speeds and currents. A second investigation involved the mechanical response of increasing layer-by-layer scans. The melts studied included a single scan, a double scan, and a triple scan. In the case of the study consisting of varying processing speeds and currents, in general, the results showed a change in properties from the standard because of parameter modifications. The E and UCS values do not change notably and fracture load observed varied considerably. A decrease in α lath width was observed as processing current decreased. In the case of the study consisting of increasing melts, in general, the change in mechanical properties showed improvements across all properties of E, UCS, and fracture load. Microstructurally, this research demonstrated the removal of the detrimental martensitic phase in lattice structures by altering the thermal environment within the build chamber (through changing scanning strategies) during the build. The study conducted in this thesis achieved the reengineering of the microstructure observed in lattice components to a complete Widmänstatten lath morphology with the appearance of α equiaxed grains.

Overall, the research outcome of this thesis provided further characterization of the EBM fabrication process and presented some potential improvements to unique lattice structures. The mechanical response obtained by increase of surface area and varying locations showed that certain variations are present and users need to be aware of these part-to-part differences. In the case of components containing lattice structures, the mechanical response obtained by variation of the processing current within a single build and increasing scan passes suggested that detrimental martensite phase that typically occurs in the standard build process can be removed from in-process modifications.

W.M. KECK CENTER FOR 3D INNOVATION

The W.M. Keck Center for 3D Innovation (Keck Center), located at the University of Texas at El Paso (UTEP), is one of the best-equipped university 3D printing facilities in the world and was the facility utilized to conduct the research for this thesis. The Keck Center has been at the cutting edge of AM for over a decade since its founding in 2000 as part of a $1 million grant from the W.M. Keck Foundation. UTEP's Keck Center has made a commitment to invest in the AM technological sector to maintain global competitiveness in manufacturing. At the writing of this thesis, the Keck Center occupies over 13,000-square-foot within the university. The laboratory houses more than 50 AM machines representing a state-of-the-art facility with research and commercial capabilities.

The Keck Center offers AM technology for all the four types of engineering materials (metals, polymers, ceramics and composites) as well as access to material characterization, mechanical testing, metrology and reverse engineering facilities (Office of research and sponsored project, 2012). The lab includes full time faculty and staff and more than 60 student researchers working on ongoing projects as well as projects under development along with affiliated faculty in various engineering departments.

Working towards an ultimate goal to evolve 3D printing for end-use products compatible for industry, success has been achieved by conducting efficient diverse interdisciplinary research. 3D structural electronics, material development for EBM technology and various areas in biomedical engineering (Wicker, 2012) are focus areas for printing end-use devices. These areas are pivotal for a successful positive presence of AM in general.

In 2015, America Makes, the National Additive Manufacturing Innovation Institute, in collaboration with UTEP's Keck Center, proudly presented the opening of its first Satellite Center, which further establishes the Keck Center as a premier facility in AM.

ADDITIVE MANUFACTURING

In 2009 the ASTM Committee F42 on Additive Manufacturing Technologies was formed as the evolving technology of AM attracted a high level of global interest (Wohlers; 2012) contributing to making it a highly researched area. From its original use for fabrication of scale models from computer-aided design (CAD), AM processes experienced rather quick improvements in final part outcome, graduating prototypes into physical structures that could be utilized in different applications depending on the material and mechanical properties. Production of difficult geometries by a simplified process established a market in terms of AM development. The layer-by-layer process became a low cost replacement for parts fabricated and utilized as a final concept, annulling the technology from its previously known term of Rapid Prototyping (RP) (Gibson *et al.*, 2010) (Wood, 2016). However, the AM process does not necessarily have to be the fabrication of a final part and implementing post-processing techniques has been widely used to achieve a better end-use product (Gibson *et al.*, 2010).

AM processes commence by making the part using a computer aided design (CAD) file. The computerized software removes design limitations, one of the things that make this technology favorable over conventional methods (Wang, 2011). The CAD file is a 3D solid model that is then converted to match specific AM machines, which tipically require an STL or AMF format that is used as a reference for each layer melting. This will ultimately make up the final part. Machine software specifications are setforth in accordance to the tehcnology and material selected. The automated build process starts accordingly.

Restricitions to the AM process that have been encountered include; size, and lack on information on part manufactured. Nonetheless, concepts of the imagination have been turned into a physical reality with the help of AM.

ELECTRON BEAM MELTING

Electron Beam Melting, or EBM, is an AM powder bed fusion technology developed by the Swedish company Arcam (Mölndal, Sweden). The system utilizes a powder spreading approach in which an electron beam selectivly melts the metal deposited through each layer that will make up the part. The approach allows for material to be added to a part making it attractive not only for new designs but also for part repairments (Gibson *et al.*, 2010).

A schematic of the EBM system is shown in Figure1.1. The machine uses a tungsten filament located within the electron beam column that is heated using 60kV. Electrons are then realease generating the energy reqiured for high melting point materials. The released electrons can be accelerated to ~0.1 to 0.4 times the speed of light. Thre grid cup filters the amount of electrons in accordance to the amount needed for the beam and the beam focus is achieved by the use of electromagnetic lenses and coils in the machine that allow precision melting corresponding to the data from a CAD file. The beam slectively melts the powder that is placed onto the building platform by a powder spreading mechanism. Before each layer is melted the building platform is heated to a predetermined temperature depending on the material selected for part fabrciation. The process takes placed in a chamber with a base pressure of 1×10^{-3} or better (Arcam AB, 2011). Control environments prevent materials from oxidizing, compliment cleanliness, and reduce post-fabrication steps. All these characteristics improve material performance. The completed part is then removed after the temperature has decreased a specific amount for handling (below 100°C) and avoidance of oxidation, nitriding or any otherwise ill effects to material performance. A

powder recovery technique used on lightly sintered powder surrounding the part is blasted away and reused for another build.

The material that is most widely used with EBM is Ti-6Al-4V ELI, a metal alloy certified by Arcam. The layer thickness distributed by the raking mechanism is of 0.05mm or 0.07mm and is typically preheated to a temperature ≥ 730°C. The high preheat temperature helps eliminate free residual stress in the parts by reducing the temperature gradient from layerwise melting and cooling. The preheat uses a beam current of ~8.8mA for this material with a scan speed of up to 14,000mm/s. A scan to melt the precursor powder follows the preheat and is performed with a beam current of 17mA and a scan speed of ~500mm/s. For Ti-6Al-4V the preheat is conducted with a low current and a high melting speed, and the melt scan is opposite to achieve the materials melting point. After the melt scan, the building platform is lowered one layer thickness which allows the next layer to be placed. This procedure repeats until the solid 3D part is complete. The part can be subjected to post processing steps such as hot isostatic pressing (HIP) or heat treatments.

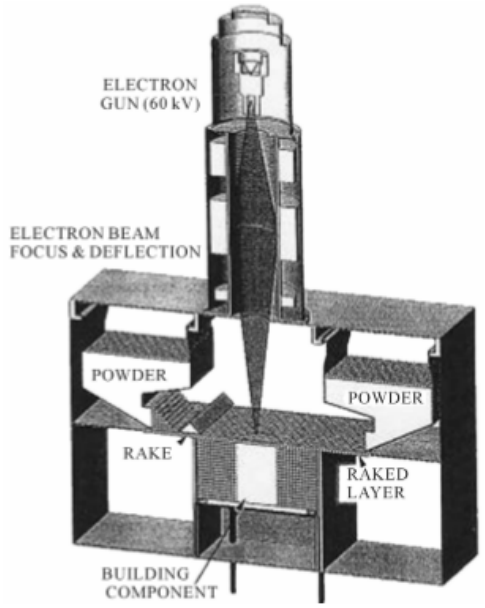

Figure 1.1: Arcam A2 EBM system schematic image courtesy of (Karina Puebla, 2012)

RESEARCH MOTIVATION

AM fabrication of metals has become an attractive and powerful tool for industries such as aerospace and automotive because it presents the possibility of manufacturing structures that will reduce weight without compromising safety or performance (Kaufui V. Wong, 2012) . Parts fabricated by this technology also find vast applications in the medical world because of the possibility of making rapid prototypes that gives doctors a better idea of the condition they are handling through pre-surgical models (Kaufui V. Wong, 2012). EBM-fabricated Ti-6Al-4V porous parts have exhibited mechanical properties comparable to those of the human bone (Peter Heinl, 2008) making them highly researchable in the medical field. The developments in the technology have provided enhancements in processing parts exhibiting outstanding properties. The high level of interest has opened new areas to study and formalized areas needing improvements. In this thesis, part performance through mechanical testing is studied to observe the impact that build variation and changes in processing parameters have on the resulting part.

Improvements in the EBM technology have been conducted for the fabrication of end-use parts. Although this has been attractive to commercial industries, post-processing steps have been a requirement to achieve the highest reliability of the part performance (Hu & Kobacevic, 2003). The extra precautions needed in industry reflected the need for better understanding of the fabrication process. Steps to better understand the process and achieve qualification have been done through studies aimed at improving the layer-by-layer temperature feedback, which is currently limited by the use of a single thermocouple that reads the temperature at the bottom of the building platform. Non-contact temperature measuring and image acquisition tools have been investigated (Rodriguez, 2013, Rodriguez *et al.*, 2012). Understaning the fabrication process thoroughly can provide insightful data to users for achieving optimum fabrication conditions.

Rodriguez *et al.;*(2015) focused on research investigating the acquisition of absolute surface temperatures using in situ infrared (IR) thermography, leading to improvements in thermal monitoring. Studies have purposely fabricated defected parts to understand how defects generate and classify processing parameters (Haijun Gong, 2014). Studies focusing in different areas of EBM have been conducted to reach the technologies maximum potential in both academia and industry.

Studies performed have mostly dealt with alterations to processing parameters; however due to the increasing implementation of EBM technologies in industry, it is important to have an understanding on how mechanical properties and microstructure of an EBM-fabricated part will be impacted by the fabrication processes. This is of importance in the commercial industry sector where only commercialized metals are use and fabrication is by the standardized building parameters. There is a need to know the output from a given input.

Repeatedly, man has looked onto nature for inspiration, and once again, natural formations provide the most efficient and enabling structures. Lattice structures, whose design reflects physical forms like those of corals and the randomness observed on cork, bone, and wood are an area of high interest regarding to EBM technology. The highly porous metal structures have exhibited astonishing properties and improvements to EBM-fabricated parts in general, and have allowed unprecedented advancements in weight reduction across a wide range of engineering components. The biomedical industry sees promise in the porous structures for medical implants because it remedies the problem of incompatible Young's modulus between metal implants and bone as well as stress shielding. The aerospace industry is delighted by their strength to weight ratio and capability of serving as heat sinks. AM has made its way to the fashion industry were designs are chiefly lattice. Other industries that have shown interest in lattice structures are

aviation, automotive, oil and gas, electronics, sports equipment, electronics and consumer goods, among others. The delightful structures, however, have been reported to exhibit a brittle behavior under mechanical testing hindering commercial opportunities. Extensive research to accurately predict the mechanical behavior of lattice structures and optimize them to achieve their multi-performance objectives has been conducted (Sophie C. Cox, 2015) (A. Butscher, 2011). In the case of metals the brittle behavior is due to α'-martensite, a phase forming due to the high cooling rates observed by the thin walls of the structures. The microstructure seen in Ti-6Al-4V in AM can be evolved depending on characteristics of the phases (J. Lin, 2016) (L. Zeng, 2005). Elastic buckling, plastic collapse, and brittle facture are areas of lattice structures that have been highly researched by computer modeling. However, experimental evaluations have been limited due to complexity of test set up and machine cost, possessing vital pieces to successfully disseminate the triggers of the undesirable characteristics.

Ultimately, this research aims to improve the fabrication of lattice structures and further understand the effects of part processing on the part microstructure and mechanical properties. The results from this thesis aim to help current and future industries of interest be aware of the potential of AM technology, but also to help users be aware of the potential issues leading to part variations and how these issues can be solved.

SUMMARY OF RESULTS

In the studies conducted for this thesis, variation of building conditions and their effect on mechanical properties are summarized. Numerous solid cylindrical geometries involving surrounding parts that were varying in dimensions were fabricated, machined, and tested. Various build locations were also tested to characterize the properties of parts at locations within a single

build. In addition, numerous rhombic dodecahedron lattice structures, with controlled density and size were fabricated and tested.

Build variations for solid cylindrical components was achieved by having a build with no surrounding parts (standard build) and two separate builds with surrounding parts of 5mm diameter and 10 mm diameter, respectively. A statistical difference in mechanical properties such as ultimate tensile strength (UTS), yield strength (YS), and the elastic modulus (E) between each build was not observed. UTS and YS measurements of up to 1021.29 MPa (± 33.24 MPa) and1053.06 MPa (±39.54 MPa) respectively, achieved for parts fabricated with no neighboring parts. Similarly, parts fabricated with neighboring parts of 5 mm and 10 mm diameter produced parts with UTS of 1025.64 MPa (± 17.29 MPa) and 1025.00 MPa (± 6.11 MPa) and YS values of 1053.06 MPa (± 20.83 MPa) and 1053.06 MPa (± 5.71 MPa), respectively. It was important to note that the standard deviation had a noteworthy decrease between the bars without neighboring parts. An increase in the percent elongation property was observed in the flowing order for EBM-fabricated parts: standard build, 5mm, and 10mm diameter with their respective values of 2.37% (±0.92 percentage), 3.02% (± 1.98%), and 4.91% (±1.63percentage). The microstructure displayed was Widmanstäten, with α-lath thickness increasing in the following order: standard build, 5 mm diameter, and 10 mm diameter.

An analysis of build location variations for cylindrical components, was also performed, by fabricating two identical build (labeled as Grid I and Grid II). These experiments provided results that conveyed dissimilar mechanical properties, suggesting the location in which a part is built impacts performance. The averaged values for the YS, UTS and E measured for both grids are summarized as; 1051.37 MPa (± 20.24 MPa), 1066.82 MPa (± 10.69 MPa), and 119.54 GPa (±2.62 GPa), respectively for the parts located in the three back rows. Parts located within the mid-

section of the build platform exhibited the yield strength, ultimate tensile strength and elastic modulus of 1027.65 MPa (± 43.81 MPa), 1046.01 MPa (± 25.81 MPa), and 118.87 GPa (± 3.42 GPa), respectively. For parts located within the front end of the machine the yield strength, ultimate tensile strength and elastic modulus measured 996.29 MPa (± 45 MPa), 1007.77 MPa (± 39.64 MPa), and 116.30 GPa (± 3.99 GPa), respectively. Percent elongation of EBM fabricated parts increased for parts located toward the back of the fabrication chamber. Percent elongation measured up to 3.27% (± 0.81 percentage), 2.98% (±0.77 percentage), and 1.68% (± 0.52 percentage) from the back to the front of the machine, respectively. The results indicate solid EBM-fabricated parts of Ti-6Al-4V exhibit better properties when located further into the chamber relative to the front of the machine in contrast with parts located further towards the front of the chamber, which exhibit the poorest properties.

For lattice structures, it was of interest to compare standardized build parameters with varying currents and number of scans. Lattice structures mechanical properties are greatly influenced by the geometry; therefore, a constant geometry was utilized in the studies to ensure the changes (if any) were not influenced by varying geometry.

The mechanical behavior of the components was investigated by three lower than standard current (15mA) at 1.7mA, 3.4mA, and 8.5mA. In general, it was determined that the mechanical properties exhibited by the standard build were similar to the values exhibited by all the other builds. It is important to note that the results for Young's modulus, ultimate compressive strength (UCS), and measured load at fracture (FL), did not exhibit varyiation as a result of varying beam currents. However, a high sensitivity was observed between the processing currents, relative density and stiffness, and porosity in which the mentioned properties increased with decreasing processing currents in the following order: standard build, 3.4mA, 8.5mA, and 1.7mA. The

opposite was observed for the thickness of the α-thickness, with values of 1.56μm (±0.14), 1.44μm (±0.17), 1.20μm (±0.11), and 1.13μm (±0.10), respectively.

One of the major concerns resulting from fabrication of lattice structures is the appearance of the detrimental brittle α'-martensite phase. Therefore, of interest in this study was to prevent the appearance of the detrimental phase by modification of scan passes increasing in the following order: single, graded, and triple. Comparing a standard fabrication to all the other builds, in general [except for the values for the UCS between standard build and triple scan pass build], there is no statistical difference concerning the mechanical behavior between the standard and all the other builds. In general the values for all the mechanical properties had the same increasing order: standard build, triple, and graded scan pass build. The lattice structures exhibited sensitivity to the high temperatures. The advancement for these components was in the re-engineered microstructure consisting of α'-martensite free for the triple scan pass and vanishing for the graded scan pass. The morphology improved as well, with globular α-phase in the triple scan pass build.

The studies performed, look to advance the metals area of AM with a focus on EBM-fabrication. The results obtain are a foundation to proceed in the correct direction, as the work discards and/or amplifies theories in the field.

THESIS OUTLINE

The chapters in this thesis present the design, experimentation and characterization methodology, and results in detail for the study on effects of fabrication conditions on mechanical properties of Ti-6Al-4V fabricated by powder bed fusion AM. Chapter two covers a literature review of AM, titanium metal, and physical metallurgy of the titanium alloy Ti-6Al-4V. Chapter three describes the mechanical response of building conditions on solid components with

increasing surface area for fabrication. Chapter four describes the mechanical response of building conditions on solid components through part location variations for a single build. Chapter five describes mechanical response of building conditions on lattice components from varying processing current. Chapter six describes mechanical response of building conditions on lattice components by controlling phase transformation through varying melt scans. Results of the basic properties of the engineering material as well as hardness values presented in the results sections of each chapter and the discussion section will provide the reader with an explanation of the impact the methodology used had on the parts in the chapter. Finally, chapter-seven is a final reporting on conclusions and recommendations for EBM users.

CHAPTER 2: LITERATURE REVIEW

ADDITIVE MANUFACTURING

In 2009 the Committee F42 on Additive Manufacturing Technologies was formed as the evolving technology of AM attracted a high level of global interest (Wohlers; 2012) contributing to making it a highly researched area. From its original use for fabrication of scale models from computer-aided design (CAD), AM processes experienced rather quickly improvements in final part outcome, graduating prototypes into physical structures that could be utilized in different applications depending on the material and mechanical properties. Production of difficult geometries by a simplified process established a market in terms of AM development. The layer-by-layer process became a low cost replacement for parts fabricated and utilized as a final concept, annulling the technology from its previously known term of Rapid Prototyping (RP) (Gibson *et al.*, 2010). However, the AM process does not necessarily have to be the fabrication of a final part and implementing post-processing techniques has been widely used to achieve a better end-use product (Gibson *et al.*, 2010). Two decades of organizations and engineers working to advance production and improve the process of AM have pave a new rode of competencies in many industries. The technology offers higher customization possibilities, material optimization, and mechanical properties compatible with traditional engineering, all that made it, very attractive at its beginning. Today industries aware of the capabilities of the products produced by AM are looking into implementing it at some point in their processing line since a more autonomous production can be achieved by eliminating third parties, which also results in a competitive edge and flexibility to the market. Companies have the freedom of locating anywhere, and still achieve mass production while mitigating capital and nearing part cost to its value rather than to the indirect cost as speculated in the *Speculations on the Impacts Additive Manufacturing Will Have*, module

. This only shows that as the technology becomes more understandable the production and application see benefits in different sectors.

AM TECHNOLOGIES

A few decades ago, it was unimaginable to be able to fabricate that which the mind imagined, but today imagination is the limit and 3D printing the reality. The layer-by-layer technology that was invented in the early 1980s is now used by numerous machines that just vary on the way in which the layer is deposited and the material that is used. For example, process categories include, but are not limited to binder jetting (liquid binding of powder materials), material extrusion (material is selectively dispensed through a nozzle), powder bed fusion (thermal energy selectively fusses powder material), sheet lamination (sheets of material are bonded), and vat photopolymerization (pre-deposited photopolymer in a vat is selectively cured by light-activated cross-linking of adjoining polymer).

AM processing of metallic parts is typically done with powder material melted by the use of a direct energy source such as laser or an electron beam. The powder is a very important aspect of the process. The size, shape, and followability of the particles influences the response to the process, hence part behavior with powder bed density preferred because it leads to higher part density. This is best achieved with spherical shape particles of moderate size (small enough to lessen the energy needed for melt and large enough to prevent damage to the system), and characteristics promoting flowability such as low surface roughness and narrow powder shape and size. Some of the most widely AM processing methods in the metals area are EBM, Selective Laser Melting (SLM), Laser Engineered Net Shaping (LENS), and Direct Energy Deposition (DED). The EBM process has been previously described in chapter one. The electron beam energy offers high power density and higher precision scanning (M.F. Zäh, 2010) resulting in significant

improvement in part performance. Via laser energy input methods, powder depositions varies. SLM is a full melting powder bed fusion process with a processing sequence alike that of the EBM, with the difference being the use of a laser for melting in this case, while LENS and DED use multiple powder feeding nozzles to spray the powder into the laser beam. Each technology has demonstrated advantages and disadvantages depending on the material use, presenting options for users.

Polymer processing is done by some of the most widely used AM technologies such as extrusion processes which includes methods such as fused deposition modeling (FDM) and fused filament fabrication (FFF) or photocuring by stereolithography (SL), all which are very similar. For this processes a thin thread like thermoplastic filament is fed to an extruder then by dual heated nozzles it is laid down in layers until part fabrication is completed. The SL process uses a UV laser that traces the first section of the computerized design in a thermosetting polymer resin, the laser is then applied curing it and bonding the layers until the part is completed. These printers provide some of the smallest as well as some of the largest parts in AM.

Ceramic materials are processed by powder binding lamination and extrusion. Via powder, biding the ceramic powder is bonded with the use of a liquid binder. The technologies available for this processing still provide poor surface finish and resolution, consequently post processing is required. Ceramics are found in a wide range of applications in which high hardness is required, this material has been tailored process by AM technologies achieving components well presented for industry.

AM technologies have extended widely capable of processing all types of engineering material. The world is excited for the potential of AM and the benefits it will bring in all sectors as limitations are overcome.

TI-6AL-4V AND ITS ROLE IN AM

The extraordinary combination of properties exhibited by titanium and its alloys have made them highly desirable for a variety of industries. The pure metal named after “Titans” was discovered in 1791 by William Gregor (Trengovem, 1972). The shiny gray, malleable, and ductile metal (Krebs, 2006) exhibits properties between those of aluminum and iron and with a density of 4.5 g cm^{-3} it is heavier than the first but lighter than the latter. Its melting point is high at 1668°C and can reach an elastic modulus of up to 107GPa. An abundant element that has transformed the world is mostly used in its alloyed form, by which the extraordinary properties including; light weight to strength ratio, high corrosion and temperature resistance, are exploited. The alloys are excellent for applications in aerospace, biomedical, and automotive industries among others. Furthermore, as a compound, it is used as pigment, as smoke screen for skywriting, and as an abrasive. However, the cost of making the alloy is high due to the nonconventional processing necessary to adapt the material to the environment it will be utilized in. Nonetheless, the versatility the alloys provide due to the properties they exhibit justify the cost.

The workhorse of industry has been highly research in AM to be able to produces parts of this material as supplementing or supporting to conventional manufactured parts in various industries (B. Dutta, 2015). Conventional manufacturing of Ti-6Al-4V parts include but are not limited to ingot casting or forging, as well as the involvement of multi-axis processes that produce up to an 85% of material waste as well as significant cost and time (S.M. Gaytan, 2009). Previously successful work has shown results are favorable for AM fabricated Ti-6Al-4V parts showing compatibility and in some cases superiority to cast parts. However, microstructure and mechanical properties anisotropy has also been reported, along with various methods to alleviate it; such as modification of process control, part orientation, and thermal monitoring. EBM-

fabricated parts have been highly evaluated for the process acceptance in industries. With this technology process scan parameters can be modified providing microstructure development, studies for processing control have included modification of speed scans in which a preferred microstructure is obtained at slow speed scans $30 \leq 100 \geq 1000$ mm/s. This range gives a coarser grain due to the slower cooling rate which controls the morphology by allowing diffusion of the alpha from the beta grain boundary. It has been shown from studies that the building direction of parts influences the mechanical properties. One of the best forms of verifying results obtained is by knowing where the error is, this approach was undertaken in studies where defected parts were fabricated by varying processing parameters. The studies suggested that via SLM and EBM porosity and voids are governed by energy input in which a fluctuation from a high or low input will result in defect generation for the following reasons but not limited to them; reduction in energy source penetration, decrease in gas flowability, and defected pre-alloyed powder.

As AM graduates into larger production it is important for users to have an idea of the variation if any the product will exhibit; build consistency has been analyzed correlation of mechanical properties and microstructure. Mechanical properties and microstructure anisotropy within a part of Ti-6Al-4V fabricated by AM have been reported previously, as a consequence of cooling rated, part location, and build direction (Beth E. Carroll, 2015) (S. Palanivel, 2016) among others. Previous work has presented the variations within a single part with most showing higher strength at the bottom because of the microstructure consisting mostly of martensitic needles due to the nature of the fabrication process. Also, studies including tensile testing for mechanical properties reporting have shown that the prior-β grins play an important role in ductility elongation rendering higher values in the transverse direction. Lattice components of Ti-6Al-4V have also been studied due to the weight and material optimization the cell shape provides above the already

mentioned advantages an AM part provides. The work on these porous structures has focus on changing the of the detrimental martensitic microstructure exhibited to a more ductile one and the deformation mechanism under compression.

Ti-6Al-4V is processed by the AM method of powder bed fusion, a technology that has proven difficult to monitor and capable of achieving the compromised needed in mechanical properties and design for the titanium alloy.

TI-6AL-4V MICROSTRUCTURE

Pure titanium has a hexagonal close packed (hcp) α-phase at room temperature, that tranforms to a body center cubic (bcc) β-phase at the transus temperature of 882°C (Wei Sha, 2009). Titanium alloys are classified as: α, near α, α + β, meta/stable β- phases dependng on the amount present. The calsification of the alloy can be altered by α or β stabilizers that either increased of decreased the temperature at which phase tranformation occurrs. The "workhorse" of industry, titanium alloy Ti-6Al-4V is α + β phase alloy and the mostly used of all titanium alloys. This is a completely heat treatable alloy that exhibits mechanical properties in between of those of the more brittle α-phase and the more ductile β- phase alloys. The additions of α (aluminum) and β (vanadium) stabilizers promote the high strength to weight ratio that make it so attractive. Also governed by the volume of phases present is the microstructure morphologies exhibited, because it is dependent on thermomechanical processing; working the material, cooling rates, and heat treatments determine the formation of the grain which can appear as lamellar, equiaxed, or bimodal (Gerhard Welsch, 1993). For the Ti-6Al-4V alloy typically a duplex Widmanstätten microstruucutre of α + β forms by a diffusion controlled nucleation and growth process and appears in various morphologies depending on the cooling rate. Under a slow cooling rate thicker α plates in organized α colonies are obtained, while faster cooling rates promote thinner laths with

a basketweved pattern. At very high cooling rates that reach the start of the martensitic temperature (M_S) β is unable to transform and the presence of α'-martensite shows (Jia-Yi Yan, 2016). This needle like hard crystalline structure forms as a diffusionless athermal transformation that inherits the chemical composition of the α-hcp. The martensitic phase exhibits outstanding strength and toughness.

CHAPTER 3: MECHANICAL RESPONSE TO BUILDING CONDITIONS ON SOLID COMPONENTS WITH INCREASING SURFACE AREA FOR FABRICATION

INTRODUCTION

As AM moves forward into large-scale production it is crucial for users to have an understanding of fabrication consistency. Also important for industrial fabrication is the consistency of the process chain therefore the fabrication receipt of interest is the standardized. In an effort to improve, the technology manufacturing scenarios for the adequate material and application were studied. Solid cylindrical Ti-6Al-4V parts with and without neighboring parts were proposed to analyze the features of interest by evaluation of mechanical behavior and microstructure of the EBM fabrication process without systematic changes to scan parameters. To evaluate the mechanical characteristics, tensile testing was performed, while microstructure characterization was done by the use of light optical microscopy (LOM) with corresponding macroindentation measured through Rockwell C-scale (HRC) with a diamond indenter. Furthermore, fractograpgy analysis was performed through the use of scanning electron microscopy (SEM).

EXPERIMENTAL METHODS AND PROCEDURES

For the solid components fabricated for this thesis, the core objective was to determine the effect that surrounding parts have on mechanical properties. Three sets of EBM-fabricated solid cylindrical Ti-6Al-4V samples were examined. Figure 3.1 shows the designs chosen for this study that consisted of Setup 1 (no neighboring parts) that will be refer to as the standard build, Setup 2 (5 mm neighboring cylinder), and Setup 3 (10 mm neighboring cylinder). The design conveys a simple geometry of four 76 mm in height cylinders with increased surface areas by neighboring

cylinders of 5 mm and 10 mm diameters, respectively. The parts were centered within the 210mm x 210mm build platform and built in a vertical orientation; having the axial direction parallel to the build platform. All sets were fabricated with processing parameters available for Ti-6Al-4V of 50-µm layer thickness, which is commercially utilized. The process commenced by elevating the temperature of the building chamber up to 745°C in a vacuumed environment of ~10^{-4}mBar. A preheating scan of 750°C follows to sinter the particles facilitating the melting and preventing thermal shock. Finally, the melt scan is performed at a speed of 500mm/s and a current of 17mA.

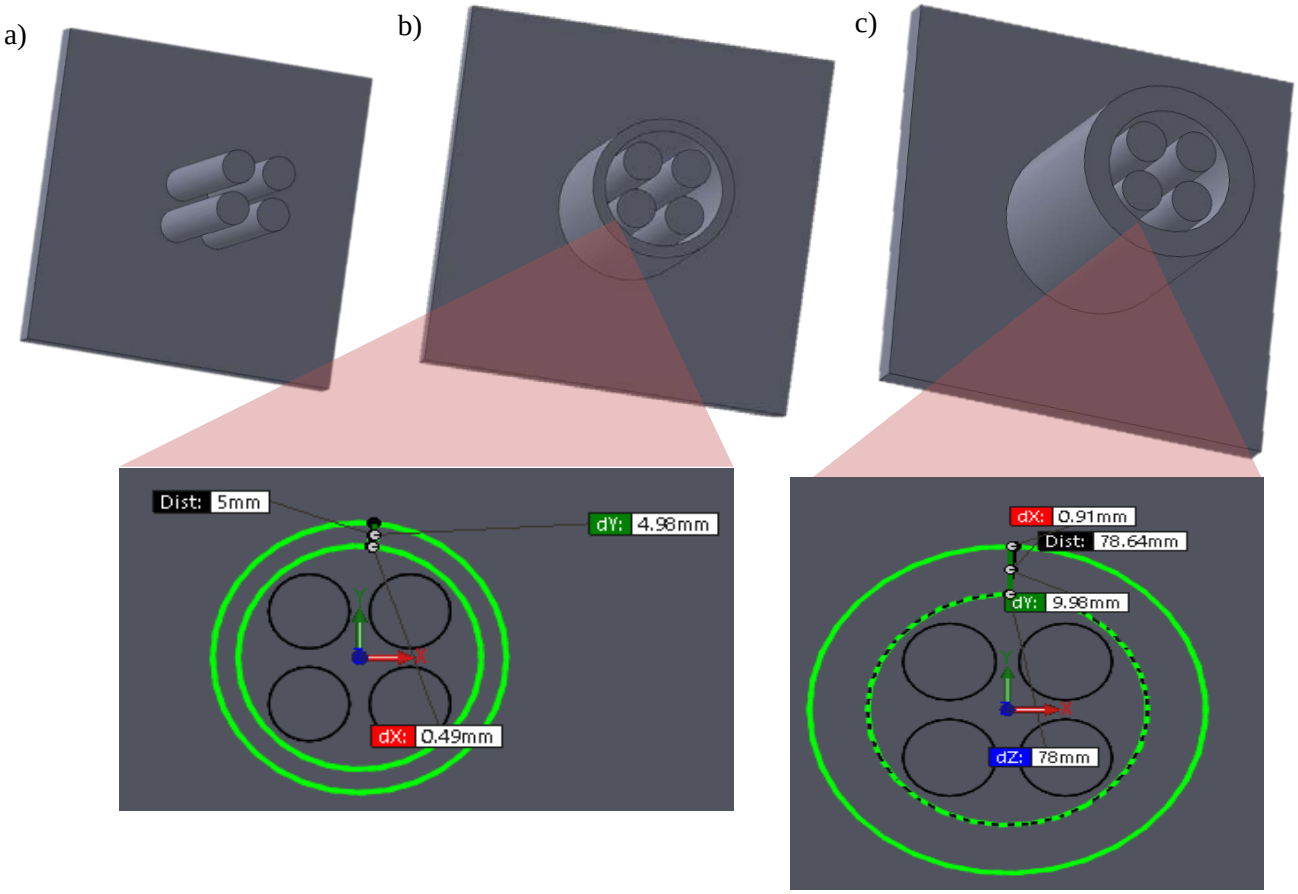

Figure 3.1: (a) Setup 1 (no neighboring parts), (b) Setup 2 (5 mm neighboring cylinder), and (c) Setup 3 (10 mm neighboring cylinder) (specimens fabricated in the longitudinal direction perpendicular to the build platform)

TENSILE TESTING

Tensile testing performed for all the cylinders complied with ASTM standards (ASTM E8M) for conventional processed Ti-6Al-4V. Tensile testing was carried in an MTS Landmark Servohydraulic test system (MTS System Corporation, Eden Prairie, Minnesota) with Series 647 Hydraulic Wedge Grips under axial load-displacement at a stain rate of $2.5 \times 10^{-3}\ s^{-1}$ and conducted at room temperature (25°C). The specimens were positioned at the loading area with the assistance of stainless steel oil-quenched fixtures that adapted to the grips of the machine. These also ensured the samples were in place preventing glitches in the data by human error. An MTS Extensometer (MTS: 634.31F-25) was placed at the gauge length of 30 mm before each test begun to monitor changes in length. An axial warm–up of the system was conducted before the first test of each day with no sample affixed for 600 cycles at a frequency of 1Hz. Figure 3.2 is a schematic of the tensile testing set up in which the blue arrows point towards the stainless steel fixtures, the red arrows indicates the position of the extensometer and the gauge length is indicated by approximate markings within the image.

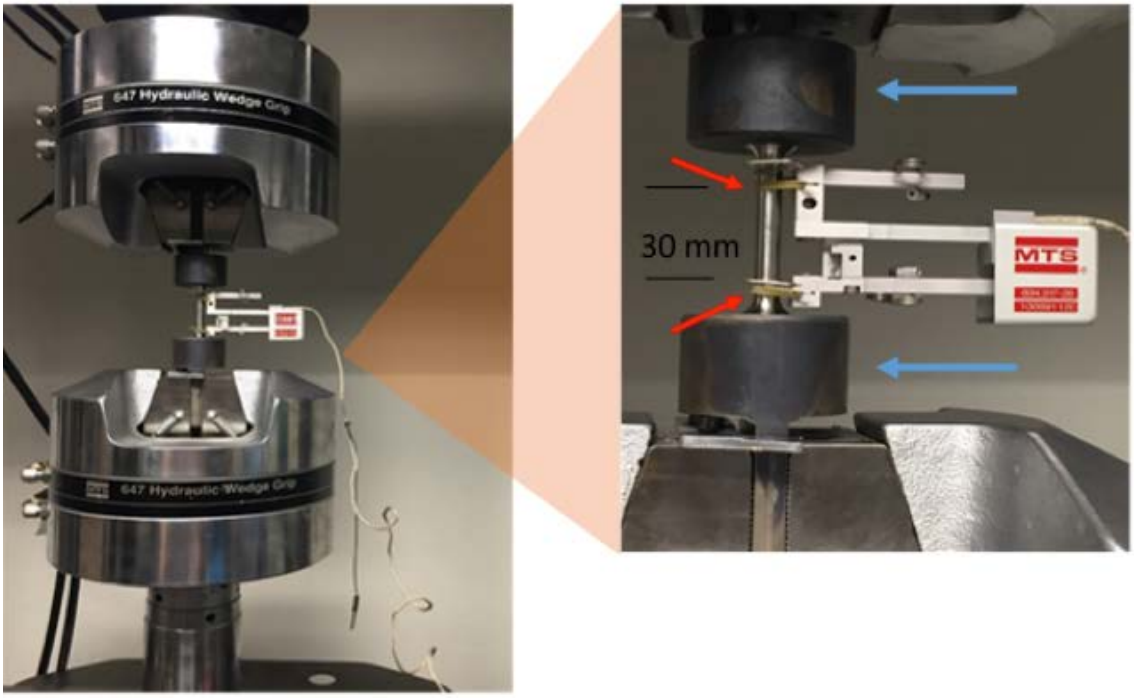

Figure 3.2: Tensile testing set up for Ti-6Al-4V EBM-fabricated with gauge length of 30mm

METALLOGRAPHY AND HARDNESS

Earlier work has focused on microstructural morphology growth influence by parameter variables; however, external modifications like fabrication orientation and geometry also influence morphology and, as such, have not been thoroughly considered. In the present study, microstructural analysis was performed on as-fabricated parts from the standard build, the 5 mm diameter build, as well as from the 10 mm diameter. The specimens were prepared by sectioning perpendicular to the build direction axis ~5mm from the top followed by a middle section cut using a Buehler IsoMet 4000 Linear Precision Saw (Buehler, Lake Bluff Illinois). The sectioned samples were then mounted using a 2:1 ratio of Koldmount acrylic resin powder (Nobilium, Albany, New York) and curing resin. Figure 3.3 shows an as-fabricated cylinder and a mounted sample. It is

important to note that the 5mm and 10mm diameter cylinders where also subjected to metallography analysis. These samples were not cut or mounted due to their size, properties, and the extensive amount of time each sample would take, which presented limitations to the equipment available. However, this should not be a factor considered to compromise data. The sample's surface was ground using silicon carbide paper of different grits while rotating 90° two times [clockwise or counterclockwise, depending on the previous rotation] in each grid to remove unwanted material. The process started with coarse grits of 80,120,130,220 and 320, followed by finer grits of 500, 600, 800, 1000 and 1200. Further on, diamond polishing of samples using monocrystalline paste of 9µ, 3µ, and 1µ with their respective cloth were used to polish the surfaces as a means to achieve a mirror like finish. The microstructure appeared visible under the LOM after etching, which was done by submerging the samples for 3-5 seconds in Kroll's reagent and rinsing them afterwards with water and ethanol to prevent stains on the surface. The Kroll's aqueous solution contained 2.5 ml hydrofluoric acid, 5ml nitric acid, and 100ml of water, which is one of the oldest and most commonly used for titanium alloys, having the alpha phase enhance and responsive to the polarized light and the beta phase exhibit in dark (Voort., 1999. Ti-6Al-4V EBM-fabricated specimens analyzed in a digital imagining Reichert MEF4 A/M optical microscope (Reichert, Inc., Depew, New York) displayed the typical Widmanstätten morphology.

The prepared metallography surfaces were subjected to Rockwell hardness measurements using Wilson Rockwell Series 2000 (Buehler, Lake Bluff, Illinois) with a C scale indenter. The samples were subjected to minimum of 10 indentations each and the results averaged for reporting.

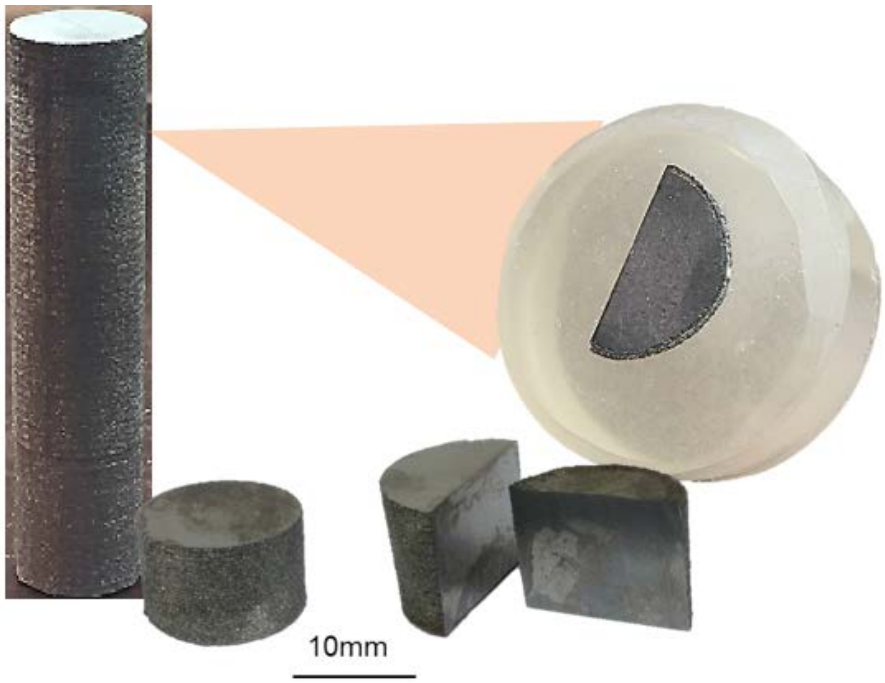

Figure 3.2: As-fabricated cylinder used for metallographic analysis and mounted cut sample

FRACTOGRAPHY

Physical characteristics such as fracture mode are often used for further correlation of design with mechanical properties. In this study, fractrography analysis was performed on the fractured surfaces of the tested tensile specimens. The specimens were prepared by sectioning 5mm below the fractured surface, the cut was made using a Buehler IsoMet 4000 Linear Precision Saw (Buehler, Lake Bluff Illinois) and the specimens were then ultra-sonicated in an ethanol bath for 10 minutes to remove debris. Figure 3.4 shows the sectioned fracture surface utilized for the analysis. The prepared surface was attached to an examination platform using conductive carbon tape, and was observed in a Hitachi S4800 (Hitachi High Technologies America, Inc., Schaumburg, Illinois) field-emission scanning electron microscope (FESEM).

Figure 3.4: Fractured tensile tested sample and sectioned sample used for fractography analysis

RESULTS AND DISCUSSION

TENSILE TESTING

To assess the effect of design variations on mechanical properties, tensile testing was performed on three samples of the standard build, 5 mm diameter-neighboring cylinder, and 10 mm diameter-neighboring cylinder. The report obtained directly from the MTS machine was read through MATLAB software which then provided values for the basic engineering properties of UTS, YS, E, and percent elongation.

The machine recorded load and displacement and the report used to calculate engineering tensile testing stress by the equation:

$$\sigma = \frac{F}{A_o}$$

were F is the instantaneous load applied, and A_o is the specimens original cross sectional area, for this study averaging 26 mm^2, and σ is the engineering stress The enginnering strain was defined according to

$$\epsilon = \frac{l_i - l_o}{l_o} = \frac{\Delta l}{l_o}$$

in which l_o is the original length and l_i is the instantaneous length calculated (William D. Callister, Fundamentals of Materials Science and Engineeing: An Integrated Approach, 2012). In the case of this study, l_o is the gauge length of 30-mm. Engineering stress vs. engineering strain graphs plotted for each sample tensile tested are presented in APPENDIX A. Mechanical properties such as ultimate tensile strength, yield strength at 0.2% off set, elastic modulus, and percent elongation at break are reported here.

A student's t-test was performed to determine the significance of the difference between the tensile tests results from the standard build versus the results from all the other builds. According to equation:

$$t = \frac{\tilde{x}_1 - \tilde{x}_2}{\sqrt{\frac{s_1^2}{n_1} + \frac{s_2^2}{n_2}}}$$

where $\tilde{x}_1$ and $\tilde{x}_2$ are the means of the two samples, and $\frac{s_1^2}{n_1}$ and $\frac{s_2^2}{n_2}$ are the variance of the difference between the two samples, and t is the ratio of the difference between the two means and the standard error (Ravindranath, 1981). From the student's t-test a t-statistic value is calculated with

a significance level of α=0.05 (5%). A critical P-value was then determined from a table and from that the probability of the null hypothesis (the starting point) being either accepted or rejected is determined with a 95% confidence interval. Anything below the critical P-value rejects the null hypothesis while anything above the critical P-value will accept the null hypothesis, that is, there is no difference statistically between the two samples. For this study, the student's t-test that was performed was under the conditions of: two-sample assuming unequal variances, due to the inter-build processing variables.

The average results for Ti-6Al-4V EBM-fabricated mechanical properties obtained from these experiments showed, in general, there is no variability between the standard build and all the other builds regarding the mechanical properties investigated. Figure 3.5 and Table 3.1 show the results for UTS between Setup 1 (no shell), Setup 2 (5 mm neighboring cylinder), and Setup 3 (10 mm neighboring cylinder). The intrinsic property exhibited a considerable increase from standard build to the other two builds. This can be attributed to grain growth as consequence of the additional thermal energy input due to the neighboring parts influencing the sensitivity of the part to microstructural change. In the case of the YS, it was determined that there was no difference between the standard build and all other builds, however a significant improvement in standard deviation was observed from the standard to Setup 3, shown in Figure 3.6 and Table 3.2. The Young's modulus reported, showed constant values and an overall equal standard deviation, these are illustrated in Figure 3.7 and Table 3.3. Samples were marginally similar in terms of size and chemical content, the results were expected. Even though, no notorious differences were observed in most of the mechanical properties between the standard build and Setup 2 and Setup 3, the results obtained for percent elongation showed a discontinuity between builds with and without neighboring parts. The proportional increase in percent elongation with the addition of surrounding

parts was very prominent with 27% and 107% from Setup 1 to Setup 2, and Setup 3, respectively. The elastic behavior correlates with coarser grains observed with the higher energy input. The results are reported in Figure 3.8 and Table 3.4.

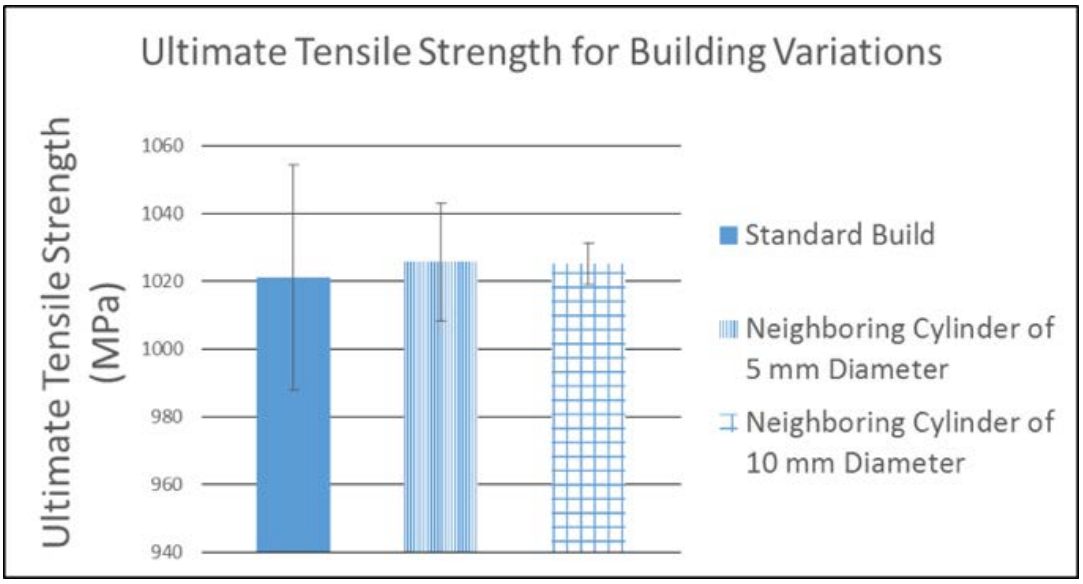

Figure 3.5: Ultimate Tensile Strength results in MPa for each build

Table 3.1: Ultimate Tensile Strength in MPa comparing standard build to each build. P-value for standard build versus

Build	Ultimate Tensile Strength (MPa) S.D.	P Value (Versus the standard build)
Standard Build	1021.29 33.24	-
5mm Neighboring Cylinder	1025.64 17.29	0.87
10mm Neighboring Cylinder	1025.00 6.11	0.88

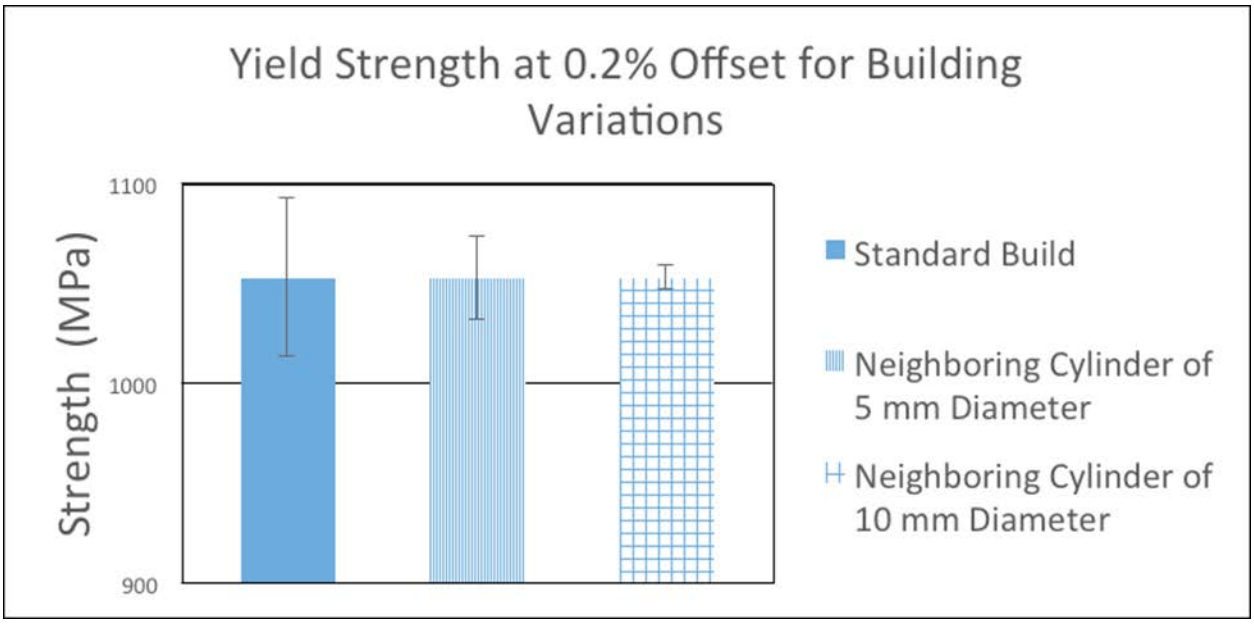

Figure 3.6: Yield Strength at 0.2% Offset results in MPa for each build

Table 3.2: Yield Strength at 0.2% Offset in MPa comparing standard build to each build. P-value for standard build versus

Build	0.2% Yield Strength (MPa) S.D.	P Value (Versus the standard build)
Standard Build	1053.06 39.54	-
5mm Neighboring Cylinder	1053.06 20.83	0.95
10mm Neighboring Cylinder	1053.06 5.71	0.97

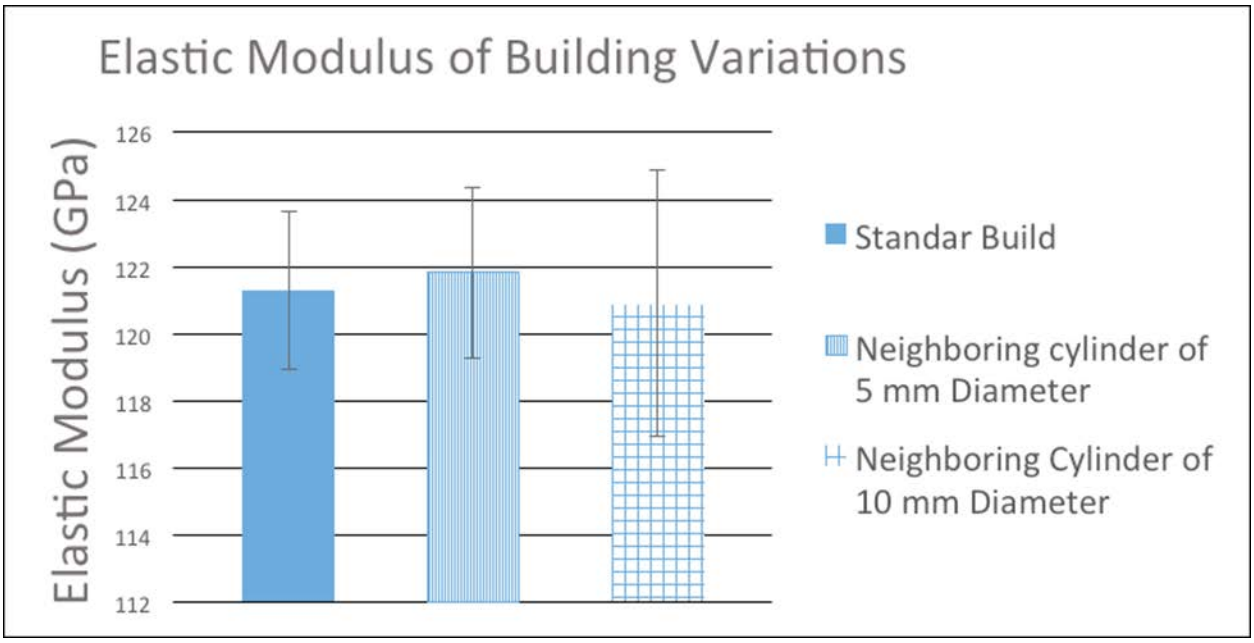

Figure 3.7: Elastic Modulus in GPa for each build

Table 3.3: Elastic Modulus of Elasticity in GPa comparing standard build to each build. P-value for standard build versus

Build	Elastic Modulus (GPa) S.D.	P Value (Versus the standard build)
Standard Build	121.29 2.35	-
5mm Neighboring Cylinder	121.83 2.53	0.84
10mm Neighboring Cylinder	120.88 3.96	0.91

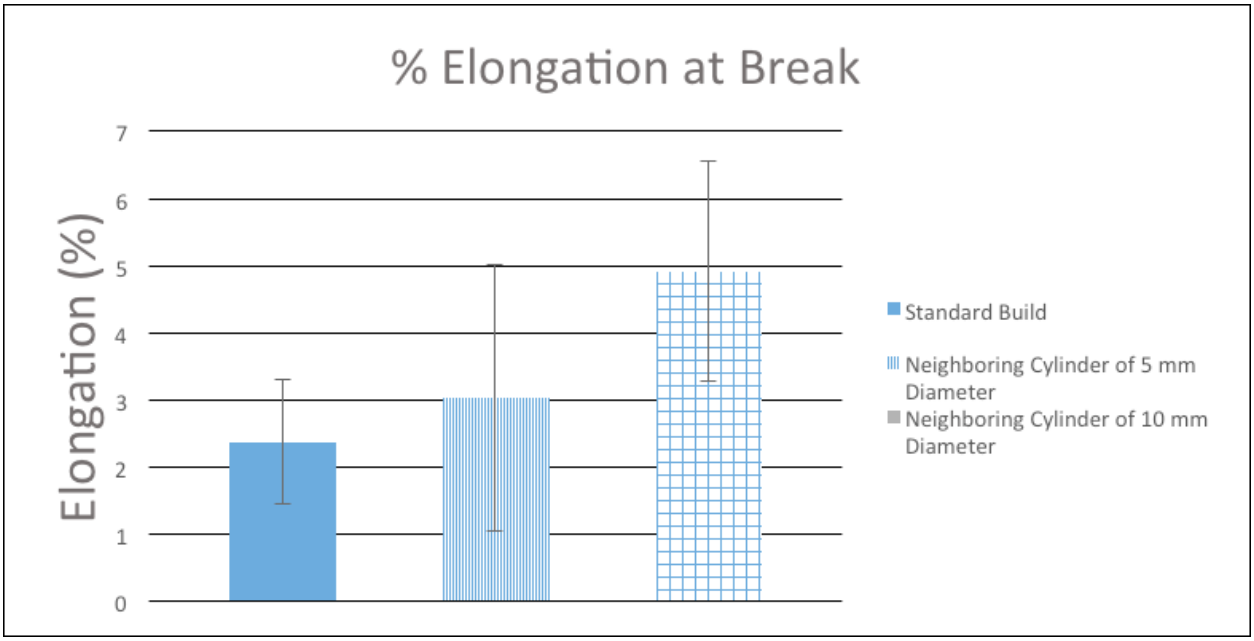

Figure 3.8: Percent Elongation at Break in % for each build

Table 3.4: Percent Elongation in % comparing standard build to each build. P-value for standard build versus

Build	Percent Elongation at Break (%) S.D.	P Value (Versus the standard build)
Standard Build	2.37 0.92	-
5mm Neighboring Cylinder	3.02 1.95	0.70
10mm Neighboring Cylinder	4.91 1.63	0.15

METALLOGRAPHY AND HARDNESS ANALYSIS

Figure 3.9 illustrates the microstructures obtained from each build. The transverse and longitudinal microstructures presented convey similarities to one another. Observing that all samples exhibited a Widmanstätten microstructure, the difference between builds was investigated by analyzing the morphology of the grains observed. The α lath width and hardness values were obtained, given that hardness of the metal also depends on the grain size, i.e. a smaller grain size will convey a greater hardness value (Hemann, 2011).

Previous work reported the observed miscrostructure consitng of a β matrix (dark) with a secondary α lamellae phase (light) growth from β (L.E Murr, 2009). The α lath widths were measured through MATLAB sofware by converting the colored images into a binary image file as illustated in Figure 3.10. Figure 3.11 and Table 3.5 show the resuls for the α widths. D.He, 2012 have reported α lath thickness of 3-5 μm on near alpha titanium alloys conventionally process displaying α lamellae, which lie in close promiximity to the meassured values of this study for the β-α titanium alloy that is EBM-fabricated. The microstructure displayed by the 39% increased surface area was more of an acicular α. The builds with the 43% increased surface area and 39% increasedsurface area had coarser grains, while the standard build refelcted finer grains. There was a 30% and 35% increase in α-lath witdth from the standard to the 5 mm neighboring cylinder, and 10 mm neighboring cylinder, respectively.

The microstructures obtained for the standard build, 39% increased surface area, and 43% increased surface area correspond to the Rockwell (HRC) values of 38 HRC (± 0.78), 37 HRC (± 0.27), and 36 HRC (±0.66), respectively. The findings are inversely proportional with grain size correlating with the previous stament, attributing higher hardness values to finer grains.

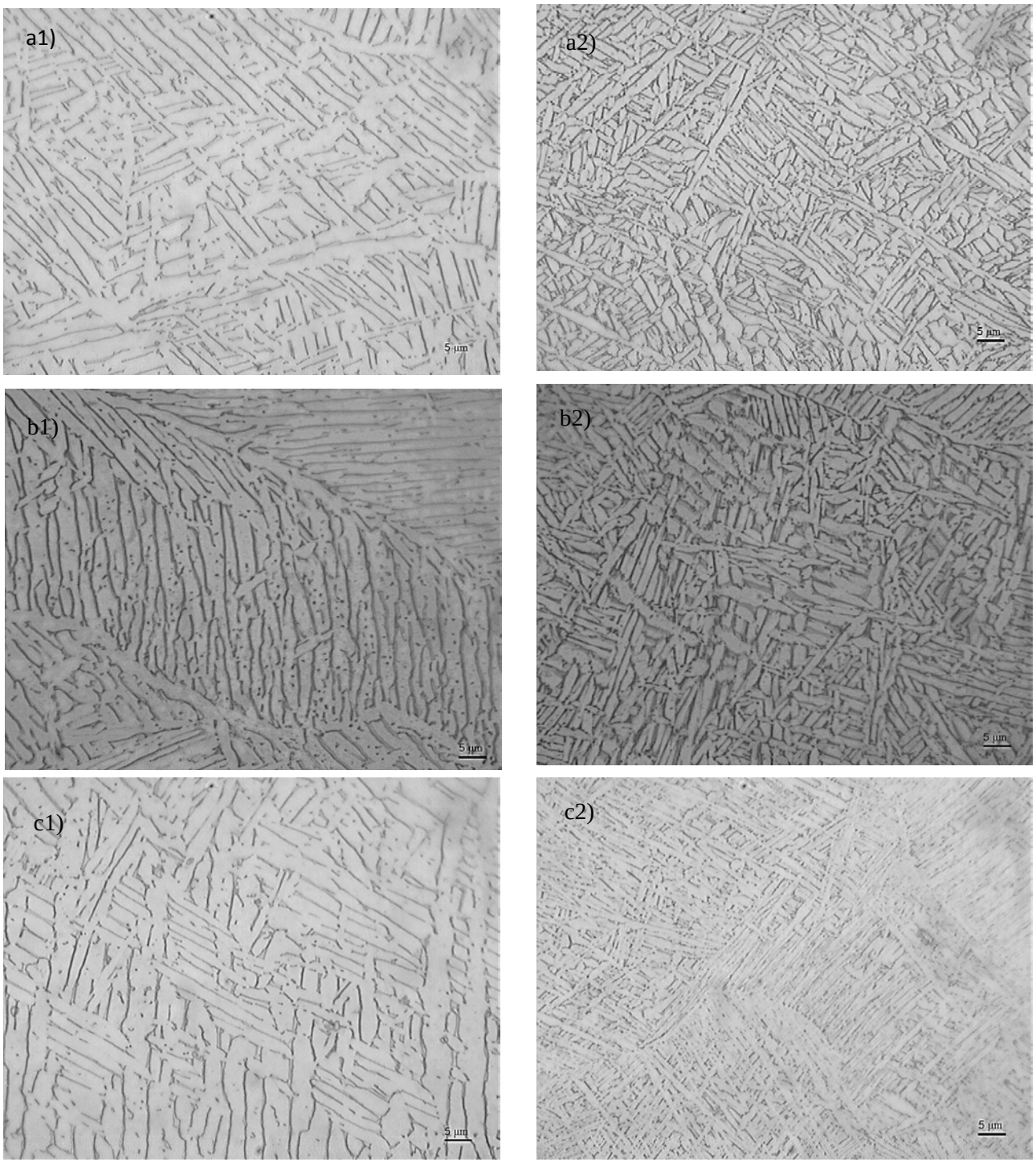

Figure 3.9:Longitudinal microstructures: a1) standard build b1) 5mm neighboring cylinder c1) 10 mm neighboring cylinder. Transverse microstructures a2) standard build b2)

5mm neighboring cylinder c2) 10mm neighboring cylinder

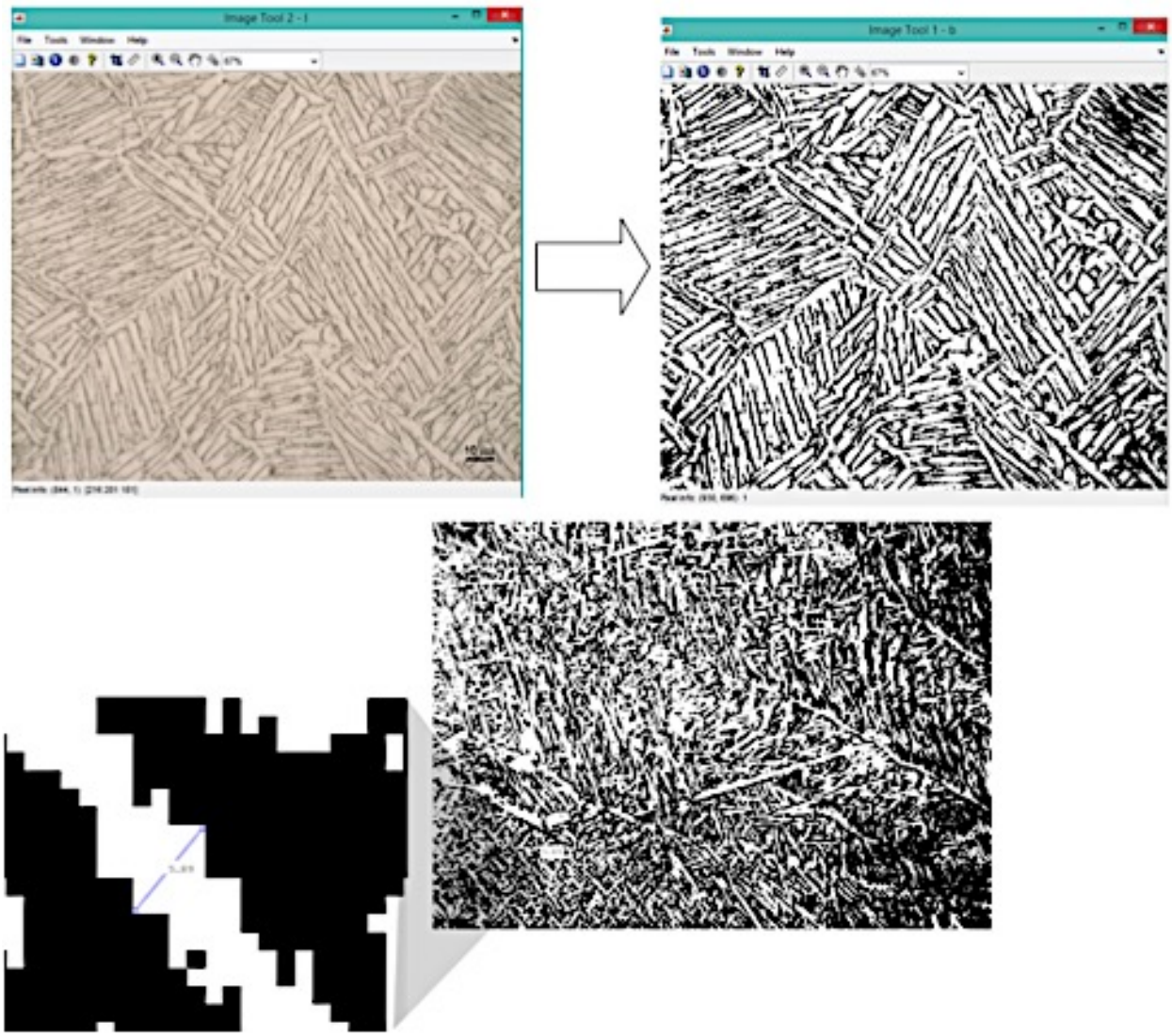

Figure 3.10: Microstructure image read by MATLAB. Microstructure image converted to a binary image and magnification of α lath measurement

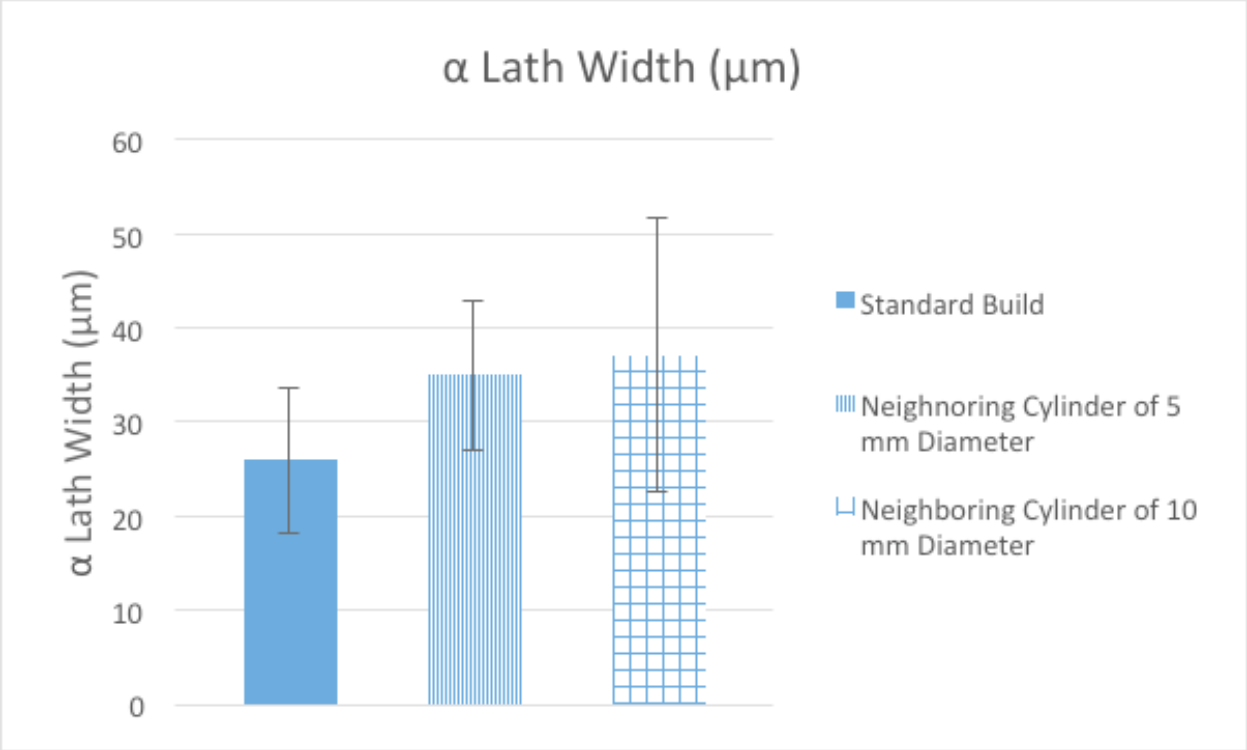

Figure 3.11: α lath width in μm for each build

Table 3.5: Comparing α lath width in μm for each build

Build	α-Lath width (μm) S.D.
Standard Build	2.46 7.63
5mm Neighboring Cylinder	3.37 3.37
10mm Neighboring Cylinder	3.5 14.48

FRACTOGRAPHY ANALYSIS

The surfaces observed in the SEM reflected a dominance of dimples, which are representative of ductile fractures. For these types of fractures, crack formation occurs by microvoid formation as the material is streesed and crack propagation is through dimple coalences. Figures 3.12 (a) is an overall image of the fractured samples displaying high magnification SEM images of Figs.3.12 (b), (c) and (d) and Figs.3.12 (b.1), (c.1), and (d.1). It is important to note that all samples tested in this study displayed a similar fracture surface, therefore the SEM images presented here are of one representative sample for each build. The material achieved extensive deformation before fracture, which can be observed in the engineering stress vs engineering strain graphs in APPENDIX A. Also, the sherically shaped voids reflect the tensile stress that the material was subjected to. The ductile fracture mode was reinforced by the cup and cone shaped morphology that the specimens displayed in Figure 3.4.

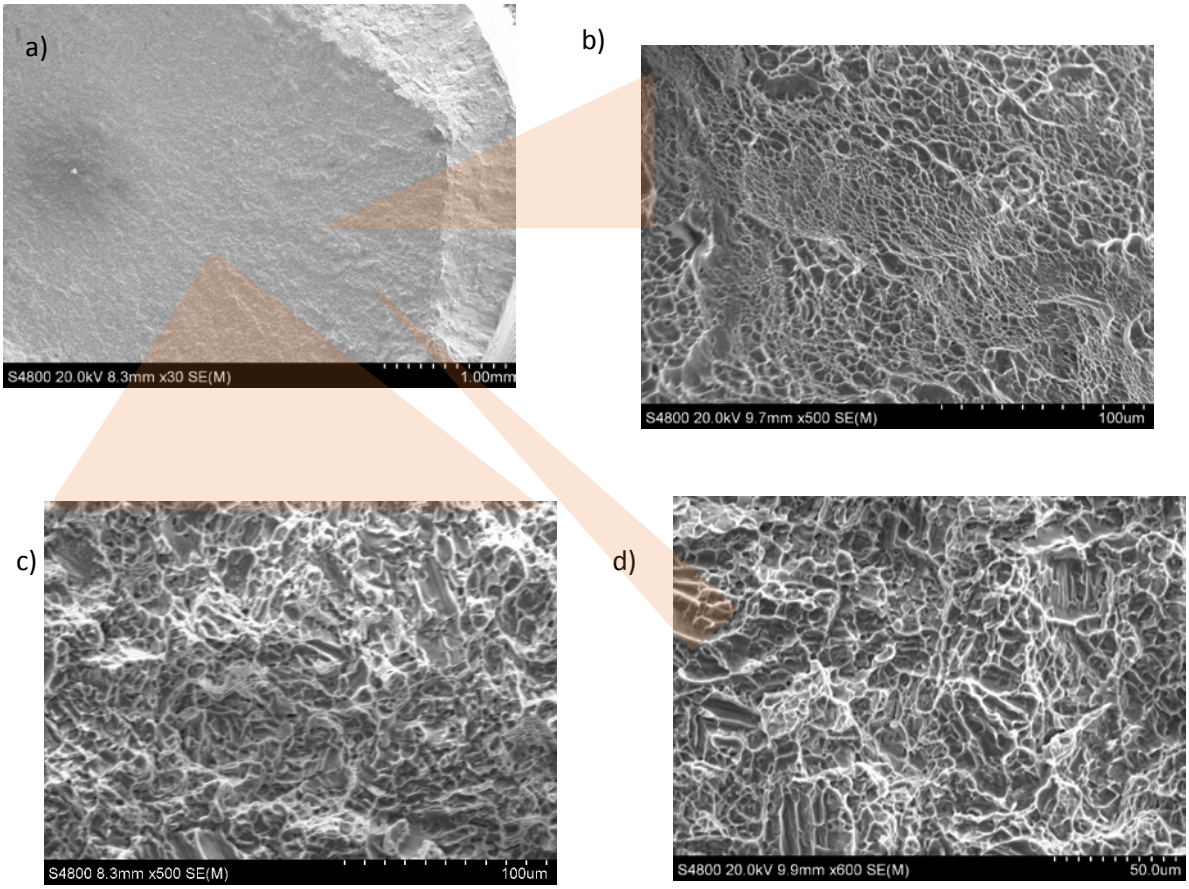

Figure 3.12: a) Low magnification SEM image of fracture surface observed in all builds. a) standard build fracture surface c) build with 5 mm neighboring cylinder fracture surface e) build with 10 mm neighboring cylinder fracture surface

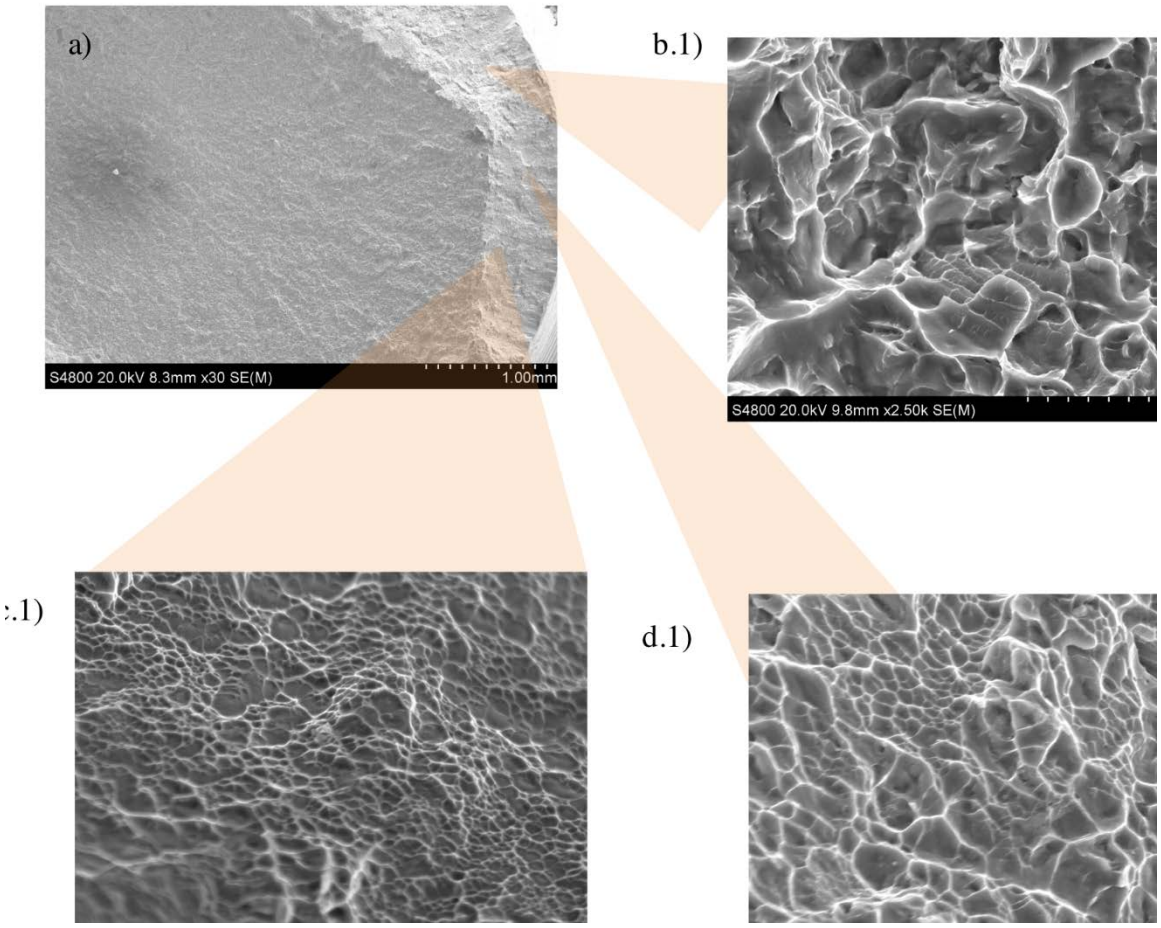

Figure 3.12: a) Low magnification SEM image of fracture surface observed in all builds.

b.1)standard build fracture surface c.1) build with fracture surface d.1) build with r

fracture surface

CONCLUSIONS

Mechanical response to building conditions on solid components with neighboring parts were studied through mechanical testing as well as through microstructure and fracture surface analysis. In this study, the principle was to compare the standard build to all other builds through tensile testing and microstructure. Base on the findings, the following conclusions can be drawn:

- The mechanical properties from builds containing neighboring parts are not statistically different from builds with no neighboring parts. This was determined at a 95% confidence level after performing students t-test in which the P-values obtained were below the significant level used of 5%, therefore the null hypothesis could not be rejected, meaning there was not enough evidence to suggest a difference between the builds.
- Microstructures of EBM-fabricated parts are governed by the thermal environment during part fabrication. Literature has descried layer deposition acts as heat sink and with an increased in surface area as in the case presented in this study the excess energy retained and experience by all the parts provided vital source for the promotion for nucleation and growth. As a consequence the 43% increase surface area build displayed the largest increase in α-lath.
- The results obtained for tensile ductility, showed that the parts fabricated with neighboring parts sustained a higher elongation prior to fracture.

Ti-6Al-4V is a material of much interest to various industries for the combination of good properties and adequate weight. It is important for AM process to be able to achieve the optimum properties for this material. Also, of importance for the AM is to have part repeatability in all aspects. The results for these studies show an improvement on part repeatability.

CHAPTER 4: MECHANICAL RESPONSE OF BUILDING CONDITIONS ON SOLID COMPONENTS THROUGH PART LOCATION VARIATIONS FOR A SINGLE BUILD

INTRODUCTION

AM presence in companies has seen a rapid increase and the future projects a further expansion along with introduction into new markets. The technology is still being explored to develop it to its full potential and improve the existing productions. This study looks to contribute to the area of understanding processing mechanical properties to part location within the EBM machine. To accomplish this, solid cylindrical Ti-6Al-4V parts were proposed to evaluate spatial distribution within a build by the AM process of EBM through mechanical behavior. Previous work conducted in understanding the effects of processing on mechanical properties and microstructure has indicated there is no systematic effect of distance on tensile properties or α lath thickness (Nikolas Hrabe, 2013). For this study, two identical builds labeled as Grid I and Grid II were fabricated with no systematic changes of EBM scan parameters. Tensile testing was performed for mechanical property evaluation and the fracture surface was analyzed through scanning electron microscopy (SEM). In general, an increase in YS, UTS and E was observed for parts towards the back of the machine, with respect to the front of the machine. Percent elongation decreased from the back to the front of the machine. The nature of the EBM process has presented a challenge to disseminate analysis results that are repeatable even under standard receipts, highlighting the focus need on application knowledge to achieve a complete acceptance and beneficiate from the advantages of metal processing technologies like EBM. The results for this study were substantiated by the fabrication of two builds of the same set up.

EXPERIMENTAL METHODS AND PROCEDURES

Of interest for this study was to identify if part location within a build area affects the mechanical properties of EBM-fabricated parts. Two identical builds labeled as Grid I and Grid II were EBM-fabricated in a vertical orientation; having the longitudinal direction perpendicular to the build platform. Previous works have reported a decrease in %EL for vertically built parts, due to the tensile axis with respect to the direction of the elongated prior-β grains and microstructural texture and no difference for UTS or YS (Nikolas Hrabe, 2013). The design consisted of nine 76 mm in height and 10 mm in diameter cylinders evenly distributed throughout the 210mm x 210mm build platform, Figure 4.1. Both builds were fabricated under processing parameters available for Ti-6Al-4V of 50-μm layer thickness commercially utilized. The process commenced by elevating the temperature of the building chamber up to 745°C in an inert environment of ~10^{-4}mBar. A preheating scan of 750°C follows to sinter the particles facilitating the melting and preventing thermal shock. Finally, the melt scan is performed at a speed of 500mm/s and a current of 17mA. The mechanical properties were evaluated by tensile testing the nine parts of each grid. The evaluation extended to determine the fracture mode of the specimens by performing fractrography analysis. In general, the values obtained continue to favor EBM application in industry; however, it was also determined that the location in which a part is fabricated impacts mechanical performance.

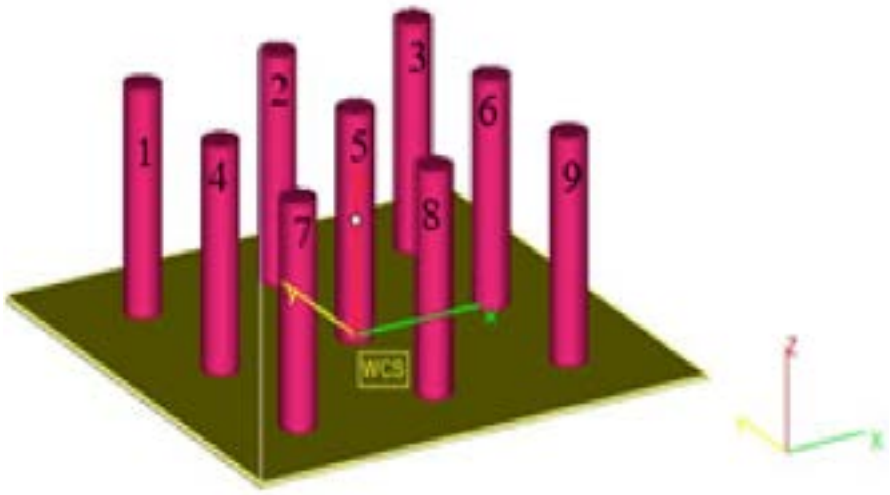

Figure 4.1: CAD model for Grid I and Grid II

TENSILE TESTING

The tensile testing performed was under the same parameters described previously in Chapter 3.

RESULTS AND DISCUSSION
TENSILE TESTING

The methodology for the results of the mechanical properties obtained from the tensile test performed was previously described in Chapter 3. Mechanical properties such as ultimate tensile strength, yield strength at 0.2% off set, and percent elongation at break are reported here. Part location variation within a single build by EBM, in general showed an increased in properties from the front to the back of the building chamber, relative to the front of the machine.

These results were shown by both Grid I and II, which suggest repeatability of mechanical behavior is completely achievable even with environmental changes from one setup to another. Mechanical properties results obtained from each build location are summarized as follows. Figure 4.2 and

Figure 4.3 show the results for UTS for Grid I, and II, respectively. The UTS values for both builds are presented in Table 4.1. The results showed, in general, that parts would be capable of withstanding a load ≥10kN. The extrinsic property of strength is responsive to the characteristics that develop under thermal energy; this is illustrated by the results obtained for YS, shown in Figure 4.4 and Figure 4.5 and Table 4.2 for Grid I and Grid II, respectively. Parts located towards the back of the machine where higher temperatures are seen reflect lesser flaws and optimum characteristic that yielded the highest values for the studies performed. In contrast, Young's Modulus did not present a pattern for property variability as consequence of part location. Figure 4.6 and Figure 4.7 and Table 4.3 show E results for Grid I and II, respectively in which the values range was 110 – 128 GPa. The percent elongation improved considerably from the front of the machine to the back as a consequence of the higher temperatures the parts in these locations were exposed too. Figure 4.8, 4.9 and Table 4.4 show the results for Grid I and II, respectively. Note* figures are presented at different angles to provide a view of each value. Note* figures are presented at different angles to provide a view of each value.

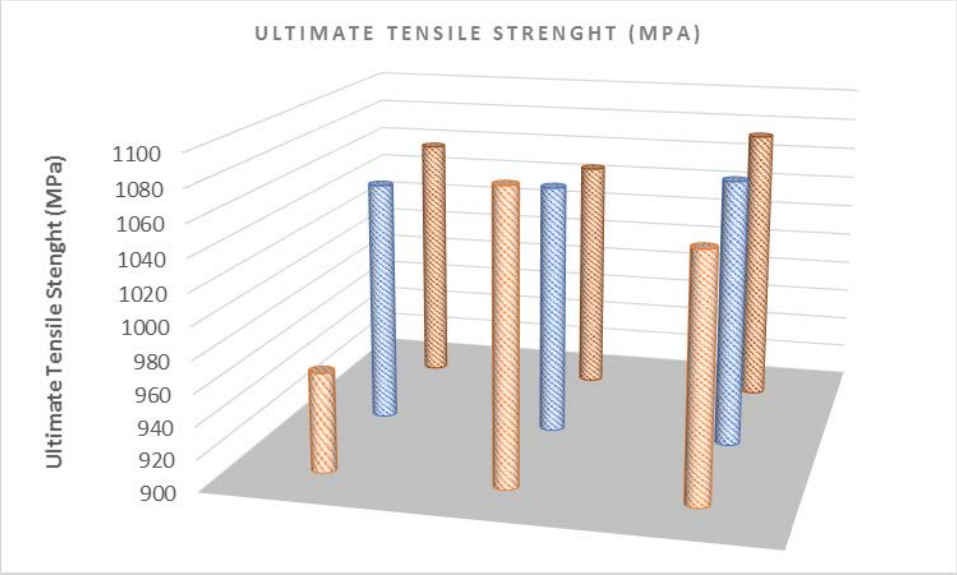

Figure 4.2: Ultimate Tensile Strength results in MPa for each cylinder in Grid I

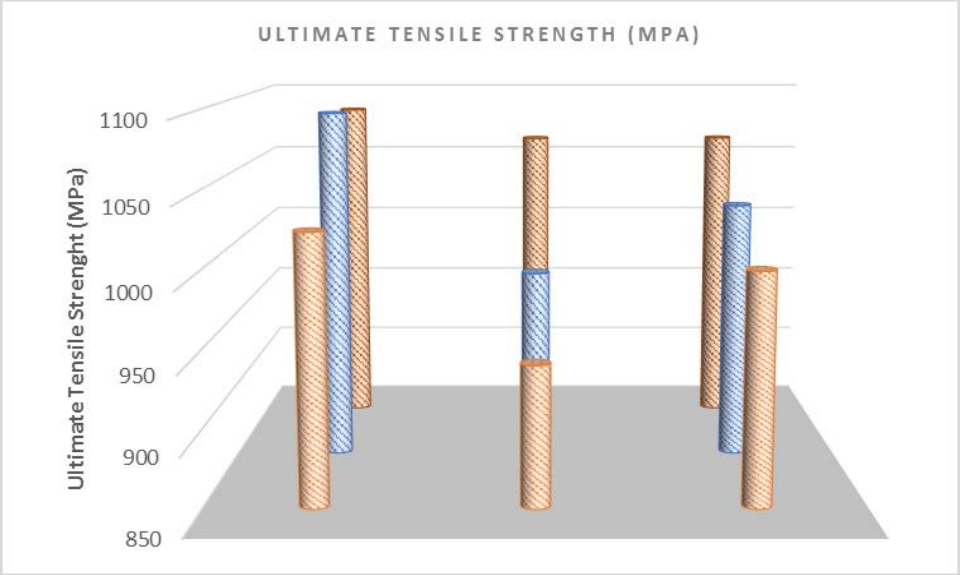

Figure 4.3: Ultimate Tensile Strength results in MPa for each cylinder in Grid II

Table 4.1: Comparing ultimate tensile strength in MPa of each cylinder in each location for Grid I and II

Build	UTS (MPa) Grid I	UTS (MPa) Grid II	S.D.
Cylinder 1	1059.10	1085.77	12.84
Cylinder 2	1049.06	1062.81	6.88
Cylinder 3	1075.98	1063.19	6.40
Cylinder 4	1053.39	1090.97	18.76
Cylinder 5	1057.75	979.37	39.19
Cylinder 6	1067.50	1027.05	20.23
Cylinder 7	962.36	1006.29	21.97
Cylinder 8	1080.83	943.19	68.82

Cylinder 9	1051.27	1002.69	24.29

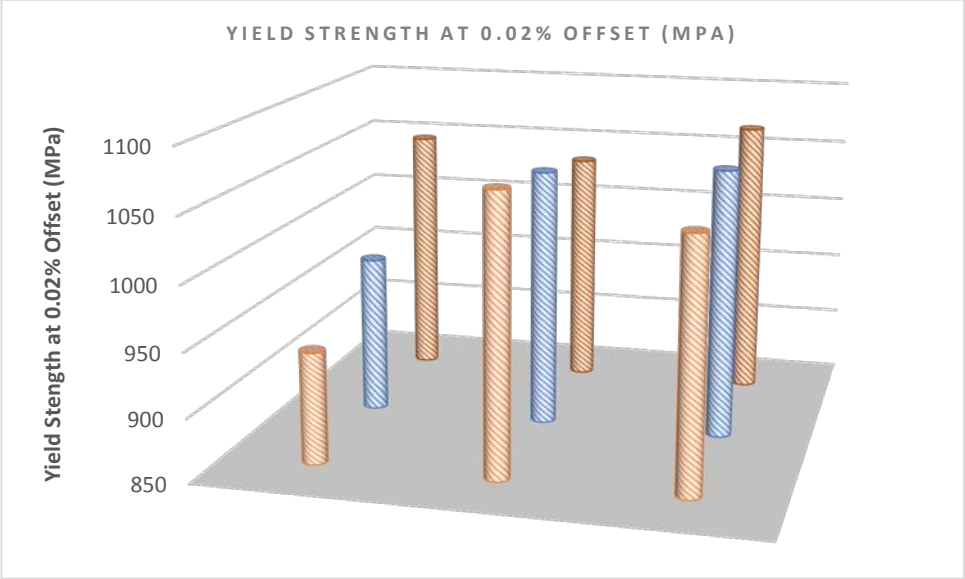

Figure 4.4: Yield Strength at 0.02% offset in MPa for each cylinder in Grid I

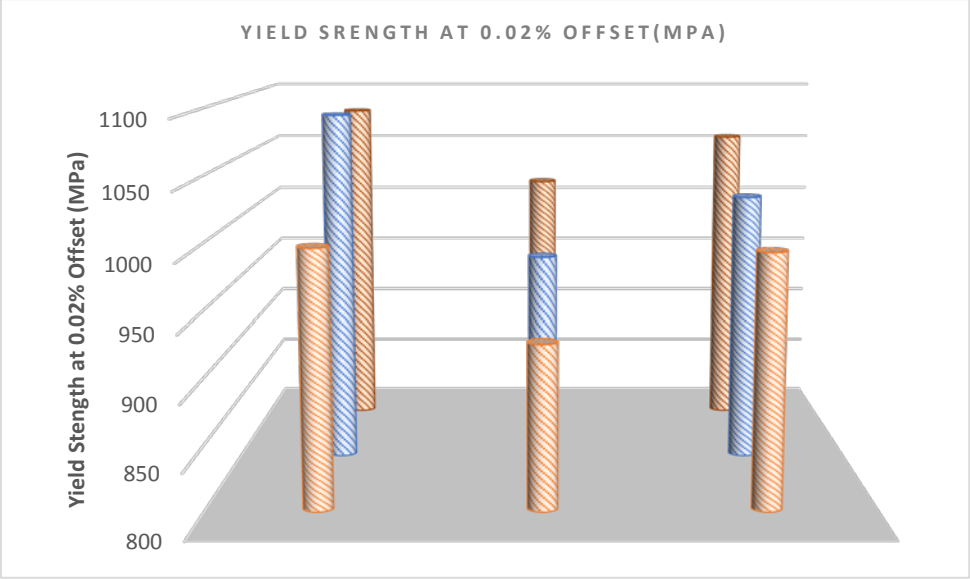

Figure 4.5: Yield Strength at 0.02% offset in MPa for each cylinder in Grid II

Table 4.2: Comparing ultimate tensile strength in MPa of each cylinder in each location for Grid I and II

Build	0.02% YS (MPa) Grid I	0.02% YS (MPa) Grid II	S.D.
Cylinder 1	1049.53	1079.99	15.23
Cylinder 2	1036.95	1015.24	10.86
Cylinder 3	1070.25	1056.26	6.99
Cylinder 4	974.53	1086.91	56.19
Cylinder 5	1053.63	969.36	45.13
Cylinder 6	1062.20	1019.28	21.46
Cylinder 7	937.51	1000.53	31.51
Cylinder 8	1068.19	928.91	69.64
Cylinder 9	1045.24	997.37	23.93

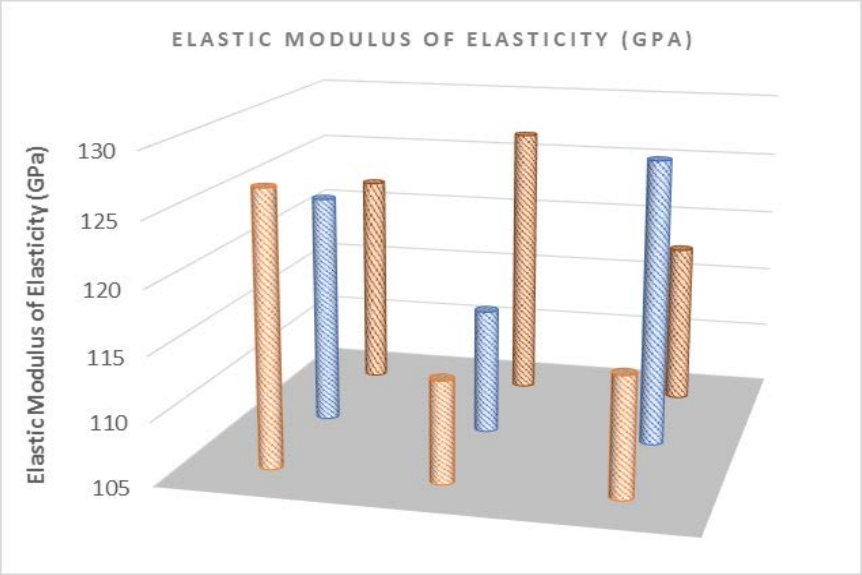

Figure 4.6: Elastic Modulus in GPa for each cylinder in Grid I

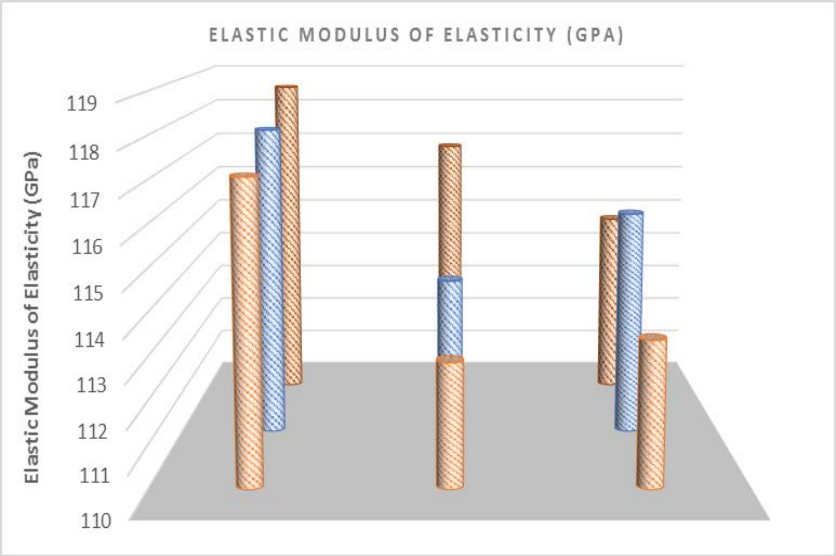

Figure 4.7: Elastic Modulus of Elasticity in GPa for each cylinder in Grid II

Table 4.3: Comparing Elastic Modulus of Elasticity in GPa of each cylinder in each location for Grid I and II

Build	Elastic Modulus (GPa) Grid I	Elastic Modulus (GPa) Grid II	S.D.
Cylinder 1	122.22	118.55	1.84
Cylinder 2	126.93	116.89	5.02
Cylinder 3	117.84	114.82	1.51
Cylinder 4	123.29	117.79	2.75
Cylinder 5	114.91	113.94	0.49
Cylinder 6	127.58	115.67	5.96
Cylinder 7	126.62	117.19	4.71
Cylinder 8	113.03	112.98	0.02
Cylinder 9	114.45	113.49	0.48

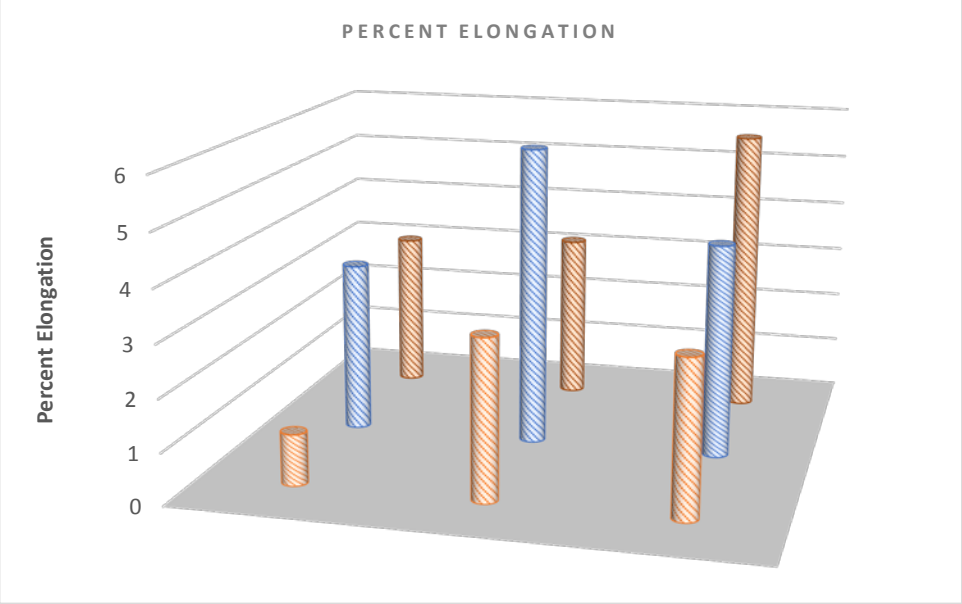

Figure 4.8: Percent Elongation for each cylinder in Grid I

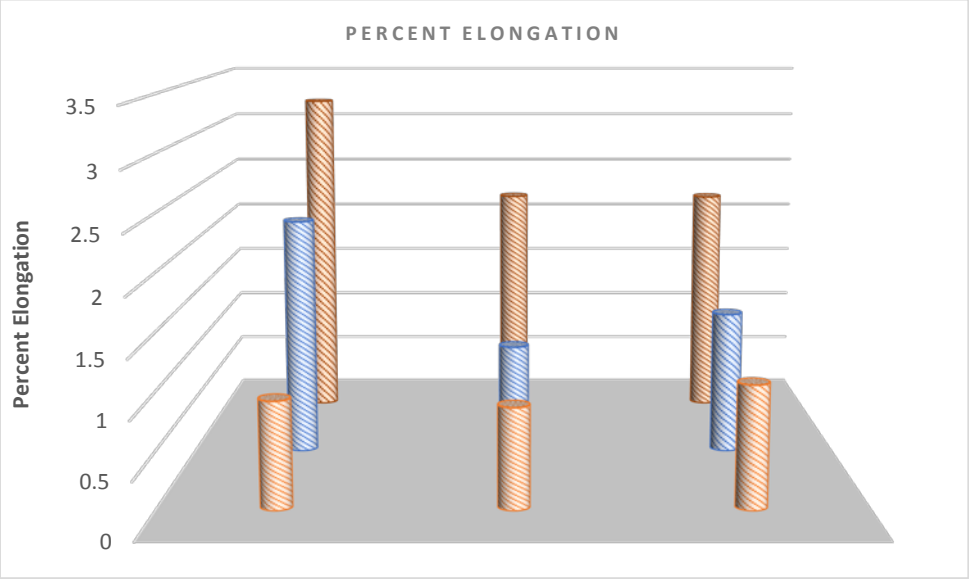

Figure 4.9: Percent Elongation for each cylinder in Grid II

Table 4.4: Comparing Percent Elongation of each cylinder in each location for Grid I and Grid II

Build	Percent Elongation (%) Grid I	Percent Elongation (%) Grid II	S.D.
Cylinder 1	3.09	3.21	0.06
Cylinder 2	3.26	2.22	0.52
Cylinder 3	5.62	2.21	1.72

Cylinder 4	3.33	2.21	0.56
Cylinder 5	5.82	1.01	2.40
Cylinder 6	4.16	1.32	1.42
Cylinder 7	0.99	0.96	0.02
Cylinder 8	3.09	0.90	1.09
Cylinder 9	3.00	1.09	0.95

FRACTOGRAPHY

The surfaces observed in the SEM reflected a dominance of dimples, which are representative of ductile fractures. For these types of fractures, crack formation occurs by microvoid formation as the material is stressed and crack propagation is through dimple coalences and fracture occurring as a result of dimple tearing. Figure 4.10 is a representative photograph of the fracture surface observed under the SEM for all Ti-6Al-4V EBM-fabricated cylinders that were CNC machined and subjected to tensile testing. Such image is from sample two in Grid I. In general, the specimens achieved extensive deformation before fracture, which can be observed in the engineering stress vs engineering strain graphs in APPENDIX A. Also, the spherically shaped voids refelct the tensile stress the material was subjected to. The ductile fracture mode rulling was also reinforced by the cup and cone shaped morphology that the specimens displayed in Figure 3.4. This is characteristic failure for EBM-produced Ti-6Al-4V samples subjected to tensile stress as previously reported by (A. Christense, 2007) and (H.K. Rafi, 2013).

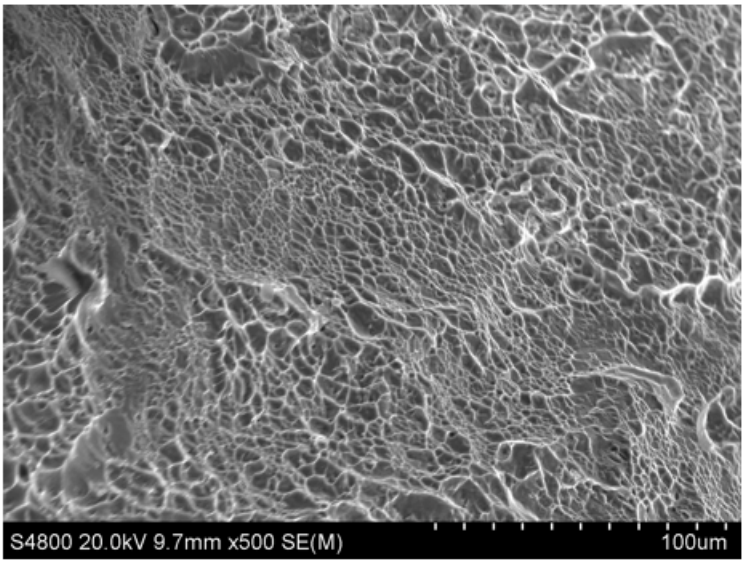

Figure 4.10: SEM image of tensile fracture surfaces showing dimple coalescence

CONCLUSIONS AND RECOMMENDATIONS

Advancing Ti-6Al-4V EBM fabrication to industry requires repeatable part reproducibility in large amounts with rapid production times. Fabrication of various parts within a single build is an alternative to satisfy such challenge. However, the certainty that every part will exhibit equal mechanical properties is an issue that has to be address, and the one targeted in this study. The principle was to evaluate mechanical response as a function to building location on solid components for a single build under a standard receipt through mechanical testing and fracture surface analysis.

The results obtained for this study suggested that location within the build platform influences mechanical properties. However, the results obtained presented scattering values. These are attributed to the nature of the EBM process, in which thermal input is constant, nonetheless unequally distributed due to various factors as are: uneven powder deposition contributing to excess cooling at some locations and heat sink at others or reaching appropriate sintering and

melting temperatures throughout the build platform. In general, an increase in YS, UTS, and %EL was observed for parts towards the back of the machine, with respect to the front of the machine. The YS and E showed a coherent change with tension deformation. It is recommended that the results of increased mechanical properties values with increase distance from the build platform be correlated with grain morphology by microstructural analysis. Also, dislocation density examination through transition electron microscopy (TEM) is recommended to confirm the results by surface area to volume ratio, which can be modified by factors affecting the EBM process mentioned.

CHAPTER 5: MECHANICAL RESPONSE OF BUILDING CONDITIONS ON LATTICE COMPONENTS FROM VARYING PROCESSING CURRENT

INTRODUCTION

Finding a safe compromised between low weight and high strength has been a crucial mission for industries and organizations. Today several materials are known to reach such compromise at competing performance at their minimum weight. The titanium alloy Ti-6Al-4V has exhibited some of the most desirable characteristics for numerous applications that go from connecting society as the most used material for aircrafts all the way to a material that can give a new opportunity to a life, as it is also use in the medical field. However, the material encounters limitations in all fields and properties are leveled against one another to achieve a decision that will yield the maximum performance. AM offers technologies for creation of lightweight parts without sacrificing properties that are important for design and performance. With a focus on high strength to weight ratios, freedom of design, material and structure optimization, compatibility with human tissue, and performance lattice structures EBM-fabricated have been highly researched to exploit materials and the technology. The process enables the manufacturing and it is well suited for it.

Previous work has found that the observed microstructure for thin walls EBM fabricated consist of a mixture of α/α' as consequence of the rapid cooling experience due to the small structure and fast scanning speed resulting from the nature of the process. Fabrication of Ti-6Al-4V ch microstructure has been observed through other AM technologies

Of interest to this investigation was the microstructure for porous structures. Studies have been conducted to determine the minimum wall thickness in which the desirable α/β

microstructure can be achieve, and (Xipeng Tan, 2015) reported for solid structures a minimum thickness of 5mm at a scanning speed of 14 mm/s. For porous structures α'-martensitic phase is dominant, yielding a brittle behavior. Literature has suggested that altering the structure can modify the properties, (L.E. Murr S. G., 2009) (Murr *et al.*, 2010), reported that the stiffness and elastic modulus vary inversely with density (specially relative density) and, the same relationship is observed with porosity of solid and hollow Ti-6Al-4V EBM-fabricated foams.

Of interest to lattice structures is removing the detrimental martensitic phase, which causes unpredictable fractures. Altering the microstructure and as a consequence mechanical behavior was approach by parameter modifications within the fabrication process, with a focus on identifying the parameter combination that will provide the most desirable microstructure. Mechanical properties, struts, and microstructure produced by EBM were characterized by compression test, scanning electron microscope (SEM), and light optical microscope (LOM). EBM has the capability for direct fabrication of these porous structures, that are isotropic and energy absorbing making them attractive to aeronautical, automotive, as well as biomedical applications among others.

EXPERIMENTAL METHODS AND PROCEDURES

Understanding the relationship between the ways a material is processed, its structure, and its properties is fundamental to the development of advance materials. Parameter dependent microstructure and mechanical properties of EBM Ti-6Al-4V lattice structure have been investigated with varying processing currents of 15 mA, 1.7 mA, 3.4 mA, and 8.5 mA.

For this study, numerous rectangular prismatic lattice structures with dimensions 25 mm x 25 mm x 40 mm were EBM-fabricated with a circular cross-sectional and of ~1mm thickness

(Figure 5.1). A repeating rhombic dodecahedron unit cell consisting of bounding cube geometry of 6 mm and relative density of 0.3 (30%) were designed using software MATERIALISE/MAGICS. These lattices have been highly examined mainly by theoretical analysis or FEM simulations due to the complexity of the analytical examination. Literature has suggested that mechanical properties are strongly influence by the geometry and optimization (graded) of lattice structures. Graded meshes have exhibited a balance of mechanical properties compared to uniform meshes of varying strut thickness, with a high strength, low Young's modulus relationship and ductile deformation under longitudinal compression behavior, unlike uniform meshes which exhibit a brittle behavior characterized by fluctuating stress at the plateau region of the stress versus strain graphs (Shangzhou Zhang, 2016). The influence of cell morphology on mechanical behavior under compressive fatigue was analyzed by (S. Zhao, 2016) with three types of meshes: cubic, G7, and rhombic dodecahedron. A decrease in strength and Young's modulus was observed in the following order: cubic, rhombic dodecahedron, and G7; and the deformation mechanism was also reported different by cell shapes in which G7 and rhombic dodecahedron are dominated by bending deformation with a fracture angle of 45° while the cubic mesh deforms by buckling at 90°. Bending-dominated lattices that are orthotropic and near-incompressible in all loading directions were also the discussion by (Sahab Babaee, 2012) for rhombic dodecahedron. Literature has highly reported rhombic dodecahedron meshes as the designed capable of attaining the most desirable properties. The focus on the lattice design now turns into intra modification such as varying relative densities and bounding cube geometries (Timothy J. Horn, 2014).

A rhombic dodecahedron unit cell was chosen for this study, in which the primary focus was to examine the mechanical response under varying processing currents. Microstructure is a

clear identifier for mechanical behavior; therefore, solid 9 mm x 9 mm x 9 mm cubes were fabricated within the build to obtained microstructural representations of each processing current. To avoid the introduction of additional variables a constant energy was maintained, for processing currents including a standard build at a high current, and three lower than standard currents with scanning speeds at a low, medium, and high, Table 5.1.

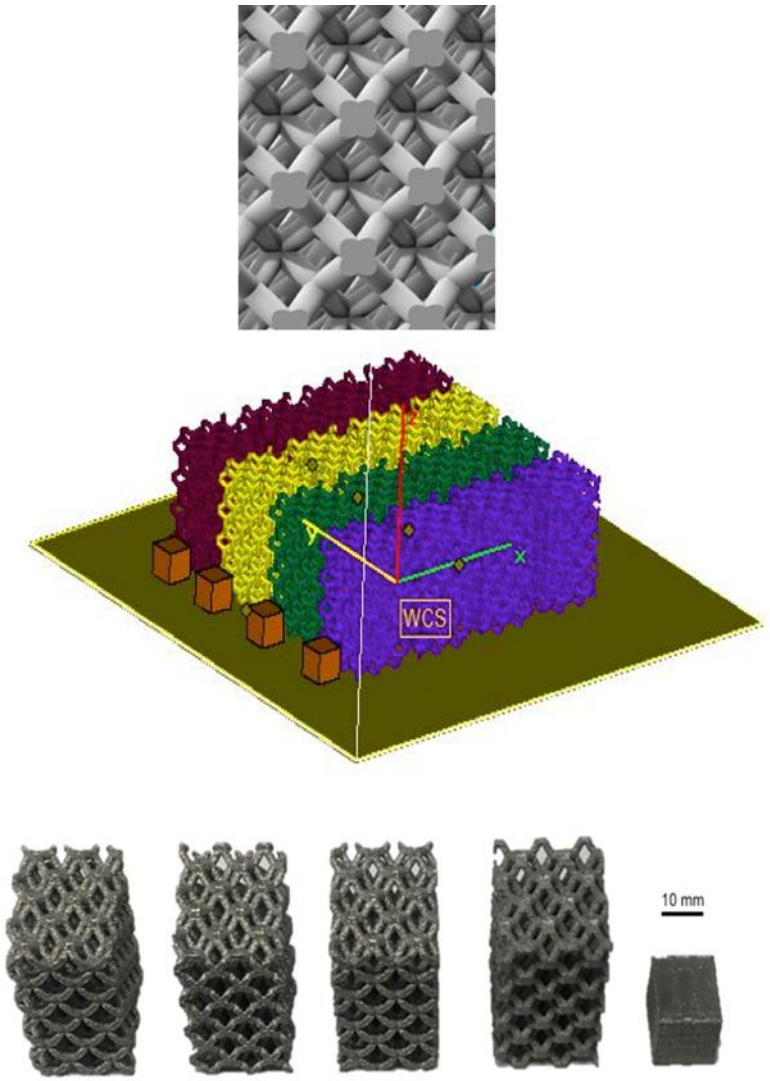

Figure 5.1: Digital design of the rhombic dodecahedron unit cell and meshes with solid cubes

Table 5.1: Processing Currents

Beam Current (mA)	Scan Speed (mm/s)
15	4530
1.7	500
3.4	1000
8.5	2500

5.2.1 COMPRESSION TESTING

Compression testing was performed on the lattice structures using an MTS Landmark Servohydraulic test system (MTS System Corporation, Eden Prairie, Minnesota) with 643 Compression Platens. An axial warm-up of the system was conducted before the first test for 600 cycles at a frequency of 1 Hz. With the assistance of concentric rings etched on the surface of the grips and lubrication between the samples and grips, the samples were positioned at the loading area in the same place throughout each test. The samples were subjected to uniaxial compression until failure with a maximum force of 100kN at a displacement rate of 1 mm per minute. Figure 5.2 is a schematic of the compression test set up.

The lattice structures were subjected to compression testing under a standard procedure. The elastic properties were calculated from the difference between two points at the beginning of the elastic slope, which was obtained from the force and displacement report generated by the testing machine. Load vs. displacement graphs plotted for each sample subjected to compression are presented in APPENDIX B. The Young's modulus (stiffness) as well as the load at fracture, the ultimate compression strength (UCS,) and the maximum deflection is reported here. Literature has suggested the importance of relating the lattice properties to the Gibson-Ashby model for open cellular materials, in which it is suggested that a reduction in relative density can have a notable reduction in the Young's modulus (stiffness) by (Ashby, 1997):

$$\frac{E^*}{E_s} = C_1 \left(\frac{\rho^*}{\rho_s}\right)^n \quad \text{(Open cells)}$$

Where E^* and E_s denote the Young's modulus (E) of the porous and fully dense material, ρ^* and ρ_s denote the density of the porous and fully dense material, and C_1 is a constant ≈1, typically n ranges from 1.8 to 2.2, with a rule of thumb of n ≈ 2 (M.F. Ashby, 2000). The compressive modulus could not be determined with the testing set up, thus Ashby also assumes an equal approximation between such and the flexural modulus. The elastic flexural and compressive properties have been determined by the use of resonant frequency and damping analysis (RFDA) and by numerical approaches.

For this study, a student's t-test was performed under the conditions of: paired tow samples for means, due to the inter-build processing variations. The average results for mechanical properties of Ti-6Al-4V EBM-fabricated obtained for these experiments showed, in general, no difference between the standard build and all the other builds.

Figure 5.2: Compression test set up

METALLOGRAPHY

Earlier work has reported the existence of the detrimental α'-martensite phase on mesh components fabricated by AM (Gaytan, 2009) due to the specimens small wall thickness which promotes a rapid cooling rate. Even though corrective actions have been implemented to obtain the desired α-β phase microstructure through post-processing operations, there is not a thorough analysis on the parameter modifications that will promote the appearance of the detrimental α'-

martensite phase. In the present study, the microstructure generated by each processing current implemented was examined by metallography analysis. A solid cube at the end of each row was representative of each current therefore was prepared for metallography analysis, and examined under the LOM. In addition, lattice structures prepared for metallographic analysis were observe the SEM.

The solid cubes were prepared for metallography analysis by sectioning perpendicular to the build direction axis ~5mm from the top as noted in Figure 5.3 by the red dash line. The lattice structures were prepared for metallography analysis by sectioning perpendicular to build direction, followed by a parallel sectioning at the middle of the part. Figure 5.4 shows the sectioning of the mesh structured by a red dash line, as well as the mounted piece. The sample preparation for metallography analysis was described in Chapter 3.

Figure 5.3: As-fabricated cubes representing microstructures for processing currents of 1.7mA, 3.4mA, and 8.5mA, respectively

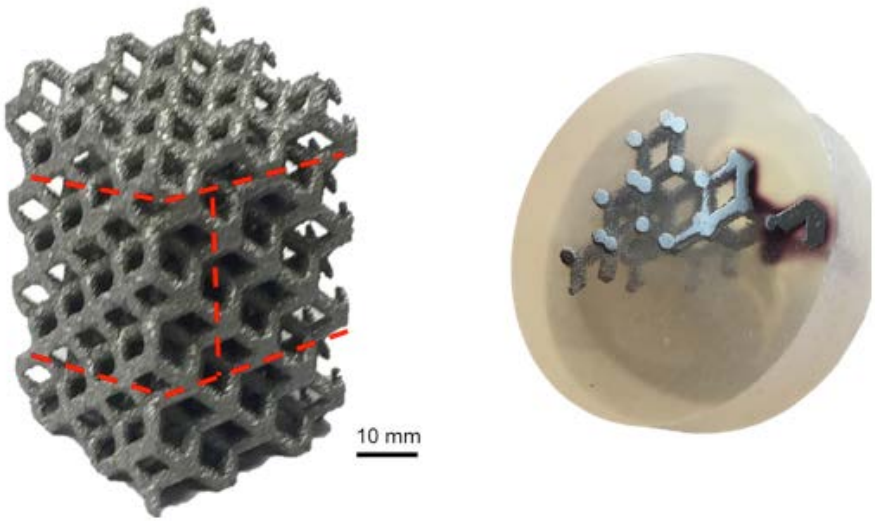

Figure 5.4: Mesh structure sectioning and mesh structure piece in Koldmount

FRACTOGRAPHY

Fractrography analysis was performed on the fractured surface. The sample preparation and analysis procedures have previously been described in chapter 3.

RESULTS AND DISCUSSION

COMPRESSION TESTING

Table 5.2 summarizes the processing currents utilized along with their measured density (ρ), relative density (ρ/ρ_o), porosity (%), and Young's modulus (stiffness) (E). The pore space porosity of all lattice structures was calculated from their respective density using equation: (ρ-

ρ_o)/ ρ. It can be observed that the relative stiffness increased with decreasing processing current Figure. 5.6 (a), thus the values did not exhibit a continuous increase; the highest and lowest processing currents do present the most considerable differences. The relative density decreased in the following order: 1.7mA, 8.5mA, 3.4mA, and 15mA with values of 8.88, 80.5, 7.43, and 6.70, respectively. Thus, the values measured by the Gibson-Ashby formula, the analysis of the lattice structures corresponded to n=2 and E_o=110GPa, in which the stiffness change proportionally to the porosity, Figure 5.6 (b). The measured porosity of the structure exhibited a decrease from the standard build in the following order: 3.4mA, 8.5mA, and 1.7mA, with respective Young's modulus values of 318.56 GPa, 370.09 GPa, and 444.02 GPa, respectively with the standard exhibited the lowest value at 260.05GPa. The values showed an increase in density as the heat input decreased, suggesting the sensitivity of the struts to the thermal experience. The UCS showed an increased with a processing current of 3.4 mA at 51 kN (± 4.71), this build also demonstrated the lowest porosity and density of 59% and 7.07 (g/ cm^{-3}), respectively. Builds under processing currents of 15 mA, 1.7 mA and 8.5mA exhibited values of 49.33 kN (± 0.94), 49.00kN (±1.41), and 48.66kN (±1.69), respectively, these values were in accordance with the expected increased strength density relationship. The UCS values for all the builds are illustrated in Figure 5.7 and Table 5.4. The results for this study regarding the load at fracture reported values of 45.33kN (± 4.11), 48.66kN (±1.70), 50kN (±2.16), and 47.66kN (±1.7) for processing currents of 15mA, 1.7mA, 3.4mA, and 8.5mA, respectively. Figure 5.8 and Table 5.5, show the results in which in which the large porosity and density measured disable a high load withstand. The displacement showed to not be affected by the parameter modifications, with all builds reaching 2mm displacement before rupture; this indicates the processing current does not have a strong influence on this property.

Table 5.2: Mesh components processed with varying processing currents properties

Processing Current (mA)	Density, (g/cm^3)[a] ρ	Relative Density (ρ/ρ_o)[b]	Space (%)	Mass (g)	E (GPa)
15 (Standard Build)	6.70	1.51	31.75	199.75	260.05
1.7	8.87	2.00	49.99	217.73	444.02
3.4	7.43	1.68	38.47	176.63	318.56
8.5	8.05	1.81	43.74	186.50	370.09

[a] Build volume: 2.5 x 2.5 x 4 (cm) = 25 cm^3

[b] ρ_o = 4.43g cm^{-3}

a)

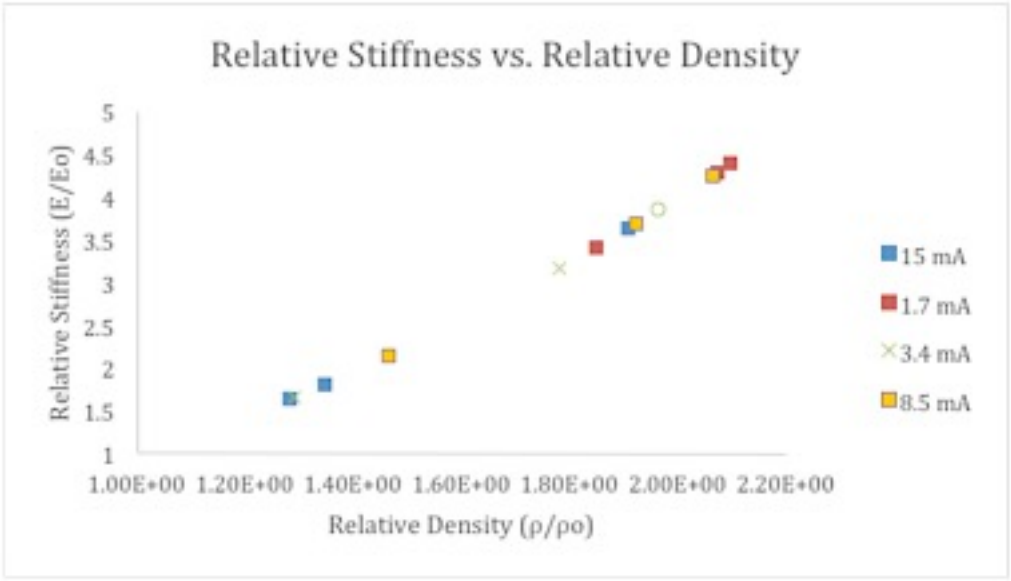

b)

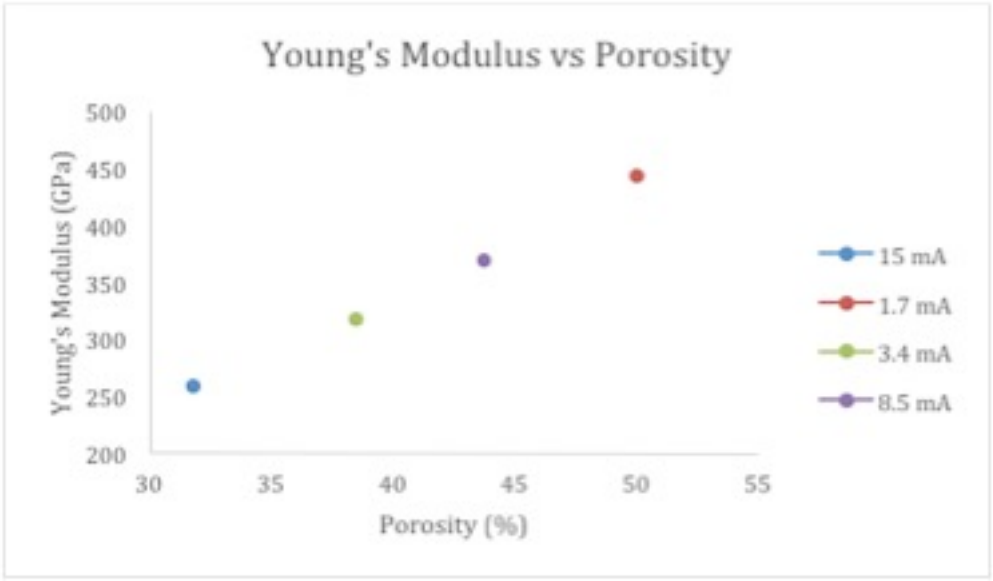

Figure 5.6: (a) Relative stiffness plotted against relative density, and (b) Stiffness (Young's modulus) versus porosity measured

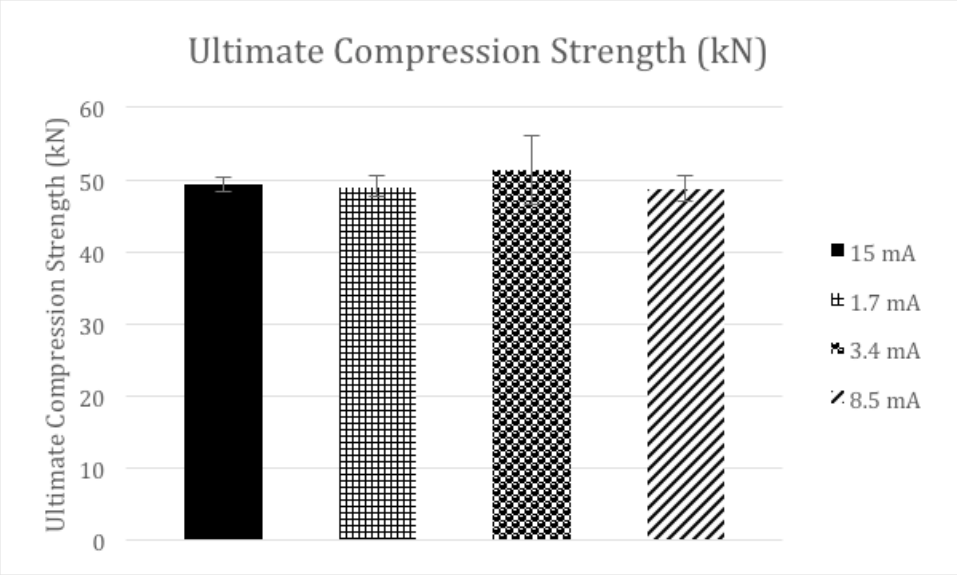

Figure 5.7: Maximum load results in kN for each build compared to the standard build

Table 5.3: Ultimate Compression Strength values comparing each build to the standard build. P value for standard build versus each build is also show

Processing Current (mA)	Ultimate Compression Strength (kN) .S.D.	P Value (Versus standard build)
Standard Build	49.33 0.94	-
1.7	49.00 1.41	0.74
3.4	51.33 4.71	0.58
8.5	48.66 1.70	0.75

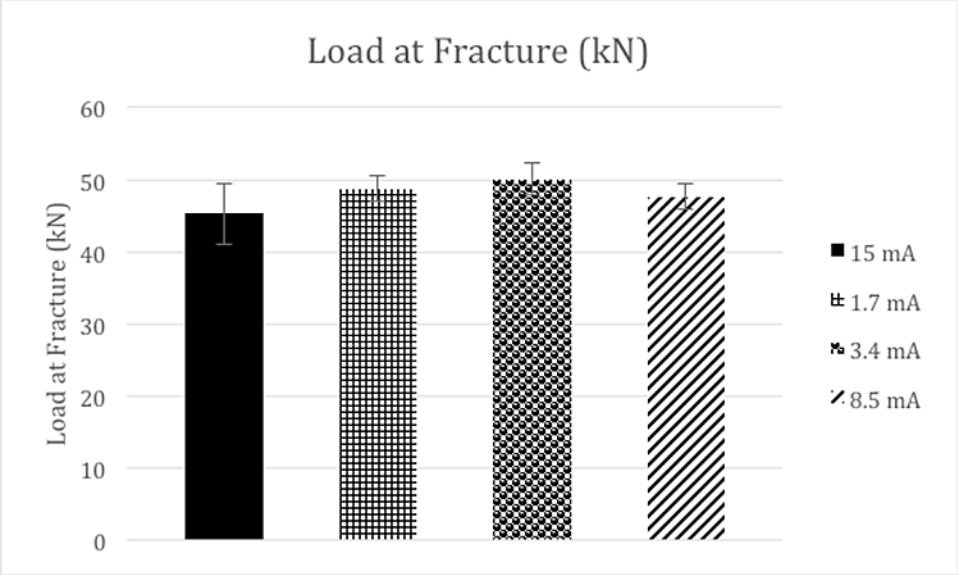

Figure 5.8: Load at rupture results in kN for each build compared to the standard build

Table 5.4: Load at Rupture values comparing each build to the standard build. P value for standard build versus each build is also show

Processing Current (mA)	Load at Rupture (kN) .S.D.	P Value (Versus standard build)
15	45.33 4.11	-
1.7	48.66 1.70	0.48
3.4	50.00 2.16	0.28
8.5	47.66 1.70	0.55

METALLOGRAPHY ANALYSIS

The microstructure is a clear indicator of how the parameter modifications influence the mechanical behavior of the structure. However, the geometry also plays an important role on the microstructure evolution during fabrication that is the reason why it was important for this study to obtain microstructure representation of the processing currents without accounting for the geometry of the part. Figure 5.9 shows the resulting microstructures from each as-fabricated solid cube from which the transverse microstructures presented conveyed an acicular α-phase more notable for the parts processed at 15 mA and 1.7mA, while the rest of the microstructures were a Widmanstäten with continuous α and β retained at the grain boundaries. Murr *et al.* 2009 reported the observed miscrostructure for the solid cubes consisted of a β matix (dark) with a secondary α lamellae phase (light) growth in standard builds. For this study, α lamellae width were meassured using MATLAB sofware by converting the color image into a binary image as illustated in Figure 3.10. Figure 5.10 and Table 5.5 illustrate the resuls for the α widths. The solid cube for the standard build had on average α-lath thickness of 1.67μ (± 0.14). The α-lath width was noted to decrease fo all the other builds in the following order 1.7mA, 3.4mA, and 8.5mA with values of 1.44 μm (±0.19), 1.20μm (±0.17), and 1.32μm (±0.10), respectively. The varying α-lath thicknesses was strongly influenced by the processing current and speed. For the EBM process, the layer depostied can act as heat sink, enableling an anneling condition, consequently the higher thermal energy inputed locally as it is for this process promotes time for the phase tranformation. Figure 5.11 illustrates the microstructures obtained from each lattice structure fabricated. Previous work by Murr *et al.* 2010 reported a mixture of α'-martensite and the hcp α-pahse with the α'-martensite as the primary phase for mesh strucutre's miscrostructure that is characterisitc of the thin walls. In

this study, a more pronounced α-phase with interphase β-phase (dark) was observed for all mesh compoents.

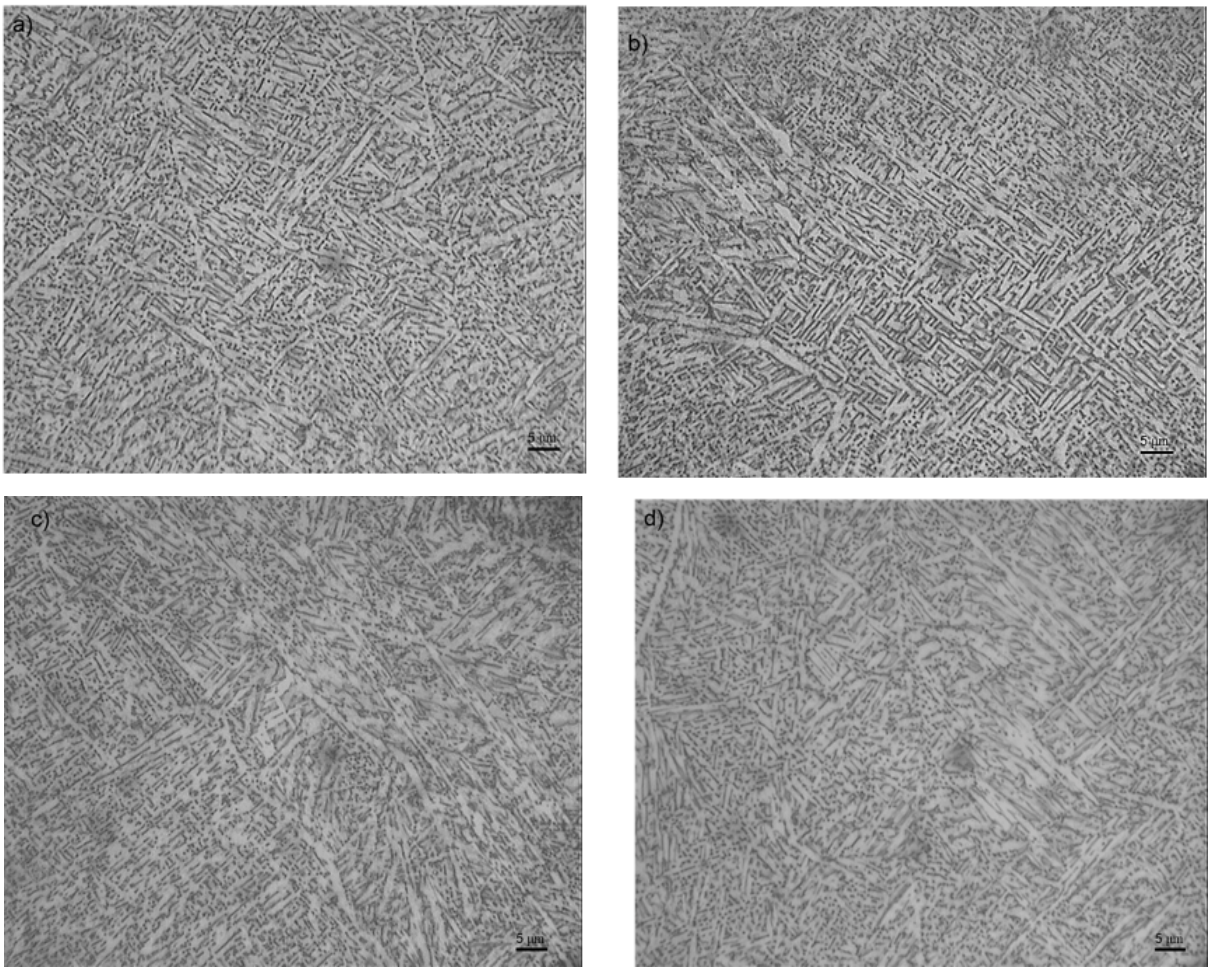

Figure 5.9: Microstructure of solid cubes fabricated under: (a) 15mA (b) 1.7mA (c) 3.4mA (d), and 8.5mA

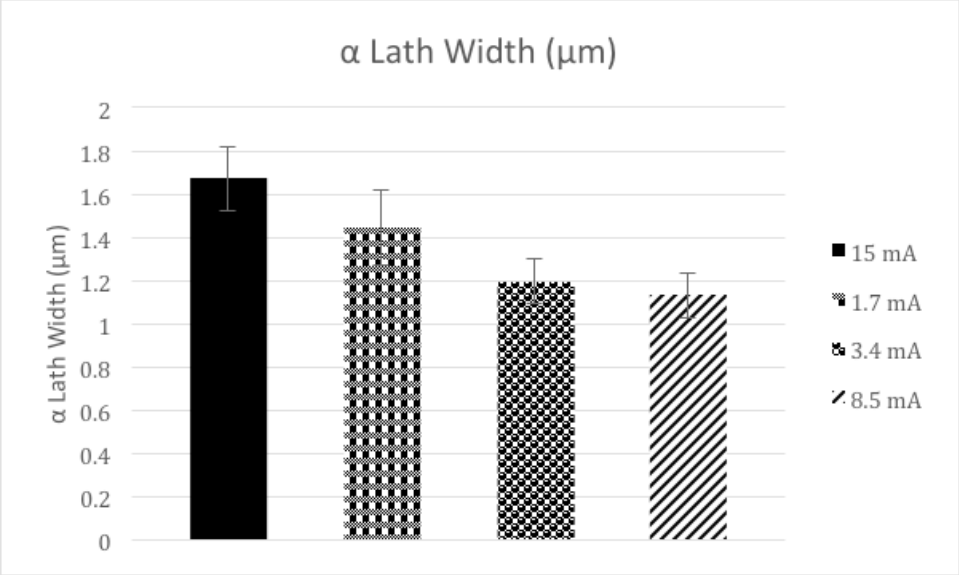

Figure 5.10: Comparing α lath width for each build for solid cubes

Table 5.5: Comparing α lath width in μm for each build for solid cubes

Build	α-lath width (μm) S.D.
Standard Build	1.67 0.14
1.7mA Processing Current	1.44 0.19
3.4mA Processing Current	1.20 0.17
8.5mA Processing Current	1.32 0.10

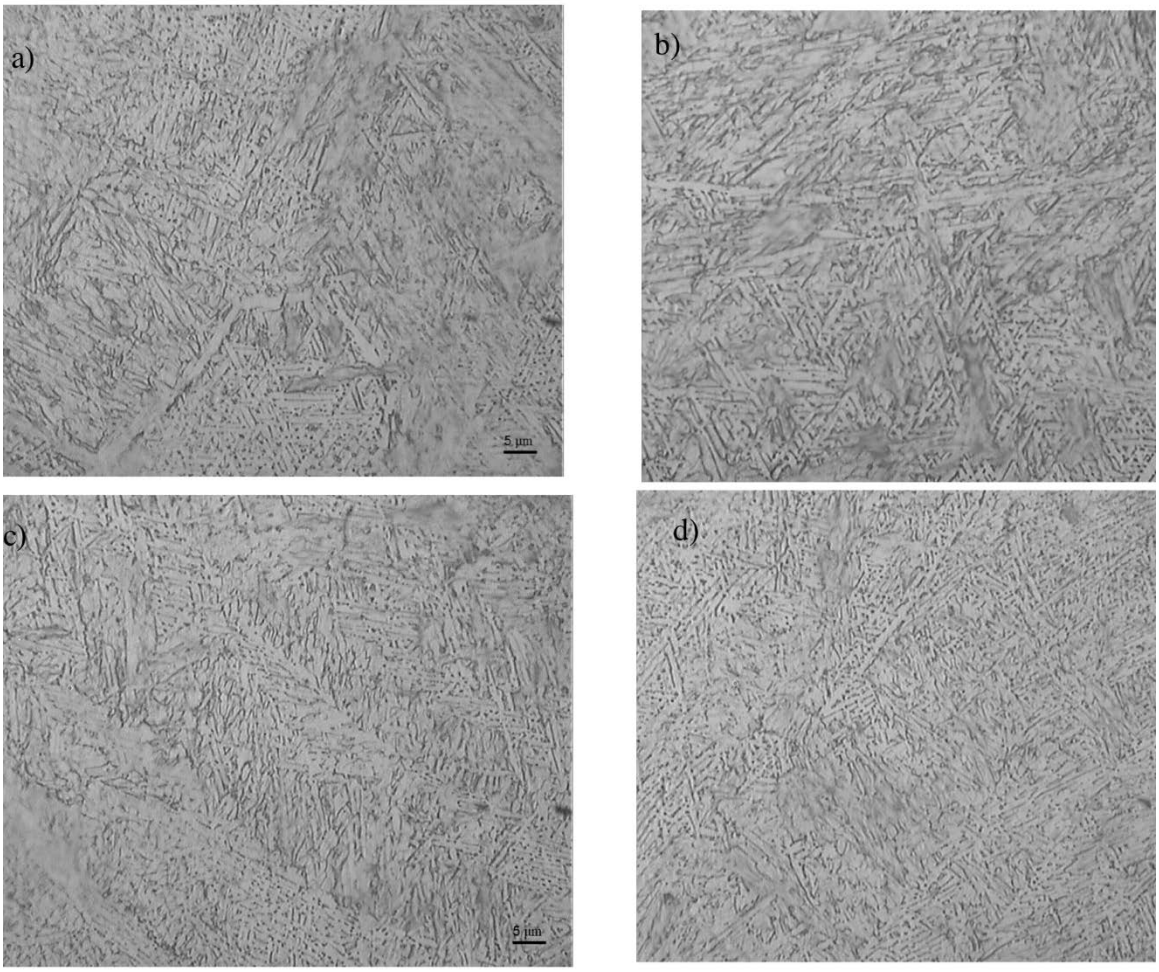

Figure 5.11: Microstructure of lattice structures fabricated under: (a) standard build (b) 1.7mA (c) 3.4mA (d), and 8.5mA

FRACTOGRAPHY ANALYSIS

Figure 5.12 shows an image of the mesh array at a target relative density of 30%. A rough surface is observed due to un-melted or sintered powder, this surface is however homogeneous throughout the struts enabling a uniform deformation, since internal pores are also contained throughout the struts. For vertical builds (as it is in this case), the roughness does not vary considerably through the lattice, this assists with obtaining an equally distributed stress concentration throughout the lattice structure. The fracture surface of the struts was examined by SEM and typical fracture modes of all the lattice structures subjected to compression are presented in Figure 5.13. The cleavage (Fig 5.13a) and dimples (Fig. 5.13b) were evident of the low energy absorption and compression fracture surface. Cracks initiated at the root of the un-melted and sintered powder on the strut surface by accumulated strain as reported by (S.J. Li, 2012) at the strut crosssectional area, finalizing in strut collapse.

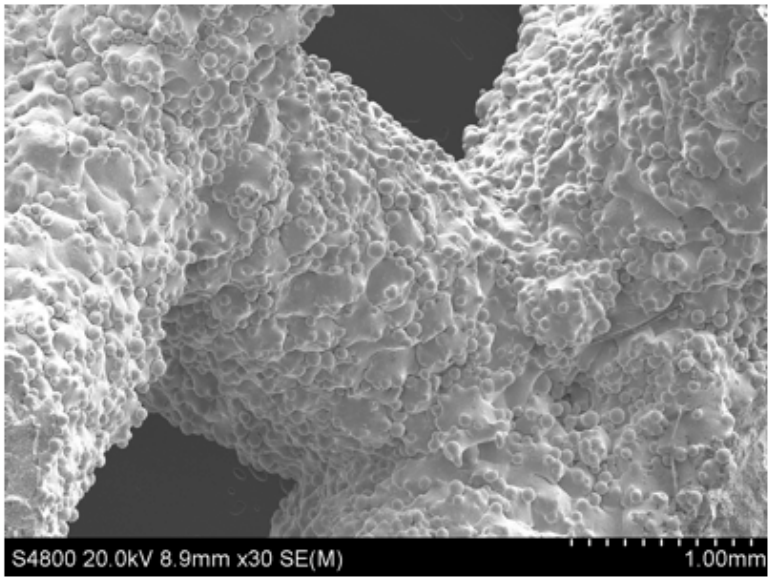

Figure 5.12: SEM image of the mesh array at a target relative density of 30%

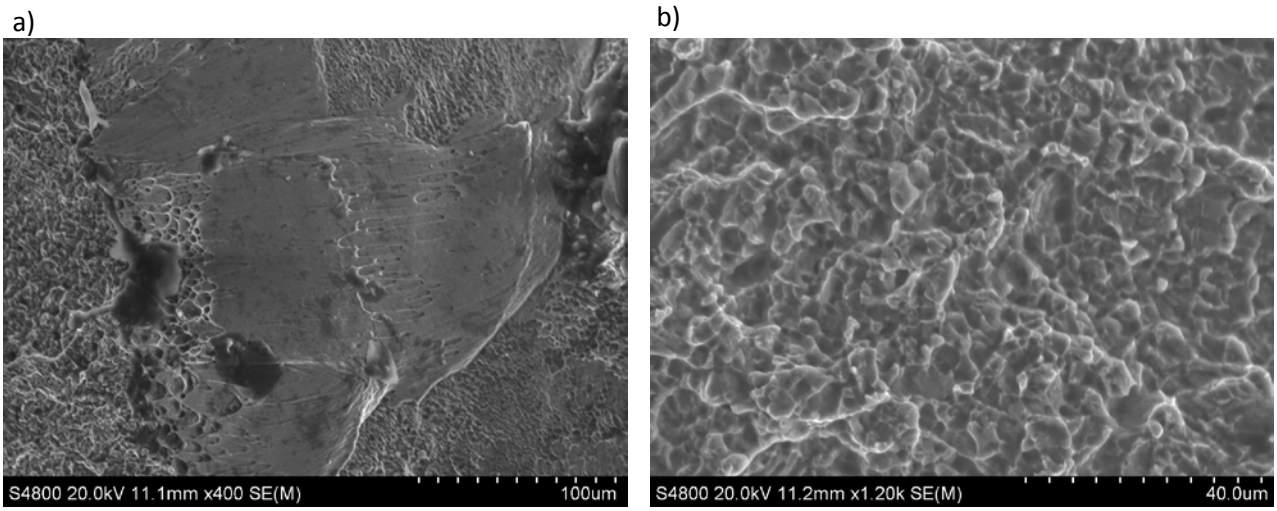

Figure 5.13: SEM image of strut fracture surface (a) cleavage facet (b) and dimple surface

CONCLUSIONS

In this study, parameter modifications effect on mechanical properties and microstructure of Ti-6Al-4V EBM-fabricated lattice structures were analyzed. Four different processing currents of 15mA, 1.7mA, 3.4mA, and 8.5mA were utilized for fabrication of lattice structures with a consistent rhombic octahedral design at a relative target density of 30%. The results are summarized as:

- Mechanical properties, in general, did not exhibit a statistical difference between the standard build and all the other builds. This was determined at a 95% confidence level though the P-critical value obtained from performing a student t-test, in which the value was lower than the t-critical.

- Mechanical properties of lattice components (especially stiffness and strength) are known to be sensitive to the design and porosity of the structure. In the study a continuous designed was use for all builds and processing current variations were introduced within the build. The results showed that at processing currents lower than the standard (15mA) the relative stiffness and increase, thus not linearly the highest and lowest current do exhibit the most notorious difference at 32% and 71% for relative density and stiffness, respectively. The thermal input along with the resulting processing speed were determined to be a governing factor to mechanical behavior.
- The α lath thickness for the solid cubes showed a decrease from the standard build to the 1.7mA, 3.4mA, and 8.5mA of 13.77%, 28.44%, and 32.22%, respectively. The sensitivity of grain growth to heat is well known, therefore the results suggest the microstructure is being affected by the nature of the process as the grains continue to refine even after a low to high energy input transition. In the case of the lattice structures the mixture of α/α' continue to be the resulting microstructure. The study did reach an improvement as the mix microstructure contained the appearance of globular α.
- Crack initiation and growth is governed by surface properties and inherent defects that increase buckling deformation on struts due to the chosen rhombic dodecahedron shape, enabling a uniform deformation by bending of the whole mesh.

CHAPTER 6: MECHANICAL RESPONSE OF BUILDING CONDITIONS ON MESH COMPONETS: VARYING PROCESSING SCAN MELTS

INTRODUCTION

Building from the ground up, this is the present of manufacturing. Additive manufacturing is a ground breaking technology that gives designers many components to successfully fabricate difficult and until now impossible parts. AM has solve many problems encountered by parts traditionally build by enhancing efficiency and durability with added benefits. The work that can be produce by AM technology can alleviate weight across multiple components on a brought range of industries. One of the most significant contribution of AM to the revolution we are seeing today is the reduction in weight, either by the successful fabrication of one components that will otherwise be numerous individual parts assembled together or yet by the even more attractive alternative of lattice structures. Lattice structures are expected to have a central role in production overtime as the design and properties improve. As it has been mentioned, the porous structures exhibit a microstructure consisting of a mixture of α/α'- martensite. Previous work has focus on removing the brittle phase by post heat treatment, design, and relative density modification, as well as by controlling strut and pore size. This study looked to contribute to the efforts on advancing the microstructures of lattice structures by taking advantage of the EBM A2 system, in which the user has access to the processing setup menu. The focus was on suppressing the appearance of α'-martensite by increasing scan passes during build to force gradient in microstructure. It addition, it was very important to correlate the microstructure and morphology with mechanical properties to determine the optimum condition of fabrication. The study uncovered several key elements the will advance the research conducted in metals AM produced by EBM

EXPERIMENTAL METHODS AND PROCEDURES

The lattice unit designed chosen for this study was that of a repeating rhombic dodecahedron due to extensive literature suggesting the design governs multiple mechanical behavior under standardized processing, this has been previously describe in chapter 5. The unit cells were designed using Magics, RP^{TM} software with specific bounding cube geometries of 6mm and target relative density of 30%. The struts designed consisted of circular cross sections, of 1mm diameter and adjusting length to meet the target relative density. Four replications of the design were fabricated in a vertical orientation, this orientation was chosen to assist with heat flux distribution, and promoted uniformity throughout the component. Figure 6.1 shows the digital model of the designs that consisted of four rows each with four lattice structures of dimensions 25 mm x 25 mm x 40 mm, and an as fabricated photograph of the built. In addition, a solid cube was built at the foot of each row as a representation of each scan pass.

The fabrication process has been previously described in Chapter 3. One standard parameter set was utilized for the fabrication of one replica of the rhombic dodecahedron lattice structure. In addition, two more replications of the design were fabricated, however in each case the processing parameters were modified by adding a scan melt in the following order: single, double, and triple.

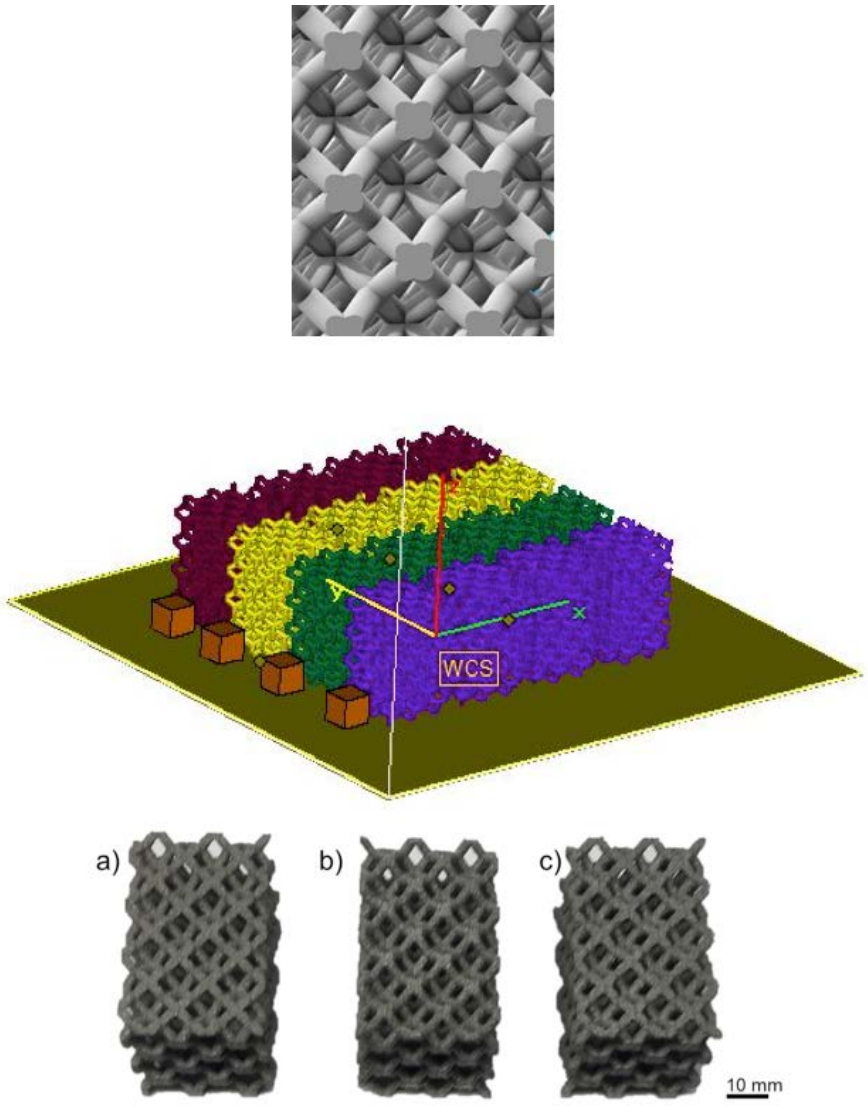

Figure 6.1: digital models of the rhombic dodecahedron unit cell design and designed use for study, as well as the fabricated lattices structures: (a) single, (b) double, and (c) triple melt

COMPRESSION TESTING

The compression test performed, set up, and analysis approach has been described in chapter 5.

METALLOGRAPHY

The metallography sample preparation and analysis has been previously described in chapter 3.

FRACTOGRAPHY

Fractrograpohy analysis was performed and it has been described in chapter 3.

RESULTS AND DISCUSSION

COMPRESSION TESTING

Table 6.1 summarizes the processing currents utilized along with their measured density (ρ), relative density (ρ/ρ_o), porosity (%), and Young's modulus (stiffness) (E). The porosity of all lattice structures was calculated from their respective density using equation: $(\rho-\rho_o)/\rho$. It can be observed in Figure 6.2 (a) and (b) that the relative Young's modulus increases with increasing relative density, and the same relationship is observed for the Young's modulus versus porosity. The highest property values were exhibited by the double scan pass build, which indicates a larger heat input will have the contrary effect; hence values decreased for the triple scan pass build. This is attributed to the chemical alteration at high temperatures as consequence of the building atmosphere and the effect of lowering the β-phase presence (B. Gorny, 2011). From the UCS comparison shown in Figure 6.3 and Table 6.3, it was seen that the property is highly affected by heat by the scan passes. The UCS between the standard build and the double, were statistically reported with no difference at their respective values of 45kN (±1.63) and 41kN (±5.01). Thus, a statistical difference was reported between the standard build and all the triple scan melt built at a value of 45kN (± 1.41). The mechanical property that presented the most variance was that of the load at fracture, thus there was no statistical difference between the standard build and all the other

builds. Figure 6.4 and Table 6.4 show the results for the standard build, double, and triple scan passes in which the values measured were 41.33kN (±1.25), 40.33kN (±1.66), and 44.33kN (±1.25), respectively. This study presented an increase in measured fracture deflection as scan passes increased by 50% from the standard build.

Table 6.1: Mesh properties under increasing heat passes

Build	Density, ρ (g/cm^3)[a]	Relative Density, (ρ/ρ_o)[b]	Porosity (%)	Mass, m (g)	E (GPa)
Standard Build	8.57	1.93	48.03	224	413.79
Double	10.37	2.34	56.74	260	609.50
Triple	9.29	2.10	50.20	283	506.39

[a] Build volume: 2.5 x 2.5 x 4 (cm) = 25 cm^3

[b] ρ_o = 4.43g cm^{-3}

a)

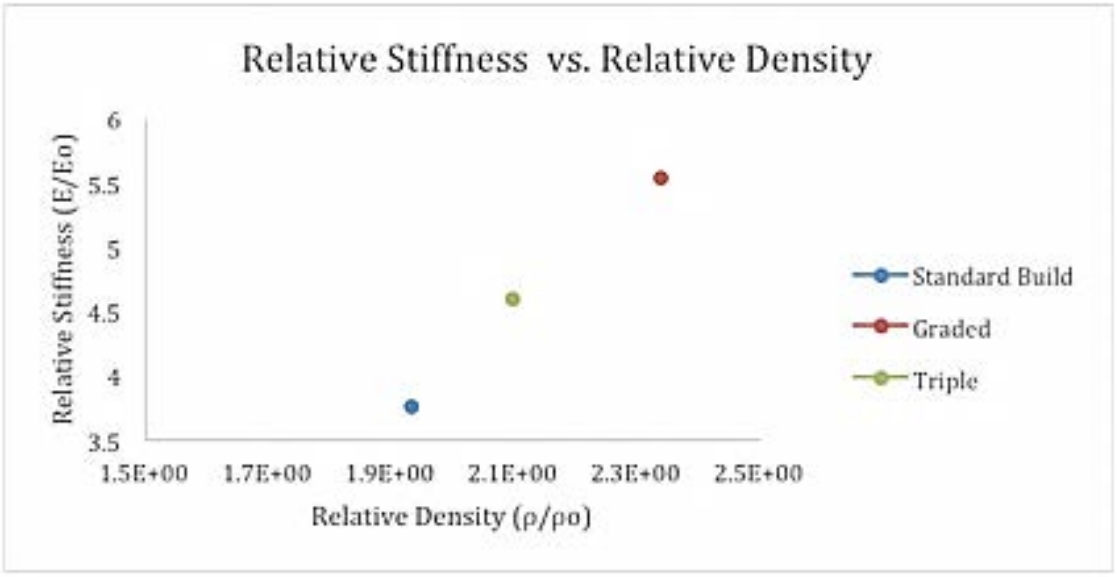

b)

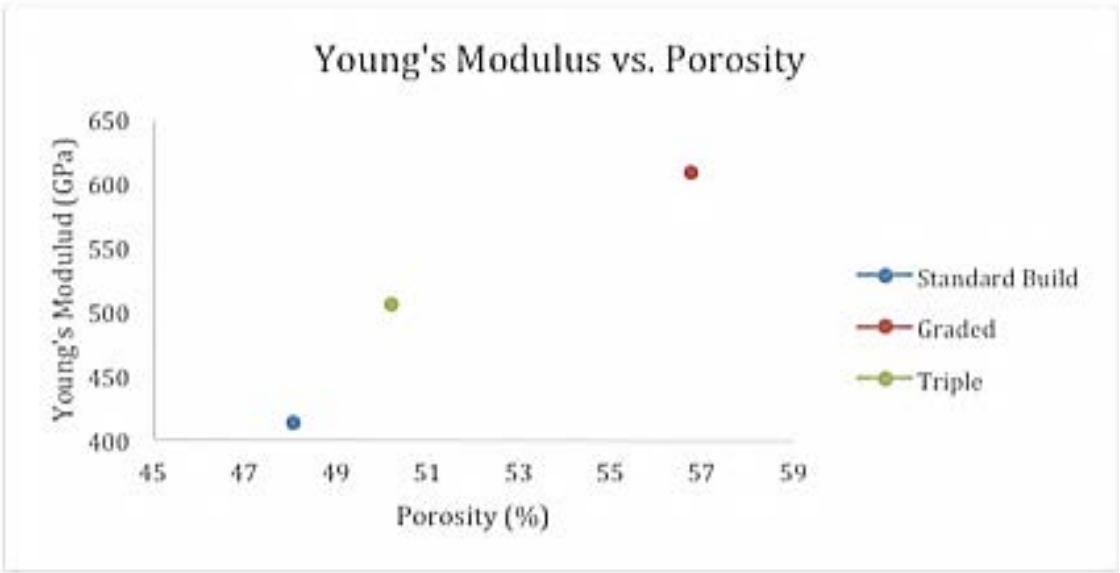

Figure 6.2 (a) Relative stiffness plotted against relative density, and (b) Stiffness (Young's modulus) versus porosity

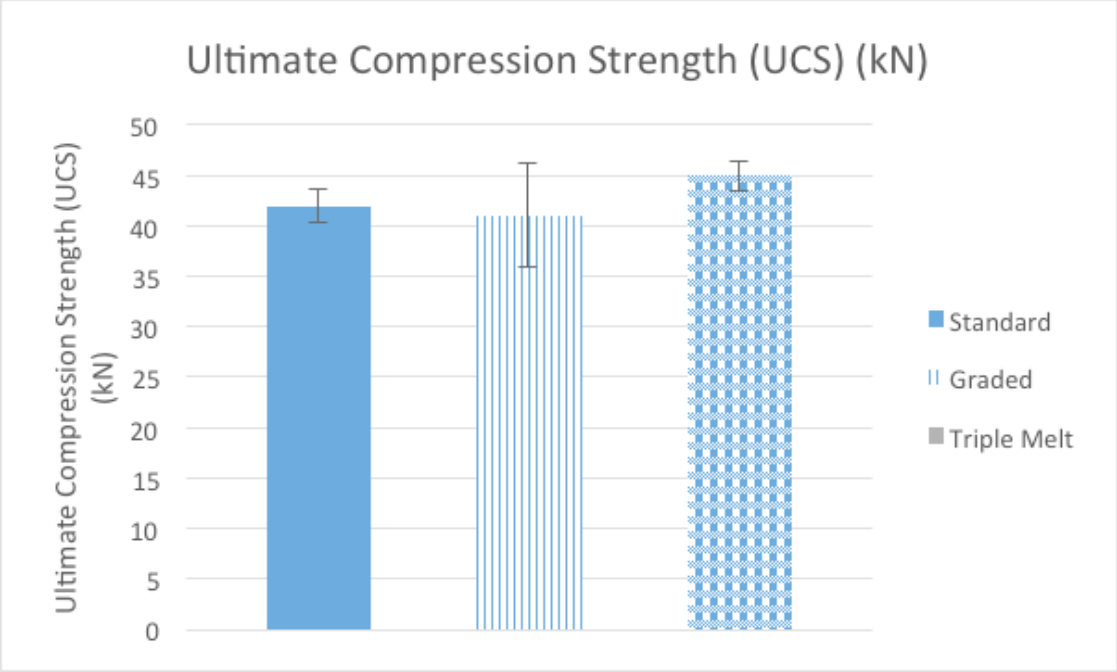

Figure 6.3: Ultimate Compression Strength results in kNfor each build compared to the standard build

Table 6.3: Ultimate Compression Strength values comparing each build to the standard build. P value for standard build versus each build is also show

Build	Ultimate Compression Strength (kN) S.D.	P Value (Versus the standard build)
Standard Build	42.00 1.63	-
Double	41.00 5.10	0.81
Triple	45.00	0.03

	1.41	

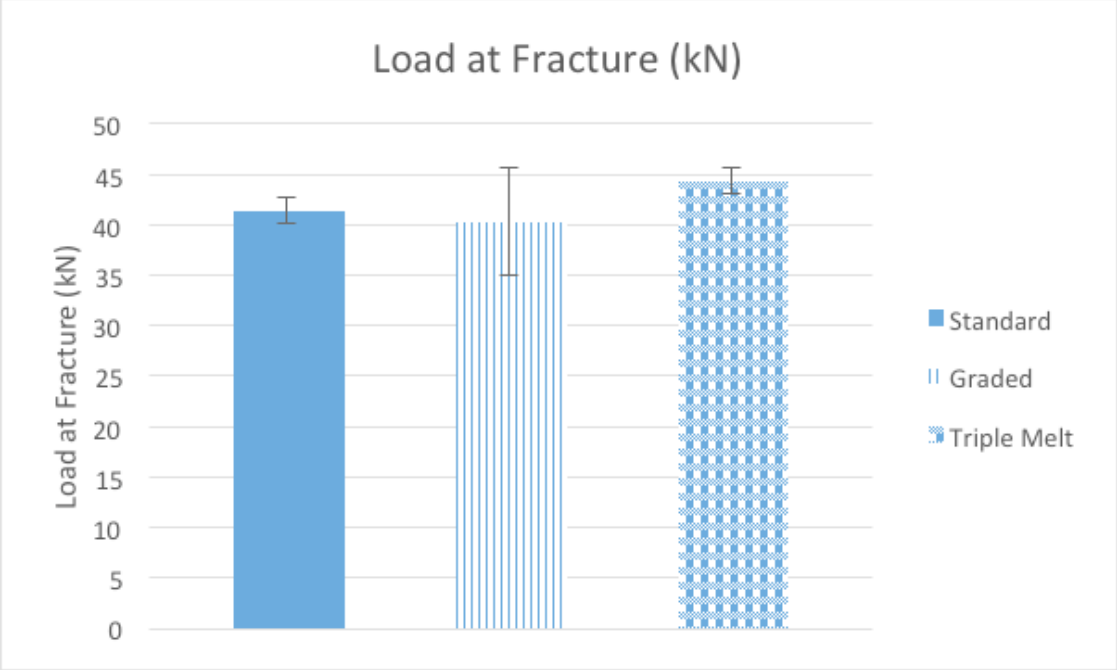

Figure 6.4: Load at rupture results in kN for each build compared to the standard build

Table 6.4: Load at Rupture values comparing each build to the standard build. P value for standard build versus each build is also show

Build	Load at Rupture (kN) S.D.	P Value (Versus the standard build)
Standard Build	41.33 1.25	-
Double	40.33 5.25	0.82
Triple	44.33 1.25	0.74

METALLOGRAPHY ANALYSIS

Increasing the number of scan passes during fabrication, resulted in microstructural optimization, and morphology. This was observed for the solid cubes and the lattice structures. The solid cubes were fabricated as a representation of the microstructure for each scan pass, without taking into account geometry of the part. The nature of the EBM process subjects parts to a continuously heat of at least 750°C, interrupted by either an increase or decrease in heat depending on the predetermined processing parameters, followed by a continuous cooling to room temperature. Due to the geometry of the lattice structures a fast cooling rate is experience preventing a phase transformation to equilibrium α and β, resulting in microstructure consisting mainly of α'-martensite lamellae with α-phase, such has been previously reported by (L.E. Murr, 2010). In the case of this study the samples experienced a heat increase, which allowed the trasformation of α' into α, as reported by (L.E. Murr S. G., 2010).

Figure 6.5 (a), (b), and (c) illustrate the microstructures obtained from each as fabricated solid cube built under the varying processing melt scans. The transverse microstructures formed as Widmanstätten lath for the standard build, double, and triple scan passes with average thicknesses of 0.79μm (± 0.30), 1.20μm (±0.20), and 2.00μm (±0.86), respectively. The α-acicular (white) was present as continuous in retained β (dark). The increasing linear relationship, between the scanning passes and the α-lath thickness, is illustrated in Figure 6.6 and Table 6.5. The increase in heat, hence slower cooling rate, promoted grain growth. The further heating from the single, grade, and to triple scan passes resulted in larger α globular as it can be observed in Figure 6.7. In the case of the lattice structures, the standard EBM-fabricated lattices presented microstructural features commonly known to the structure which consisted mainly of α'-martensite lamellae with α-phase with an average lath thickness of 0.53μm (± 0.15). In contrast, the resulting α-lath

thickness for the double and triple scan passes were of 0.58μm (±0.09) and 0.75μm (±0.15), respectively. The α-lath thickness for the lattice structures are presented in Figure 6.8 and Table 6.6.

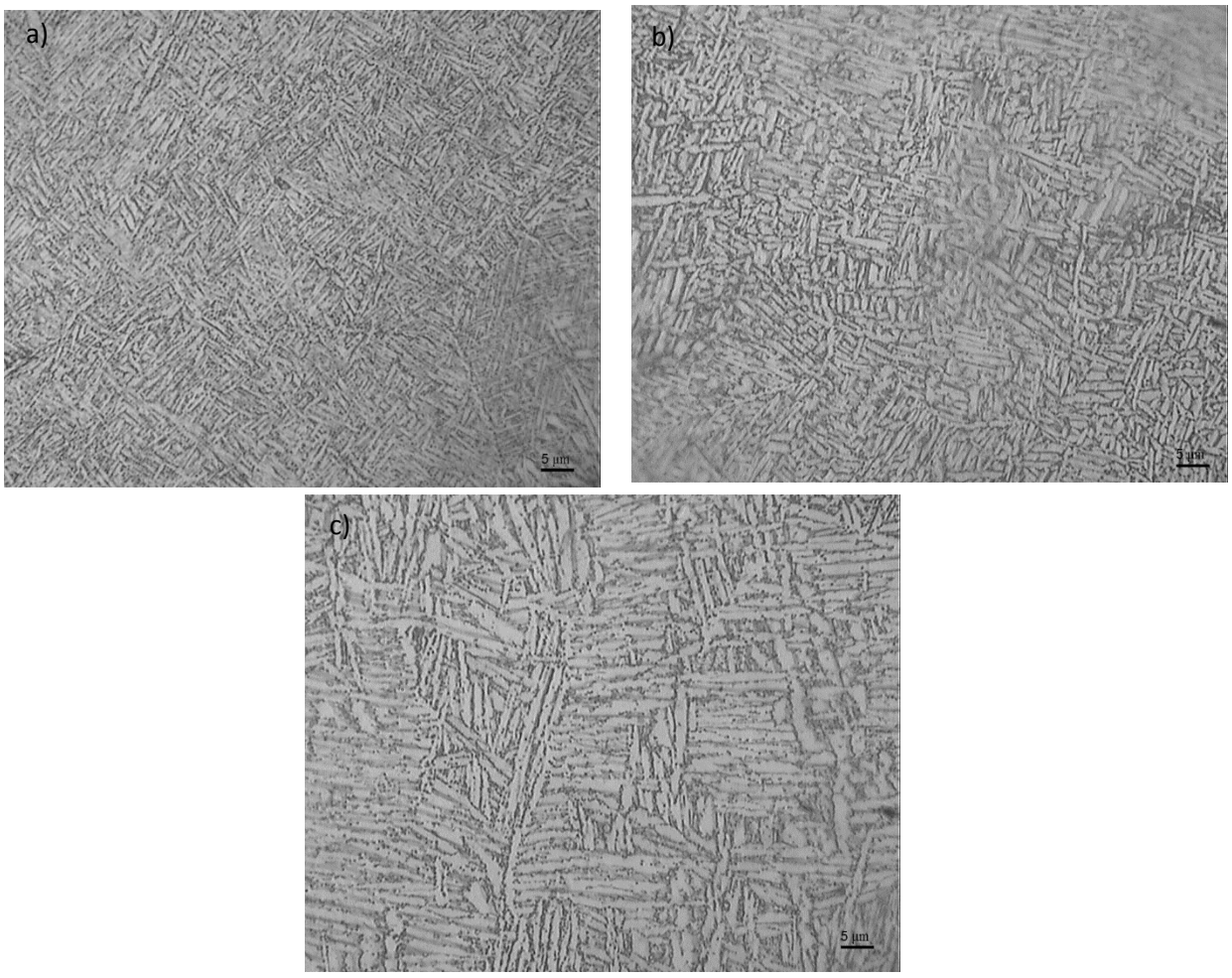

Figure 6.5: Transverse microstructures: a) standard build b) double melt c) and triple scans

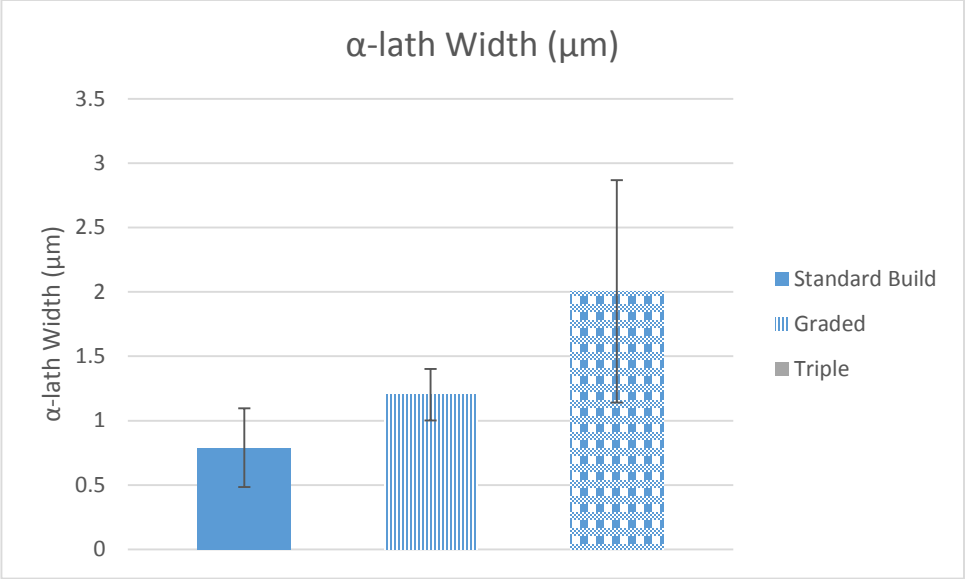

Figure 6.6: α-lath width for each solid cube fabricated under standard build, double, and triple scan melt

Table 6.5: Comparing α lath width in μm for each solid cube build

Build	α-lath witdth (μm) S.D.
Standard Build	0.79 0.31
Double	1.20 0.20
Triple	2 0.86

Table 6.6: Comparing α'-martensite thickness in μm for each lattice structure build

Build	α-martensite thickness (μm) S.D.
Standard Build	0.53 0.15
Double	0.58 0.09
Triple	0.75 0.15

FRACTOGRAPHY ANALYSIS

Figure 6.9 (a, b) shows an image of the mesh array at a target relative density of 30%. A rough surface is observed due to un-melted or sintered powder, this surface is however homogeneous throughout the struts enabling a uniform deformation, since internal pores are also contained throughout the struts, thus acting as crack nucleation sites. For vertical builds (as it is in this case), the roughness does not vary considerably through the lattice, this assists with obtaining an equally distributed tensile and compressive stresses concentration throughout the lattice structure. The fracture surface of the struts was examined by SEM and typical fracture modes of all the lattice structures subjected to compression are presented in Figure 5.12. The cleavage (Fig 5.12a) and dimples (Fig. 5.12b) were evident of the low energy absorption and compression fracture surface. Cracks initiated at the root of the un-melted and sintered powder on the strut surface by accumulated strain as reported by (S.J. Li, 2012) at the strut crosssectional area, finalizing in strut collapse.

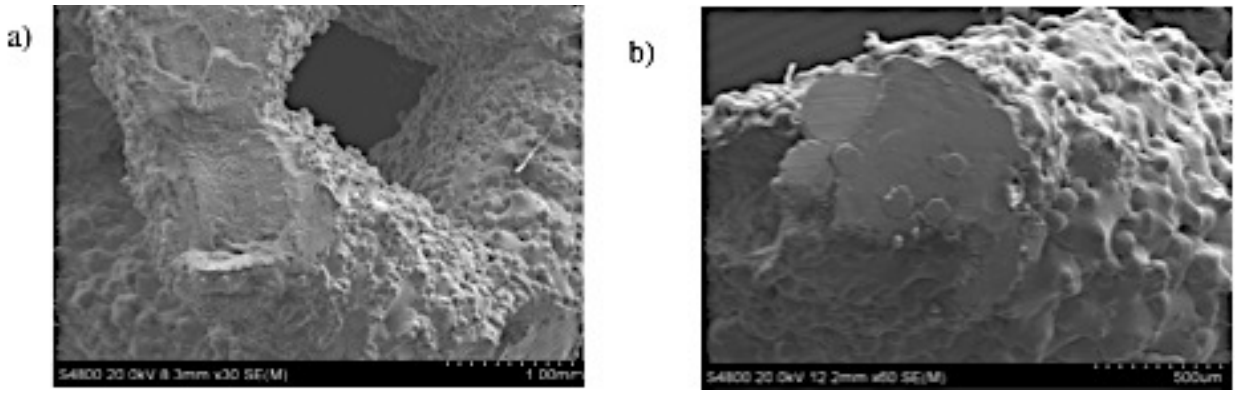

Figure 6.9: (a) (b) SEM image of the mesh array at a target relative density of 30% and the fracture surface

CONCLUSIONS

In this study, a method to prevent the appearance of the detrimental α'-martensite phase reported in the fabrication of this walls (<5mm) by the AM method of EBM was implemented, in the desire of configuring the optimum processing parameters for the attractive parts. The microstructure was analyzed through varying scan passes of single, double and triple. In addition, the mechanical behavior was correlated through compression test. The major features of the approach are as follows:

- The mechanical behavior between the standard build and all the other builds, in general, was determined to be statistically the same at a 95% confidence level. Aside for the UCS between the standard and the triple melt, the probability of the mechanical response to be assumed equal is accepted. This by the P-value calculated to be less than the significance level of 0.05 (5%) used.
- The relative stiffness, increased with increasing heat; however, it was concluded that the property was not governed by the amount of heat, given the triple scan pass

build did not report higher values than the double scan pass rather the opposite was observed.

- The results for the microstructure of the solid cubes showed there was a 52% increase in α-lath thickness from the standard build to the double, but the most notorious increase was for the standard build to the triple melt, in which the α-lath thickness saw an increase of 154%.
- The results obtained for this study for the lattice structures correlated with Murr's findings, conveying an increase in the α-phase regardless of the part geometry and dimensions. From the single melt to doubling the melt passes, there was a 10% increase in thickness of the α'-martensite, while increasing the melt passes from single to triple resulted in an increase of 42%.
- Literature has suggested that increasing heat input conveys a change in morphology of [larger grains by nucleation and growth yielding a relaxation of internal stresses. This was observed through the increase in deflection from the standard build to all the other builds, as well as superior properties from the standard build to all the other builds.

CHAPTER 7: CONCLUSIONS AND RECOMMENDATIONS

CONCLUSIONS

This research concentered on evaluating mechanical properties, analyzing microstructures, and correlating the fabrication process to inherent characteristics of solid and porous parts fabricated utilizing EBM. The effects of building parts in the presence of neighboring parts was explored as well as the location in the build chamber of the part being fabricated. In the case of mesh structures, or lattice structures, the effects of parameter modifications, such as; processing currents and number of scan passes, on the final part were explored. An Arcam A2 system was used in this investigation as the means for the fabrication of all parts. Testing equipment included an MTS Landmark Servohydraulic with exchangeable features for the two types of mechanical test performed for these studies, which were tensile and compression. Each test performed was tailored to the material, dimension and structure of part through modification of parameters and external features (e.g. extensometer and/or lubricants). Solid components were subjected to tensile testing while lattice structures were evaluated under a compression test. In the case of the tensile test, the data provided by the machine were evaluated by the use of Matlab computer software that is capable of reading the acquired report and providing values for the basic engineering properties of: Young's modulus (E), ultimate tensile strength (UTS), yield strength (YS), and percent elongation . In the case of the compression testing, the properties reported were obtained through the use of the well known Gibson-Ashby equations for cellular structures. It is well known that the microstructure influences the mechanical behavior; therefore, for solid components, it was important to report if consistency was achievable for intra-build and inter-builds or if microstructural anisotropy was a factor for similar build setups of the EBM-process for Ti-6Al-4V

parts. In the case of the lattice structures, the focus was on removing the well-documented α martensite microstructure.

Solid components were fabricated under standardized Ti-6Al-4V parameters as a means to study the mechanical properties and microstructure. In the case of additional surrounding parts of different diameters, the mechanical behavior was determined to be statistically different. The addition of surrounding parts meant an increase in heat experience by the main parts in the build, altering the microstructures (increase in α-lath width) and as a consequence there was an increase in UTS with increasing diameter size. In the case of the varying locations for solid components EBM-fabricated under standardized parameters, it was determined that mechanical behavior varies for an intra-build. The parts towards the back of the machine, reported a higher UTS and noticeably higher in percent elongation. The E, and YS, varied in a scattering manner. A ductile fracture was observed for all the parts subjected to tensile testing. The parts displayed similar macro and micro evidence of the ductile mode such as necking, dull and fibrous surface, and dimples were observed under SEM analysis.

Lattice structures were fabricated taking advantage of the accessibility Arcam offers EBM users to customize the parameters from the process menu Modifications to processing parameters were made as means to study the mechanical behavior and intentionally grade microstructure to remove the detrimental martensitic phase. Three lower than standard currents were utilized, to evaluate mechanical behavior under compression testing. It was determined that between the standard build and all the other builds there was no statistical difference for the mechanical behavior exhibited. The mechanical properties measured such as, density, relative density, porosity, and stiffness showed an increase from the standard build values. It is important to note highest values were observed for the lowest current utilized for the properties mentioned above.

This was attributed to the fine grain morphology due to the fast scan low energy promoting the appearance of the α-martensite. Of interest was to prevent the appearance of the detrimental α-martensite phase that appears as the size of the lattice structure decreases. This is due to rapid solidification for these geometries. The results obtained from the study showed removal of the martensite phase is possible by increasing the scan melt pass. The double scan reported the highest measured properties and an increased in α-lath width. However, it was the triple scan pass in which a globular α-phase was observed, allowing research to move to the next chapter for these very attractive structures.

RECOMMENDATIONS

Much research has been performed to characterize EBM-fabricated parts. The following recommendations are provided based on the results described in this research.

- Fabrication by EBM occurs in a controlled environment and in this study with a prealloyed powder that aided the control of chemical composition. A quantification of crystalline phases present by X-ray Diffraction is recommended as this too highly influences properties just as microstructure and morphology.
- In the case of lattice structures the experimental value for the Young's modulus (stiffness) is crucial for mechanical behavior evaluation. This value can be complicated to obtain due to the geometry of the structure as it proved to be the case for this study. It has been reported that the value can be obtained ultrasonically by the use resonant frequency and damping analysis (RFDA) or with the use of numerically analysis software.
- Materials are subjected various stresses at times in combinations, the work here presented compressive and tensile stress. However, it is recommend investigating the behavior under fatigue, bending, and shear.

- Simulation of thermal distribution of the EBM AM process and monitoring of thermal history for thermal models for materials properties.

Additive manufacturing is a technology projected to become a manufacturing alternative by the efforts of minds that work in conjunction to understand it and seek to evolve it for the ultimate goal of industrialized production. The work presented in this thesis looked to contribute to the research on the metals area of additive manufacturing, specializing in the biocompatible and "work horse" of industry, the titanium alloy Ti-6Al-4V. The need to understand the effects that contribute to part behavior and microstructural evolution were the motivation behind the studies performed. The innovating products resulting from EBM-fabrication have the potential to contribute largely to the world by exploiting beautiful designs and performance; a combination originally believed to contradict.

As technology advances, materials are changing to extract a new alternative from them, in the hopes of transforming our world, all while taking care of it.

REFERENCES

A. Butscher, M. B. (2011). Structural and material approaches to bone tissue engineering in poweder-based three-dimensional printing. *Acta Biomaterialia*, 907-920.

A. Christense, R. K. (2007). Qualification of Electron Beam Melted (EBM) Ti6Al4V-ELI for Orthopaedic Applications. In J. Gilbert, *Medical Device Materials IV* (pp. 48-53). Palm Desert: ASM International .

Ashby, L. I. (1997). *Cellular solids: Structure and properties - Second edition.* New York : Cambridge Univiersity Press.

B. Dutta, F. H. (2015). The additive manufacturing (AM) of titanium alloys. In F. H. Ma Qian, *Titanium Powder Metallurgy science, technology, and applications* (pp. 447-468). Elsevier.

B. Gorny, T. N. (2011). In situ characterization of the deformation and failure behavior of non-stochastic porous structures processed by selective laser melting. *Materials Science and Engineering A*, 7962-7967.

Beth E. Carroll, T. A. (2015). Anisotropic tensile behavior of Ti–6Al–4V components fabricated with directed energy deposition additive manufacturing. *Acta Materialia*, 309-320.

D. Cooper, J. T. (2015). Design and manufacture of high performanec hollow engine valves by Additive Manufacturing. *Materials and Design*, 44-55.

D.He, J. Z. (2012). Influences of deformation strain, strain rate and cooling rate on Burges orientation relationship and variants morphology during beta to alpha phase transformation in a near alpha titanium alloy. *ELSEVIER*, 20-29.

Emmanuel Rodriguez, J. M. (2015). Approximation of absolute surface termperature measirements of powder bed fusion additive manufacturing technology using in situ infrared termography. *Additive Manufacturing*, 31-39.

Gerhard Welsch, R. B. (1993). *Material Properties Handbook: Titanium Alloys.* Materials Park .

H.K. Rafi, N. K. (2013). Microstructures and Mechanical Properties of Ti6Al4V Parts Fabricated by Selective Laser Melting and Electron Beam Melting. *Journal of Materials Engineering and Performance* , 3872-3883.

Haijun Gong, K. R. (2014). Analysis of defect generation in Ti-6Al-4V parts made using powder bed fusion additive manufacturing processes. *Additive Manufacturing*, 87-98.

Hemann, K. (2011). *Hardness Testing: Principles and Applications.* Materials Park: ASM International.

J. Lin, Y. L. (2016). Microstructural evolution and mechanical properties of Ti-6Al-4V wall deposited by pulse plasma arc additive manufacturing. *Materials and Desing*, 30-40.

Jia-Yi Yan, G. O. (2016). Computational Thermodynamics and kinetics of displacive transformations in titanium-based alloys. *Journal of Alloys and Compounds*, 441-454.

Jonathan Minjares, J. M. (2014). Installation and Thermal Feedback from a Multi-wavelength Pyrometer in Electron Beam Melting.

Karina Puebla, L. E. (2012). Effect of Melt Scan Rate on Microstructure and Macrostructure for Electron Beam Melting of Ti-6Al-4V. *Scinetific Research*, 259-264.

Kaufui V. Wong, A. H. (2012). A Review of Additive Manufacturing. *International Scholarly Research Network*.

Krebs, R. E. (2006). *The History and Use of Our Eath's Chemical Elements: A Reference Guide.* London: Greenwood Publishing Group.

L. E. Murr, 1. S. (2009). EFFECT OF BUILD PARAMETERS AND BUILD GEOMETRIES ON RESIDUAL MICROSTRUCTURES AND MECHANICAL PROPERTIES OF Ti-6Al-4V COMPONENTS BUILT BY ELECTRON BEAM MELTING (EBM).

L. Zeng, T. B. (2005). Effects of working, heat treatment, and aging on microstructural evolution and crystallographic texture of α, α′, α″ and β phases in Ti–6Al–4V wire. *Materials Science and Engineering:A*, 403-414.

L.E Murr, E. E. (2009). Microstructures and mechanical properties of electron beam-rapid manufactured Ti–6Al–4V biomedical prototypes compared to wrought Ti–6Al–4V. *Materials Characterization*, 96-105.

L.E. Murr, S. G. (2009). Characterization of Ti-6Al-4V open cellular foam fabricated by additive manufactruing using electron beam melting. *Materials Science and Engineering A*, 1861-1868.

L.E. Murr, S. G. (2010). Characterization of Ti-6Al-4V open cellular foams fabricated by additive manufacturing using electron beam melting. *Materials Science and Engineering* , 1861-1868.

L.E. Murr, S. G. (2010). Next-generation biomedical implants using additive manufacturin of complex, cellular and functional mesh arrays. *Philosophical Transactoins of The Royal A Society*, 1999-2032.

M. Svensson, U. A. (2009). Titanium Alloys Manufactured with Electron Beam Melting Mechanical and Chemical Properties. *Medical Device Materials V: Proceedings from the Materials & Processes for Medical Devices Conference*, 189-194.

M.F. Ashby, A. E. (2000). *Metal foams: A Design Guide.* Buirlington: Butterworth Heinemann.

M.F. Zäh, S. L. (2010). Modelling and simulation of electron beam melting. In *Production Process Research and Develpment* (pp. 15-23).

Nikolas Hrabe, T. Q. (2013). Effects of processing on microstructure and mechanical properties of a titanium alloy (Ti–6Al–4V) fabricated using electron beam melting (EBM), part 1: Distance from build plate and part size. *Material Science and Engineering: A*, 264-270.

Nikolas Hrabe, T. Q. (2013, March 13). Effects of processing on microstructure and mechanical properties of a titanum alloy (Ti-6Al-4V) fabricateed using electron beam melting (EBM), Part 2: Energy input, orientation and location. *Materials Science and Engineering: A, 573*, 271-277.

Peter Heinl, L. M. (2008). Cellular Ti-6Al-4V structures with interconnected macro porosity for bone implants fabricated by selective electron beam melting. *Acta Biomaterialia*, 1536-1544.

Ravindranath, M. (1981). STUDENTS "t" TEST. *Manual of Reserach Methods for Crustacean Biochemisty and Physiology*, 153-156.

S. Palanivel, A. D. (2016). Spatially dependent properties in a laser additive manufactured Ti–6Al–4V component. *Material Science and Engineering: A*, 39-52.

S. Zhao, S. L. (2016). The influence of cell morphology on the compressive fatigue behavior of Ti-6Al-4V meshes fabricated by electron beam melting. *Journal of the Mechanical Behavior of Biomedical Materials*, 251-264.

S.J. Li, L. M. (2012). Compression fatigue behavior of Ti-6Al-4V mesh arrays fabricated by electron beam melting. *Acta Materialia*, 793-802.

S.M. Gaytan, L. M. (2009). Advanced metal powder based manufacturing of complex components by electron beam melting. *Materials Technology*, 180-190.

Sahab Babaee, B. H.-H. (2012). Mechanical properties of open-cellular rhombic dodecahedron cellular structures. *Acta Materialia*, 2873-2885.

Shangzhou Zhang, C. L. (2016). Longitudinal Compression Behavior of Functionally Graded Ti–6Al–4V Meshes. *Journal of Materials Science & Technology*.

Sophie C. Cox, J. A. (2015). 3D Printing of porous hydroxyapatite scaffolds intended for use in bone tissue engineering application. *Materials Science and Engineering C*, 237-247.

Timothy J. Horn, O. L.-L. (2014). Flexural properties of Ti6Al4V rhombic dodecahedron open cellular strucutres fabricated with electron beam melting. *Additve Manufacturing*, 2-11.

Trengovem, L. (1972). William Gregor (1761-1817) Discoverer of Titanium. *Annals of Science* .

Voort., G. F. (1999). *Metallography, principles and practice.* Materials Park: ASM International.

Wang, W. (2011). *Reverse Engineering Tehcnology of Reinvention.* Boca Raton: Taylor and Francis Group,LLC.

Wei Sha, S. M. (2009). *Titanium alloys; modeling of microstrucutre, properties and applications.* Boca Raton: Woodhead Publishing Limites .

William D. Callister, D. G. (2012). *Fundamentals of Materials Science and Engineeing: An Integrated Approach.* John Wiley & Sons.

William D. Callister, D. G. (2012). Mechanical Properties. In D. G. William D. Callister, *Fundamentals of Material Science adn Engineering: An Integrated Approach* (p. 910). John Wiley & Sons.

Wood, B. M. (2016). Multifunctionality in Additive Manufacturing. In B. M. Vannessa Goodship, *Design and Manufacture of Plastic Components for Multifunctionality* (pp. 171-204).

Xipeng Tan, Y. K.-W. (2015). An experimental and simulation study on build thickness dependent microstructure for electron beam melted Ti–6Al–4V. *Journal of Alloys and Componds* , 303-309.

APPENDIX A: STRESS VERSUS STRAIN

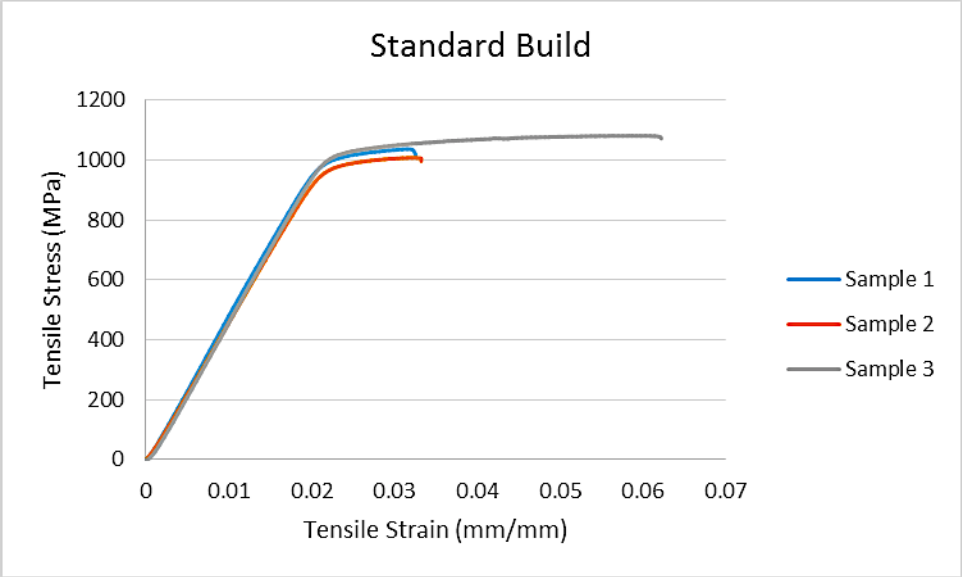

Figure A-1: Engineering stress versus tensile strain data for each cylinder tested under the standard build for, mechanical response of building conditions on solid components: increasing surface area of surrounding part

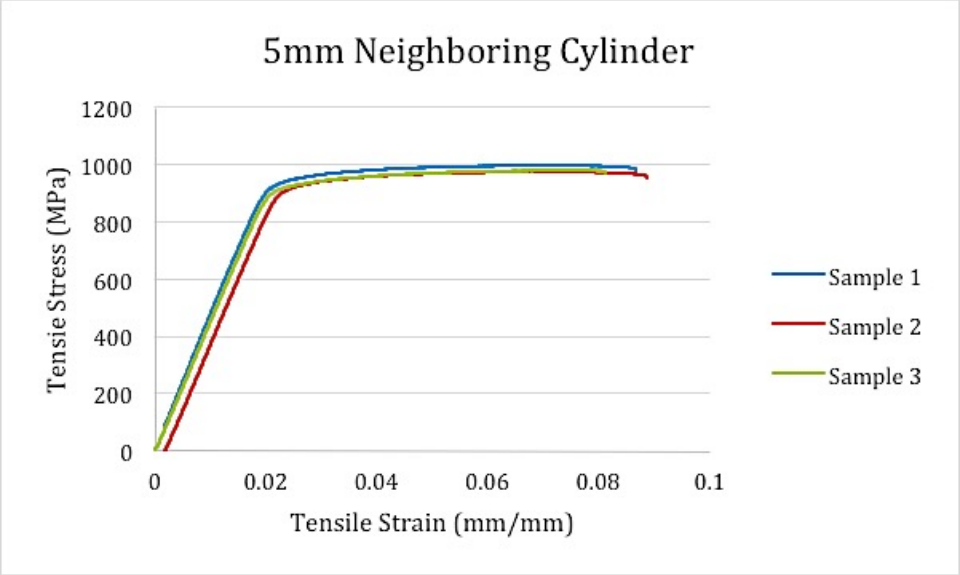

Figure A-2: Engineering stress versus tensile strain data for each cylinder with 5mm neighboring cylinder design for, mechanical response of building conditions on solid components: increasing surface area of surrounding parts

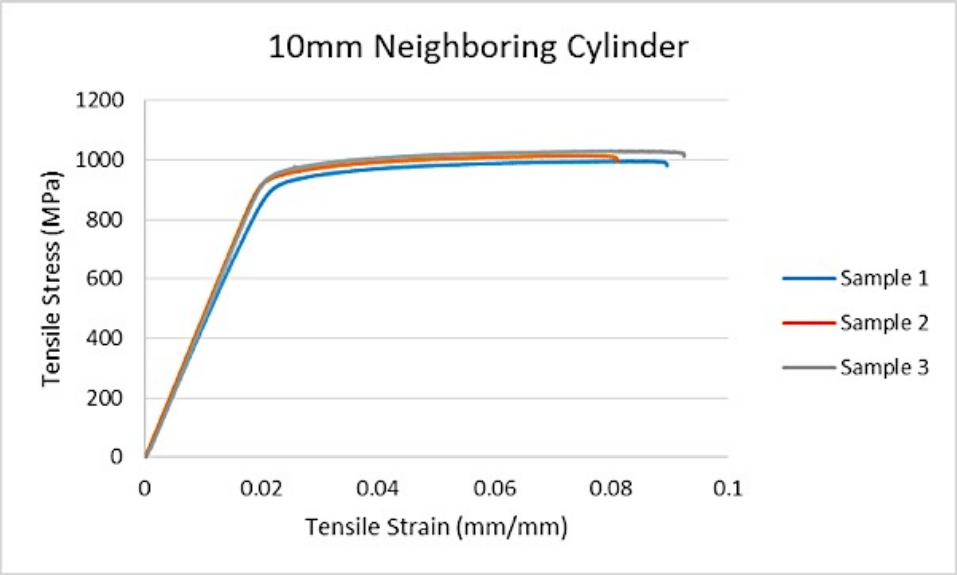

Figure A-3: Engineering stress versus tensile strain data for each cylinder with 10mm neighboring cylinder design for, mechanical response of building conditions on solid components: increasing surface area of surrounding parts

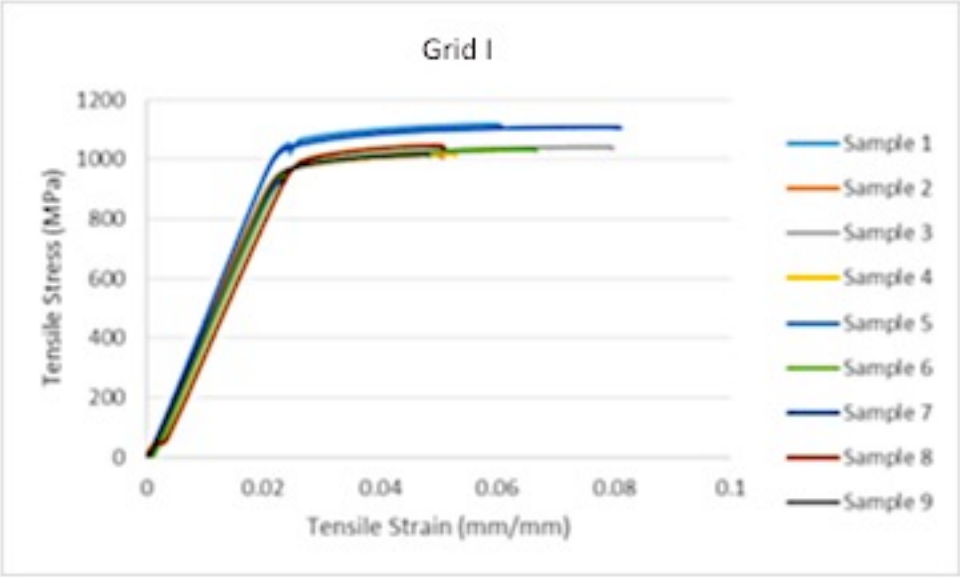

Figure A-4: Engineering stress versus tensile strain data for each cylinder tested for Grid I for, mechanical response of building conditions on solid components: location variations for a single build

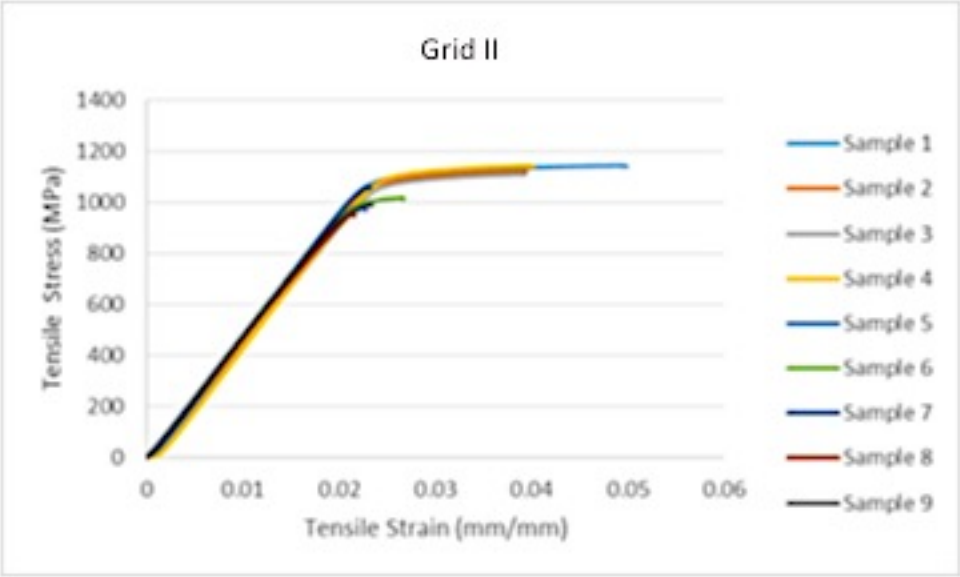

Figure A-5: Engineering stress versus tensile strain data for each cylinder tested for Grid II for, mechanical response of building conditions on solid components: location variations for a single build

APPENDIX B: LOAD VERSUS DISPLACEMENT

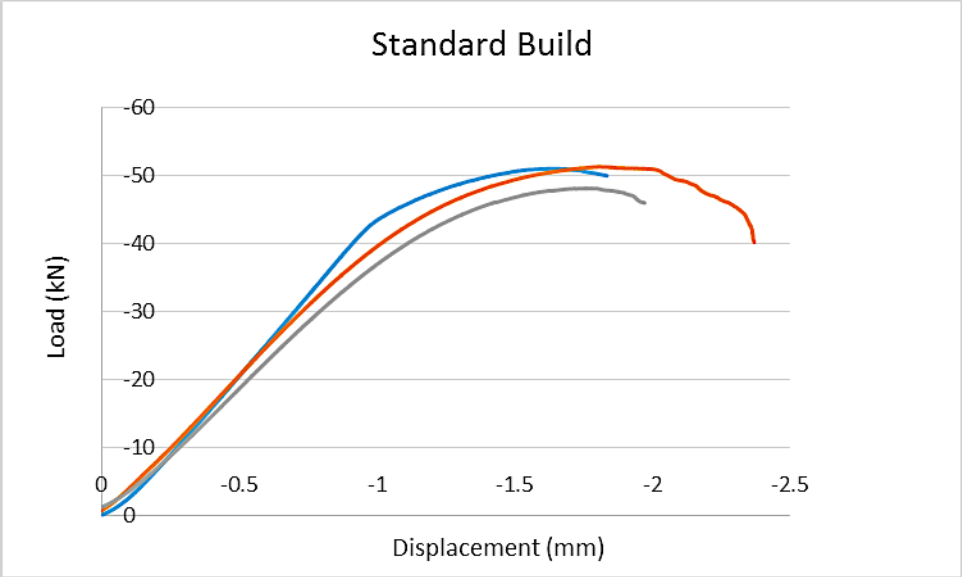

Figure B-1: Load versus displacement data for all the samples tested under the standard build

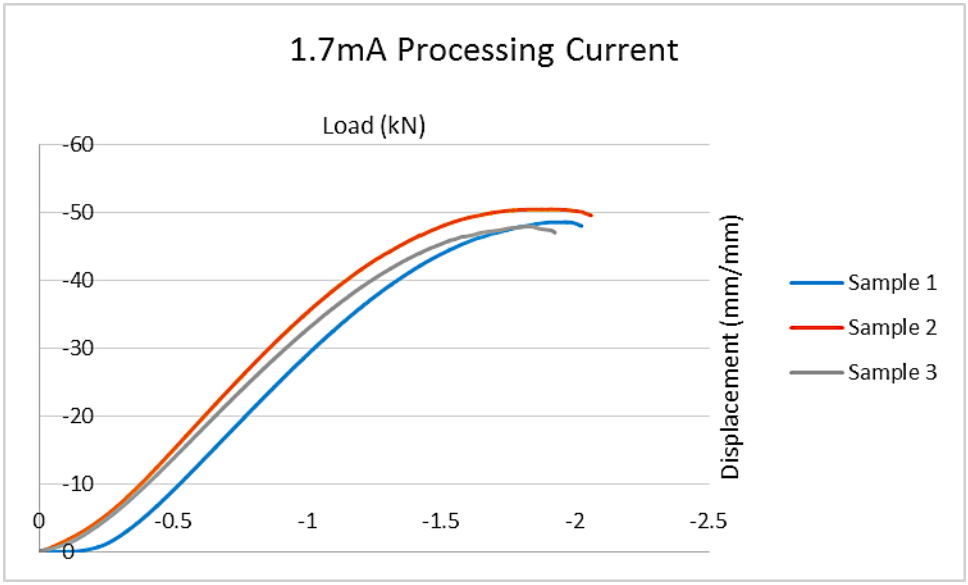

Figure B-2: Load versus displacement data for all the samples fabricated at 1.7mA

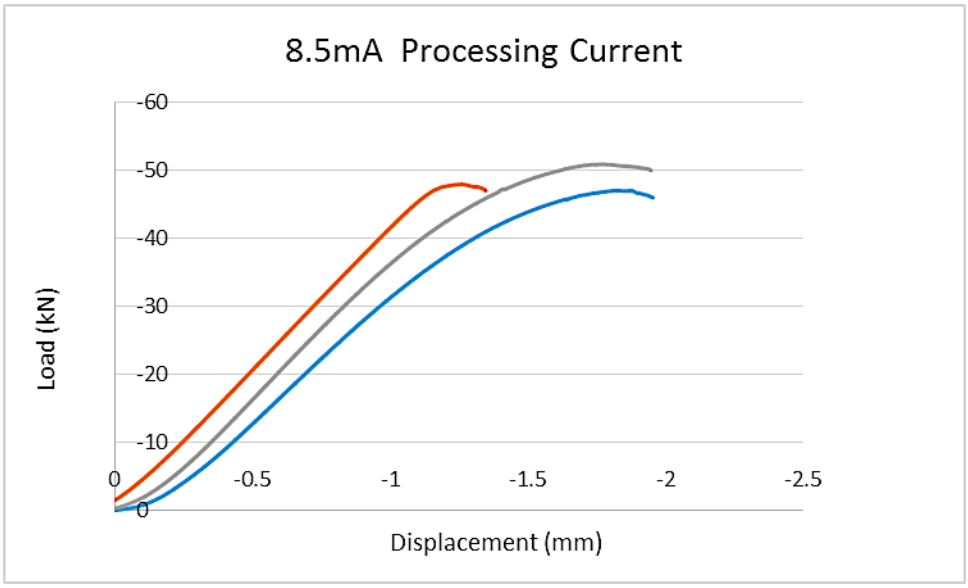

Figure B-3: Load versus displacement data for all the samples fabricated at 8.5mA

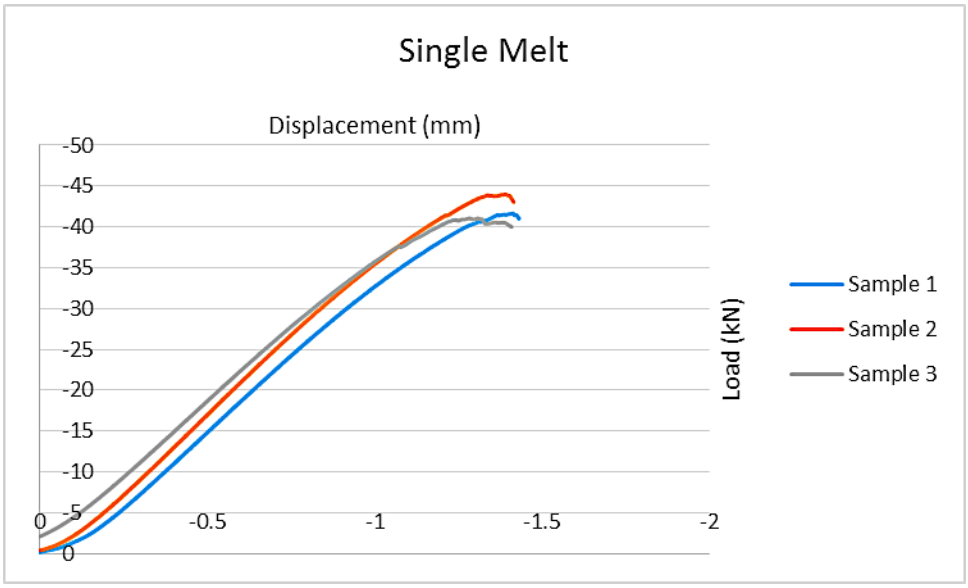

Figure B-4: Load versus displacement data for all the samples fabricated with a single melt

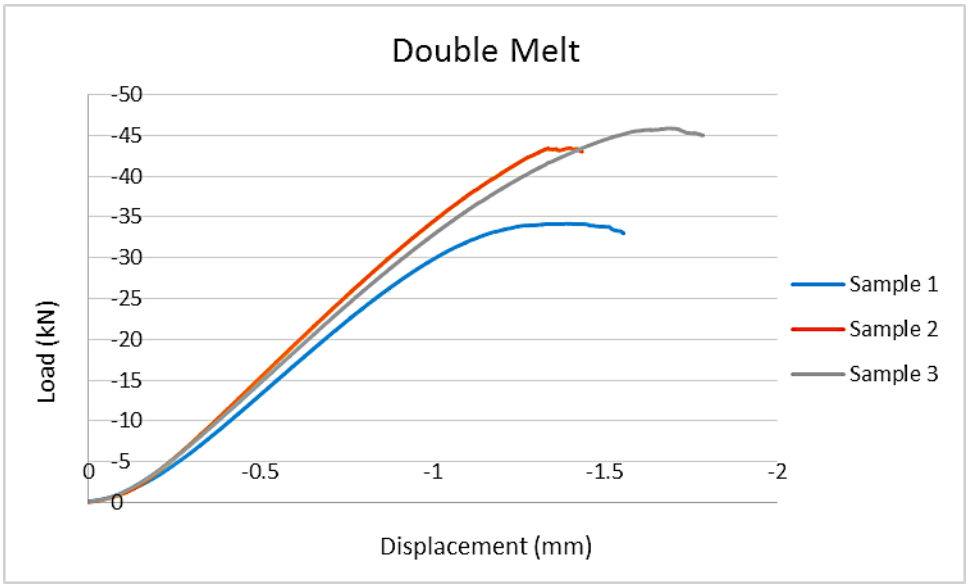

Figure B-5: Load versus displacement data for all the samples fabricated with a double melt

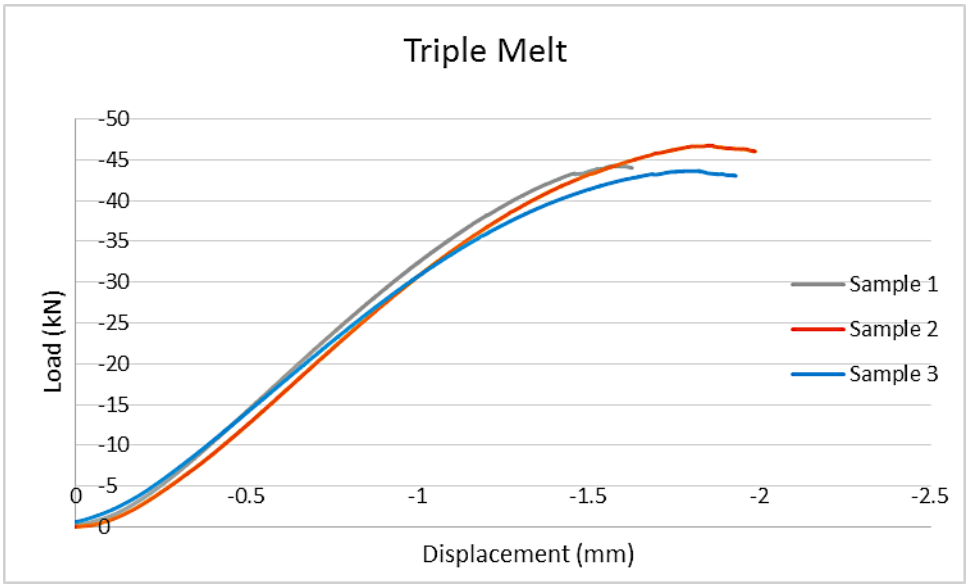

Figure B-6: Load versus displacement data for all the samples fabricated with a triple melt

VITA

Paola Azani was born in El Paso, TX, on January 23, 1990. After completing her high school studies at J.M. Hanks High School in 2008, she enrolled at the University of Texas at El Paso (UTEP). Between 2008 and 2014 she studied metallurgy and materials engineering, receiving the degree of Bachelor of Science. In August 2014, Paola commenced as a graduate student at UTEP perusing a masters in metallurgy and materials engineering. During her stay at the University, she was provided with a research experience through the National Science Foundation (NSF) starting in the summer of 2014. NSF allowed Paola to work at the W.M. Keck Center for 3D Innovation (Keck Center) where she performed research on the metals area of Additive Manufacturing (AM).

Contact Information: pmcordero@miners.utep.edu

This thesis was typed by Paola Azani.